

THE UNIVERSITY OF HULL

Characterisation of reverse grading in ignimbrites through image analysis and
experimental granular currents

being a Thesis submitted for the Degree
of

MSc by Research Geology

in the University of Hull

by

Matthew Johnson

September 2022

Abstract

Pyroclastic density currents (PDCs) are hot, density-driven fast-moving flows of gas, rock and ash produced by volcanic events such as explosive eruptions, the fallback of eruption columns or the collapse of lava domes. They are deadly geological hazards which have caused >90 000 deaths since 1600 AD. We must improve our understanding of PDCs and their deposits to improve our ability to prepare for future events. PDCs are rarely observed up close due to their hazardous nature and as such real time analysis is difficult. Through the use of models and the interpretations of deposits, known as ignimbrites, we can improve our understanding of the flow dynamics of PDCs. The deposits of PDCs can provide important information about how these deadly volcanic hazards behave in time and space. Reverse grading of clasts is often observed in these deposits and can be interpreted in different ways such as growing eruption intensity where larger clasts are introduced over time. Alternatively, it could record kinematic sorting (the 'muesli effect') where small grains percolate downwards and large grains rise. The link between current dynamics and reverse grading is previously untested in aerated granular currents.

This study used aerated granular currents created in an analogue flume to investigate how reverse grading may be related to kinematic sorting. These experiments are complemented by sedimentological characterisation of ignimbrites through image analysis along with static tests of kinematic sorting. Our results show that aerated currents are stratified through kinematic sorting whereby larger grains are carried towards the top of a current and smaller grains are closer to the base. Stratification of the current controls the composition of the flow boundary zone and therefore the clasts which are able to deposit. Through quantitative analysis, we show that kinematic sorting during flow is directly linked to creating reversely graded deposits.

Acknowledgements

This work would not have been possible without the support of many people and organisations. Firstly I would like to thank my supervisors Rebecca Williams, Natasha Dowey and Pete Rowley who have supported and guided this project and helped design new methods when the Covid-19 pandemic prevented access to laboratories. I would like to thank the University of Hull for allowing me to carry out this research.

I would like to thank Peter Rowley and the University of West England for providing the space, time and equipment to carry out the flume experiments that made this study, and huge thanks to Leah Sier for her assistance in conducting the experiments. The experimental work could not have been completed without the financial support of the Geologist Association for which I am extremely grateful.

I am thankful all my friends who have been there for me, Tom, Charlotte, Rebecca, David, Tom, Elizabeth, Hannah, Preyash and Kathryn thanks for providing me with the much needed breaks from work and the support you have given. Finally, I would like to thank my family who have supported me throughout my life and who always provided encouragement throughout my time at university.

Contents

1. Introduction	14
1.1. Aim and objectives.....	14
2. Literature review.....	16
2.1. Deposit Characteristics	16
2.2. Granular material.....	16
2.3. Fluidisation.....	16
2.4. Grain characteristics	17
2.5. Deposit analysis methods	18
2.5.1. Sieving	18
2.5.2. Image analysis	18
2.6. Deposit aggradation.....	19
2.6.1. Reverse grading.....	20
2.6.2. Reverse grading theories	20
2.6.3. Dispersive pressure.....	20
2.6.4. Gravitational settling.....	23
2.6.5. Kinematic sieving	23
2.7. Modelling	25
2.7.1. Bedforms.....	26
3. Quantifying reverse grading in ignimbrites with image analysis.....	27
3.1 Introduction	27
3.1.1 Aims.....	28
3.1.2 Objectives.....	28
3.2 Methods.....	28
3.2.1 Image selection	28
3.2.2 Image Analysis.....	29
3.2.3 Data Analysis.....	29
3.3 Images used for analysis	30
3.3.1 Packages 1 and 2.....	30
3.3.2 Package 3	31
3.3.3 Package 4	32
3.3.4 Package 5	33
3.3.5 Package 6	33
3.4 Results.....	33

3.4.1	Package 1	35
3.4.2	Package 2	36
3.4.3	Package 3	37
3.4.4	Package 4	38
3.4.5	Package 5	39
3.4.6	Package 6	40
3.4.7	Composition	42
3.5	Discussion.....	43
3.5.1	How is reverse grading characterised?	43
3.5.2	The effectiveness of image grain size analysis of volcanic outcrops	45
3.6	Conclusions	46
4.	Quantitative analysis of the Muesli effect	47
4.1.	Introduction	47
4.1.1	Aim and objectives.....	47
4.2.	Background	47
4.2.1.	Particle segregation theory.....	47
4.2.2.	Applicability to polydisperse volcanic granular currents	49
4.3.	Methods.....	51
4.3.1.	Experimental design.....	51
4.3.2.	Materials	52
4.3.3.	Parameters and experimental runs	53
4.3.4.	Analysis	54
4.4.	Results.....	55
4.4.1.	Type 1 experiments (different sizes, similar density)	55
4.4.2.	Type 2 experiments (different sizes, different densities)	63
4.5.	Discussion.....	70
4.5.1.	Impact of grain size of segregation.....	70
4.5.2.	Role of density in segregation.....	71
4.5.3.	Impact of shape on segregation.....	73
4.5.4.	Sorting.....	73
4.6.	Conclusions	74
5.	Experimental analysis of particle sorting in fluidised conditions.....	75
5.1	Introduction	75
5.1.1	Aims.....	75
5.1.2	Objectives.....	75
5.2	Background	75

5.3	Methods.....	76
5.3.1	Flume set-up	76
5.3.2	Analogue density current material	77
5.3.3	Experimental runs.....	79
5.3.4	Documentation	79
5.3.5	Image Analysis.....	80
5.3.6	Video analysis.....	81
5.4	Results.....	81
5.4.1	Deposit analysis.....	81
5.4.2	Experiments with varied grain size and same density particles	84
5.4.3	Experiments with varied grain sizes and different density.....	85
5.4.4	Bedforms.....	86
5.4.5	Reverse grading.....	88
5.4.6	Analysis of experiments with varied grain sizes and the same density.....	88
5.4.7	Analysis of experiments with varied grain sizes and different density.....	95
5.4.8	Current velocity.....	98
5.4.9	Current stratification.....	99
5.5	Discussion.....	102
5.5.1	Deposit Characteristics	102
5.5.2	Flow behaviour.....	104
5.5.3	Stratified currents	104
5.5.4	Applications to field volcanology.....	105
5.6	Conclusions	105
6.	Discussion.....	107
6.1.	Key factors involved in segregation processes	107
6.1.1.	Grain size range.....	107
6.1.2.	Grain density	108
6.1.3.	Grain shape	109
6.1.4.	Grain size distribution	109
6.1.5.	Impact of fluidised flow	109
6.2.	Implications for PDC behaviour	113
6.3.	Applications to field volcanology	114
6.4.	Conclusions	115
7.	Appendix I	124
7.1.	Digital version of all JMicrovison and Gradistat data used in Chapter 3	124
8.	Appendix II	124

8.1. Digital version of all JMicrovison and Gradistat data used in Chapter 4 with videos of all experiments	124
9. Appendix III	124
9.1. Digital version of all JMicrovison and Gradistat data used in Chapter 5 with videos of all representative experiments.....	124
10. Appendix IV	124
10.1. Link to online versions of highspeed videos	124
10.2. Link to online version of High resolution photos.....	124

List of Figures

- Figure 2.1 The outer drum A, solidly built of Perspex and brass, could be rotated through change-wheels at a series of known speeds ranging from 0-25 to 8-6 rev/sec. The periphery C of the inner drum B, permanently filled with water, consisted of sheet rubber sealed to the drum flanges, attached to the head D was a calibrated spring for torque measurement. the end-spaces FF, was filled with water up to a convenient level in the open stand-pipe G. this level was reproduced in the wide reservoir H. A pump K enabled air bubbles to be driven out of the whole apparatus when needed. (rotating parts shown in hatched) (Bagnold, 1954)..... 21
- Figure 2.2 flume used in the second experiment with a length of 5ft and a constant angle of 33°, and a sliding gate that can be opened at various heights to create sand flows of the required heights (Bagnold, 1954)..... 22
- Figure 2.3 deposition in a traction carpet via gradual aggradation (Sohn, 1997)..... 24
- Figure 3.1 Packages 1 (blue) and 2 (red), showing reversely graded ignimbrite in the Poris Formation, Tenerife (A) and marked up for analysis (B). Note that this image contains two packages for analysis (1i, 1ii, iii, iv, Av and 2i, 2ii, iii, iv, Av). Photo courtesy of N. Dowey..... 31
- Figure 3.2 Package 3, ignimbrite from Bandas Del Sur, Tenerife, (left) and marked up for analysis (3i, 3ii, etc) (right) Resolution = 923x692 (± 1.25 mm). Photos courtesy of Rebecca Williams 31
- Figure 3.3 Package 4 ignimbrite located in Bandas Del Sur, Tenerife (left) Same image, but with linework added to map packages into five sections of equal thickness (right). resolution = 4608x2592 (± 0.33 mm). Photo courtesy of Rich Brown 32
- Figure 3.4 Package 5 reversely graded ignimbrite located in Bandas Del Sur, Tenerife (left) Same image, but with linework added to map packages into five sections of equal thickness (right). Resolution = 2848x2316 (± 0.47 mm). Photo courtesy of Rich Brown 33
- Figure 3.5 Package 6 ignimbrite from Bandas Del Sur, Tenerife (left) Same image, but with linework added to map packages into five sections of equal thickness (right). Resolution = 2848x2316 (± 0.90 mm). Photo courtesy of Rich Brown..... 33
- Figure 3.6 (a) Lithofacies package 1 with five equal subsections (2.7 cm tall) marked in red, accompanied by (b) grain size distribution charts for each subsection (1i, 1ii, 1iii, 1iv and 1v). (c) sorting values calculated using Gradistat within each subsection of package 1, (D) Mean average grain size of the 10 largest (qualitatively selected) pumice and lithic clasts 35
- Figure 3.7 (a) Lithofacies package 2 with five equal subsections (3.4 cm tall) marked in red, accompanied by (b) grain size distribution charts for each subsection (2i, 2ii, 2iii, 2iv and 2v). (c) sorting values calculated using Gradistat within each subsection of package 2, (d) Mean average grain size of the 10 largest (qualitatively selected) pumice and lithic clasts 36
- Figure 3.8 (a) Lithofacies package 3 with five equal subsections marked in Black, accompanied by (b) grain size distribution charts for each subsection (3i, 3ii, 3iii, 3iv and 3v). (c) sorting values calculated using Gradistat within each subsection of package 3, (d) Mean average grain size of the 10 largest (qualitatively selected) pumice and lithic clasts..... 37
- Figure 3.9 (a) Lithofacies package 4 with five equal subsections marked in Black, accompanied by (b) grain size distribution charts for each subsection (4i, 4ii, 4iii, 4iv and 4v). (c) sorting values calculated using Gradistat

within each subsection of package 4, (d) Mean average grain size of the 10 largest (qualitatively selected) pumice and lithic clasts..... 38

Figure 3.10 (a) Lithofacies package 5 with five equal subsections marked in black, accompanied by (b) grain size distribution charts for each subsection (5i, 5ii, 5iii, 5iv and 5v). (c) sorting values calculated using Gradistat within each subsection of package 5, (d) Mean average grain size of the 10 largest (qualitatively selected) pumice and lithic clasts..... 39

Figure 3.11 (a) Lithofacies package 6 with five equal subsections marked in black, accompanied by (b) grain size distribution charts for each subsection (6i, 6ii, 6iii, 6iv and 6v). (c) sorting values calculated using Gradistat within each subsection of package 6, (d) Mean average grain size of the 10 largest (qualitatively selected) pumice and lithic clasts..... 40

Figure 3.12 Ternary Plot showing the composition of Pumice ash and lithics for the images used. 43

Figure 4.1 (A) interpreted movement of grains according to dispersive pressure model suggested by Bagnold (1954). (B) Concept of kinematic sorting through sieving in the collisional zone, and squeezing in the compressional zone (Le Roux, 2003)..... 49

Figure 4.2 Sketch of the experimental setup used for the shaking experiments 52

Figure 4.3 Grain size distribution of Type 1 uniform mix (with equal amounts of giant couscous, couscous, and semolina) before and after 2 minutes of shaking at 12000 rpm. (A) Type 1 uniform mix before shaking occurred, split into five equal subsections, (B) Grain size distribution of each deposit subsection before shaking, (C) Sorting values for the 5 subsections before (black) and after (grey) shaking, calculated using Gradistat, (D) Grain size distribution of each deposit subsection after shaking, (E) Type 1 uniform mix after shaking. 56

Figure 4.4 Video frames taken from type 1 uniform mix with equal parts couscous, semolina, and giant couscous. The numbers in bottom left corner of frames are time in seconds since shaking began. **A** instant percolation of finer material leads to almost full segregation of finest material from the deposit. **B** Larger couscous begins to vibrate increasingly, areas of couscous in between larger grains (Highlighted in red) begin to shrink **C** medium sized grains now segregating from the largest grains, areas between the larger grain (highlighted in red) shrinking as grains percolate downwards, increasing level of fine material at the base as rapid segregation continues. **D** areas between the largest grains disappeared as the medium sized grains percolated through, full segregation of finest material. 57

Figure 4.5 Grain size distribution of Type 1 fines rich mix (with 50% semolina, 40% couscous and 10% giant couscous) before and after 2 minutes of shaking at 12000 rpm. (A) Type 1 fines rich mix before shaking occurred, split into five equal subsections, (B) Grain size distribution of each deposit subsection before shaking, (C) Sorting values for the 5 subsections before (black) and after (grey) shaking, calculated using Gradistat, (D) Grain size distribution of each deposit subsection after shaking, (E) Type 1 fines rich mix after shaking..... 58

Figure 4.6. Grain size distribution of Type 1 medium rich mix (using a mix of 40% semolina, 50% couscous and 10% giant couscous) before and after 2 minutes of shaking at 12000 rpm. (A) Type 1 fines rich mix before shaking occurred, split into five equal subsections, (B) Grain size distribution of each deposit subsection before shaking, (C) Sorting values for the 5 subsections before (black) and after (grey) shaking, calculated using Gradistat, (D) Grain size distribution of each deposit subsection after shaking, (E) Type 1 medium rich mix after shaking..... 60

Figure 4.7 Video frames taken from type 1 uniform mix with equal parts couscous, semolina, and giant couscous. The numbers in bottom right corner of frames are time in seconds since shaking began. **(A)** segregation of the smallest particles begins. **(B)** small particles continue to percolate down, now majority lie at the base, and coarse grains begin to rise through the mixture and emerge at the surface. **(C)** coarse grains rise

in lower sections with increased exposure at the surface **(D)** surface now littered with the coarse grains, throughout the mid and base layers, large grains are moving more laterally than vertically 61

Figure 4.8 Grain size distribution of Type 1 coarse rich mix (using a mix of 10% semolina, 40% couscous and 50% giant couscous) before and after 2 minutes of shaking at 12000 rpm. (A) Type 1 fines rich mix before shaking occurred, split into five equal subsections, (B) Grain size distribution of each deposit subsection before shaking, (C) Sorting values for the 5 subsections before (black) and after (grey) shaking, calculated using Gradistat, (D) Grain size distribution of each deposit subsection after shaking, (E) Type 1 coarse rich mix after shaking. 62

Figure 4.9 Grain size distribution of Type 2 fines rich mix (using a mix of 50% poppy seeds, 20% oats, 20% raisins and 10% nuts) before and after 2 minutes of shaking at 12000 rpm. (A) Type 1 fines rich mix before shaking occurred, split into five equal subsections, (B) Grain size distribution of each deposit subsection before shaking, (C) Sorting values for the 5 subsections before (black) and after (grey) shaking, calculated using Gradistat, (D) Grain size distribution of each deposit subsection after shaking, (E) Type 2 fines rich mix after shaking. 64

Figure 4.10 Grain size distribution of Type 2 uniform mix (using a mix of 25% poppy seeds, 25% oats, 25% raisins and 25% nuts) before and after 2 minutes of shaking at 12000 rpm. (A) Type 1 fines rich mix before shaking occurred, split into five equal subsections, (B) Grain size distribution of each deposit subsection before shaking, (C) Sorting values for the 5 subsections before (black) and after (grey) shaking, calculated using Gradistat, (D) Grain size distribution of each deposit subsection after shaking, (E) Type 2 uniform mix after shaking..... 66

Figure 4.11 Frames of video footage showing the movement of small oats and poppy seeds in type 2 uniform mix. yellow boundary marks the original spread of small grains in A with the same area overlain on B and C showing the difference in particle spread. Time in seconds is noted in the top right corner of each frame 67

Figure 4.12 **(A)** video frame showing a gap created by the movement of two large grains with a pile of smaller grains resting on top. **(B)** a void opens slightly allowing the pile of smaller particles to fall and fill the gap created. Time in seconds is noted in the bottom right of each frame 68

Figure 4.13 Grain size distribution of Type 2 medium rich mix (using a mix of 20% poppy seeds, 50% oats, 20% raisins and 10% nuts) before and after 2 minutes of shaking at 12000 rpm. (A) Type 1 fines rich mix before shaking occurred, split into five equal subsections, (B) Grain size distribution of each deposit subsection before shaking, (C) Sorting values for the 5 subsections before (black) and after (grey) shaking, calculated using Gradistat, (D) Grain size distribution of each deposit subsection after shaking, (E) Type 2 medium rich mix after shaking..... 69

Figure 5.1 longitudinal section of the experimental flume 77

Figure 5.2 sketches of steep backset bedforms (left) and shallow backset bedforms (right) (Smith et al., 2020) 83

Figure 5.3 A) Profile type B deposit from experimental deposit 4, using Mix 5 (60% 45 μm -90 μm 20% 125 μm - 425 μm 20% 425 μm -600 μm). B) Annotations on delineate bedforms and grading patterns visible. (red = reverse grading, blue= normal grading, yellow = no grading)..... 84

Figure 5.4 (A) Experimental deposit 14 using mix 4 (50% 45-90 μm white beads, 30% 125-425 μm orange beads, 20% 425-600 μm green beads and 10% 600-800 μm purple beads). (B) photograph of experiment 14 deposit with sketch overlain showing types of grading and bedforms present. Red shading indicates reverse grading and yellow shading indicates no grading; this picture shows no normal grading however it was observed more distally in the deposit..... 85

Figure 5.5 (A) Deposit from experiment 31 using a mix of 60% fines (White), 20% medium light beads (Orange), and 20% medium dense beads (Black) 86

Figure 5.6 (A) Deposit from Experiment 3 using mix 5: 60% fines (White), 20% medium (Orange) and 20% coarse (Green). (B) Deposit from experiment 3 overlain with a sketch detailing the changing bedforms upstream	87
Figure 5.7 the progression from planar beds to steep backset bedforms through a granular bore, numbers in red give representative values for Froude number (Fr), Savage number (NS), Bagnold number (NB) and Friction number (NF) (Smith et al., 2020)	88
Figure 5.8 A) Reversely graded packages identified in experimental deposit 28 using mix 2 (80% 45-90 μm (White), 20% 125-425 μm (Orange)) . B) Package 1 with 5 equal horizontal subsections outlined for image analysis (Fig 5.9)	89
Figure 5.9 A package from experimental deposit 28 split into 5 equal subsections, the image has been cropped for presentation purposes B Grain size data for each subsection collected using JMicrovison C sorting data from each subsection calculated using Gradistat	90
Figure 5.10 A) Reversely graded packages identified in experimental deposit 11 (top) using mix 6 (50% 45-90 μm (White) 30% 125-425 μm (Orange) 15% 425-600 μm (Green) 5% 600-800 μm (Purple)). B) Package 1 with 5 equal horizontal subsections outlined for image analysis (Fig 5.11). C) Package 2 with 5 equal horizontal subsections outlined for image analysis (Fig 5.12).D) average grain size for each subsection for packages 1 and 2	91
Figure 5.11 A package 1 from experimental deposit 14 split into 5 equal subsections B Grain size data for each subsection collected using JMicrovison C sorting data from each subsection calculated using Gradistat.....	92
Figure 5.12 A package 2 from experimental deposit 14 split into 5 equal subsections B Grain size data for each subsection collected using JMicrovison C sorting data from each subsection calculated using Gradistat.....	93
Figure 5.13 A) Reversely graded packages identified in experimental deposit 4 using mix 5 (60% 45-90 μm (White) 20% 125-425 μm (Orange) 20% 425-600 μm (Green)). B) Package with 5 equal horizontal subsections outlined for image analysis (Fig 5.14).....	94
Figure 5.14 A package 2 from experimental deposit 4 split into 5 equal subsections, the image has been cropped for presentation purposes B Grain size data for each subsection collected using JMicrovison C sorting data from each subsection calculated using Gradistat.....	95
Figure 5.15 reverse graded bed from experiment 31 using mix 3 (80% 45-90 μm (White) 20% 125-425 μm (orange) 20% 125-425 μm dense (Black)) (left) same bed with linework splitting into 5 equal subsections (right)	96
Figure 5.16 A reverse graded bed from experimental deposit 31 split into 5 equal subsections B Grain size data for each subsection collected using JMicrovison C sorting data from each subsection calculated using Gradistat	97
Figure 5.17 average flow front velocity vs current mixture from finest (mix 1) to coarsest (mix 8).	98
Figure 5.18 Timelapse of current showing segregation of larger beads from the bulk of the current (timestamps mark time passed since current enters video frame).....	98
In figure 5.19 a small package of coarser material is seen moving within the current in experiment 9	99
Figure 5.20 stratification of currents shown across different grain sizes and densities. Red lines show the deposit surface, frames timestamped in the top right corner, and time in seconds since the current entered frame. Experiment 21 shows a fine rained current with small levels of stratification particularly evident on the	

left of the frame. Experiment 11 shows a coarse-grained current with a much greater level of stratification than shown in a fine-grained current across two waves, grain size change is abrupt in the lower section and gradual in the upper section. Experiment 30 shows a fine-grained current with mixed density grains. the stratification shows a grain size segregation and a density segregation, with fines at the base of current, underneath coarse dense grains which are underneath coarse light grains. 100

Figure 5.21 (A) fine-grained experimental deposit (experiment 28) using Mix 2, (B) Medium grain size experimental deposit (experiment 4) using mix 5, (C) coarser grained experimental deposit (Experiment 17) using mix 6, (D) coarse grained experimental deposit (experiment 14) using mix 8, (E) dense experimental deposit (experiment 31) using mix 3..... 101

Figure 6.1 (A) Stepwise aggradation of granular surges. A schematic diagram of density (q) and velocity (u) profiles is also presented; (B) sketch of a transverse section through unconfined deposits; (C) sketch of a transverse section through valley pond deposit (Sulpizio et al., 2007)..... 111

Figure 6.2 Video frames from experimental current showing an aggrading deposit from a stratified current, flow head enters the frame at 4.84 seconds. At 4.96 seconds a new graded bed is formed and the current behind continues to flow and overpass the deposited bed for the process to begin again and force the deposit to aggrade regressively. 112

Figure 6.3 elutriation pipes at the surface of the distal end of the deposit, displaying evidence of fine grains elutriating and transporting down current after deposition 113

List of tables

<i>Table 3.1 Bins used to analyse data in excel along with conversions from mm to phi and microns.</i>	<i>29</i>
<i>Table 3.2 Sorting value parameters used by the Gradistat for the logarithmic method of moments (Blott & Pye, 2001).....</i>	<i>30</i>
<i>Table 4.1 Densities for the materials used in the shaking experiments.....</i>	<i>53</i>
<i>Table 4.2 different compositions of Semolina, couscous, and giant couscous used similar density experiment..</i>	<i>54</i>
<i>Table 4.3 Composition of poppy seeds, oats, raisins, and nuts used in different density experiments</i>	<i>54</i>
<i>Table 4.4 diameter differences D_s/D_l across all grains used in Type 1 experiments</i>	<i>70</i>
<i>Table 4.5 diameter differences d_s/D_l across all grains used in Type 2 experiments.....</i>	<i>71</i>
<i>Table 5.1 Types of beads used in flume experiments</i>	<i>78</i>
<i>Table 5.2 Different mixes of beads used in the flume experiments, colour is used to distinguish between mixes in following tables and figures.</i>	<i>78</i>
<i>Table 5.3 Experimental runs with mix number (mix numbers are colour coded, matched with those outlined in Table 5.2)</i>	<i>79</i>
<i>Table 5.4 sketches of deposit of profiles A, B and C with descriptions of key features.....</i>	<i>82</i>

1. Introduction

PDCs are hot, density-driven, fast-moving flows comprised of volcanic ash, gas, and tephra. PDCs are produced by multiple phenomena including but not limited to the collapse of lava domes, collapse or fallback of eruption columns and lateral explosions (Druitt, 1998). They are one of the most hazardous volcanic phenomena, attributed to the deaths of over 90,000 people between 1600-2010, accounting for 33% of all volcanic-related deaths in that time (Auker et al., 2013). It is estimated that 29 million people live within 10 km of an active volcano and 800 million within 100 km where PDCs are at their most dangerous (Brown et al., 2017).

A major aim of modern volcanology is to achieve a quantitative understanding of pyroclastic density currents (PDCs). Multiphase modelling and new geophysical methods will provide insights into the internal flow structure of PDCs, combining the experimental, computational and field approaches that must be used to validate and advance PDC hazard models to save lives (Lube et al., 2020). Many aspects of PDCs are still only understood qualitatively due to the lack of up-close observations.

PDCs are rarely observed up close and are difficult to analyse in real-time due to the inhospitable environment. Volcanologists investigate these flows by interpreting deposits (ignimbrites), experimental modelling and computer modelling. By understanding the processes of deposition, we will increase our understanding of flow dynamics in aerated currents and the volcanic processes that create them.

Deposit analysis provides crucial data required to understand the behaviours of PDCs. The key details collected often include; location/distance from the source, largest grain size, sorting, grading and grain type composition and sedimentary structures. Each of these provides insights into different characteristics of the flow through time and space (See chapter 2.1). Grain type and grain size changes vertically through an ignimbrite have been thought to show changing conditions in a current over time, such as a change in the supply of material or a change in the energy a current has (i.e. waxing and waning) (Giannetti & De Casa, 2000; Branney & Kokelaar, 2002; Brown & Branney, 2004a; Brown et al., 2007; Smith & Kokelaar, 2013). This grading is often observed in field deposits, and so understanding the flow behaviours that lead to graded deposits is crucial for interpreting field deposits.

Experimental modelling uses controlled and safe conditions to investigate specific changes to current conditions allowing volcanologists to explore the effects on flow and depositional behaviour. Understanding how PDCs move is critical in planning for future eruptions with evacuation plans, hazard maps etc.

1.1. Aim and objectives

This project aims to investigate sorting behaviours of polydisperse granular currents to better understand reverse grading in ignimbrites and associated PDC dynamics. This aim will be met through the following objectives:

1. To quantify the characteristics of reversely graded ignimbrites
2. To investigate sorting behaviours that occur in a static system
 - How do different-sized particles of the same density sort in a static system?
 - How do different-sized particles of different densities sort in a static system?
3. To investigate behaviours responsible for reverse grading in a polydisperse fluidised granular current

- How do different-sized particles of the same density sort in a gas fluidised system?
- How do different-sized particles of different densities sort in a gas-fluidised system?

2. Literature review

Pyroclastic density currents are one of the deadliest volcanic phenomena (Auken et al., 2013; Brown et al., 2017) and, as such, they are rarely observed up close. The best tool for investigating PDCs is the deposits known as ignimbrites. Ignimbrites provide volcanologists with a detailed account of current behaviour over time and space.

Through interpretation and analogue modelling of ignimbrites along with eyewitness accounts and video footage, PDCs can be split into 3 distinct regions: head, body, and tail. The head is at the front of the current where air ingestion allows for fluidisation and turbulent flow, followed by the body making up the bulk of the current where most segregation of material occurs. Bringing up the rear is the tail of the current which is the slowest part, lagging behind the rest of it (Wilson & Walker, 1982).

2.1. Deposit Characteristics

The deposits of PDCs can be categorized according to sedimentary structure and lithology. Two categories that have been identified are ignimbrites, and block and ash flow (Branney & Kokelaar, 2002). Ignimbrites are pumice and ash rich with a matrix of vesicle wall-type shards and crystal fragments usually in a poorly sorted mixture as one end member, ranging to an end member lithofacies with somewhat better sorting and stratification. Block and ash flows however are a mixture of juvenile lava blocks with predominantly non-pumiceous ash of similar composition (Branney & Kokelaar, 2002). Most ignimbrites are relatively poorly sorted, typically containing a continuous range of grain sizes from many centimetres down to a few microns (Sparks, 1976).

2.2. Granular material

Pyroclastic density currents are an example of a granular material flow. Granular material is a collection of many discrete solid particles with interstices filled with fluid or gas making these currents a multiphase process (Campbell, 1990). These currents show a distinct behaviour that manifests itself as that of solids liquids or gases, for example, powders pack like a solid but can flow like a liquid (Pudasaini & Hutter, 2007). In granular flows where the particles are closely packed or the material is denser than the interstitial fluid the particles alone will play the greatest role in momentum and transport (Campbell, 1990). Due to this behaviour PDCs exhibit many interesting properties in their flows which are recorded in the deposit. Examples of this are segregation, normal and inverse grading, and the Muesli effect/ Brazil Nut Effect (BNE).

The internal transport rates of mass, momentum and energy are governed by granular temperature (Campbell, 1990). Instead of moving in many-particle blocks, every particle in the granular mass is moving independently. In the rapid-flow regime, the velocity of each particle may be decomposed into a sum of the mean velocity of the bulk material and a component to describe the random motion of the particle relative to the mean. The analogy between the random motion of the granular particles and the thermal motion of molecules in the kinetic-theory picture of gases is so strong that the mean-square value of the random velocities is commonly referred to as the "granular temperature". Granular temperature is maintained by external energy components for example gravitational energy acting upon a granular flow or an input of kinetic energy during the shaking of a bag of muesli, without the constant addition of this energy temperature will rapidly dissipate due to inelastic particle collisions (Walton & Braun, 1986; Campbell, 1990).

2.3. Fluidisation

PDCs are multiphase flows consisting of solid particles dispersed in a gas phase where the main components are water vapour and air. Gas fluidisation is held accountable for the mobility and

grading in ignimbrites. The upwards flow of gas exerts a drag force on clasts partially supporting them to make them behave like a fluid (Branney & Kokelaar, 2002). PDCs are never fully fluidised, they can only be semi-fluidised; full fluidisation would separate the small particles away from the current almost completely. The large clasts are supported by other means within the current (Sparks, 1976; Branney & Kokelaar, 2002). Complete fluidisation can only be possible in very fines-rich granular mixtures (Gravina et al., 2004).

The fluid that supports a PDC has multiple sources that are explored in Branney and Kokelaar (2002):

A. Flow fluidisation where gas moves upwards from the substrate into the current at a rate that supports the clasts. This can be created experimentally but real examples are not known. Gas may be locally supplied by surface water, snow, ice, vegetation or degassing substrate but would not be sufficient to support a large current. **B.** Bulk self-fluidisation where clasts are supported through the upward escape of air that is engulfed from the flow front e.g. Walker (1980). This is most effective in short-lived currents, whereas sustained currents, especially those with slow-moving fronts, may not be supported fully by this form of fluidisation. **C.** Grain self-fluidisation involves gas exsolved from pyroclastic material (Sparks, 1978), steam from ice, snow and water and gasses from burning of material entrained in the current (Wilson, 1980; Branney & Kokelaar, 2002). In the head of the current most fluid comes from the surrounding air as the current passes through. **D.** Sedimentation fluidisation is driven by interstitial fluid during hindered settling. **E.** Proximal currents may undergo decompression fluidisation where gas fluxes are produced by rapid decompression of gas either at the base of a tall collapsing fountain or in a lateral blast (Branney & Kokelaar, 2002).

2.4. Grain characteristics

Whilst volcanologists cannot observe the currents up close, they can observe the deposits created by them. Detailed analysis of these deposits has allowed volcanologists to correlate features displayed in the deposit with characteristics shown by the events that produce the PDC. Pyroclastic deposits are composed of pyroclasts. Pyroclasts can have a wide range of sizes ranging from micron to decimetre scale, irrespective of their origin. Fragments greater than 64 mm in diameter are called blocks or bombs, those between 64 mm and 2 mm in diameter are called lapilli, and those less than 2 mm in diameter are called ash. Average lithic fragments have a density of over 2000 kg/m³ depending on their specific rock type, while pumice has a density usually less than 1000 kg/m³ (Cas & Wright, 1987; Choux et al., 2004). Grain size data collected from deposits provides insight into important current characteristics. Changes in grain size within a deposit can tell us about current capacity during flow; during a waxing phase larger clasts may be introduced into a current, however, it may also be indicative of a waning current as when the current loses energy it is no longer able to support larger clasts and will begin to deposit its load (Branney & Kokelaar, 2002).

Detailed recording of grain size and grain type across a deposit (logging) may allow the observer to interpret current conditions. Grain size data is also used to infer source parameters such as eruption column height, eruption rate and volume (Burden et al., 2011; Bonadonna et al., 2013; Buckland et al., 2021). In addition to current characteristics, grain size data can provide information on the sorting and grading of clasts, which can reveal depositional behaviours exhibited by PDCs. Vertical grain size changes within a deposit can be used to interpret changing conditions during the flow such as waxing and waning of a current or source dynamics over time ('unsteadiness' through time; Branney and Kokelaar, 2002). Lateral changes reflect non-uniformity (Branney and Kokelaar, 2002) in space, including current capacity over time through maximum distances of clast size and type.

Grain size distribution can be used to give a more detailed analysis of the sorting mechanisms within currents, by analysing sorting patterns within a deposit. Analogue modelling can be used to create

currents and interpret what conditions are needed to produce them (Rowley et al., 2014; Smith et al., 2018; Smith et al., 2020). By understanding these conditions, we can more accurately model PDCs which in turn will assist in creating hazard mitigation strategies for people in volcanic regions.

2.5. Deposit analysis methods

2.5.1. Sieving

Traditionally, in field deposits, inverse grading is often described qualitatively based on the investigator's observations, characterising reverse graded deposits based on appearance and estimating the composition of ash pumice and lithic clast. They are often investigated quantitatively by sieving or collecting measurements of sampled clast, which will confirm the composition of outcrops and are rarely used to investigate grading (Walker, 1980; Shultz, 1984; Giannetti & De Casa, 2000). Sampling and sieving techniques are used to quantify the grain size distribution of pumice, lithics and ash in ignimbrite lithofacies (Sparks, 1973; Sparks, 1976; Walker, 1980). This requires excavating a representative sample from the lithofacies and sieving the materials which can be done in the field or a laboratory setting. Obtaining a grain size distribution from sieving usually involves separating a sample using sieves and weighing the material collected from each size range. The largest clasts from outcrops are usually measured in the field, as they may be too large for transport.

The sampling method allows for the analysis of large amounts of material and (in theory) provides measurements of whole clasts, rather than just the visible area of clasts at the surface. However, sieving ignimbrite facies is not ideal. Deposits must be loose; deposits that are cemented or lithified cannot undergo sieving. Excavating these types of deposits will cause the breakup of clasts, causing data to be inaccurate (Buckland et al., 2021). Even unlithified pumice clasts are prone to breakage both during sampling and during the sieving process, therefore impacting the accuracy of grain size representation. Achieving a representative sample across multiple ignimbrites can require large numbers of samples (Sparks, 1976; Walker, 1980). This level of sampling is destructive to the outcrop and detrimental from a geo-conservation and geo-ethical standpoint. This is particularly an issue for coarse-grained ignimbrites, where collecting a sample representative of all size ranges can result in unfeasibly large volumes (large clasts in PDCs have been known to be several meters in some deposits (Cas & Wright, 1987). Furthermore, whether or not a clast will pass through a given sieve is dependent upon its shape and not necessarily its size; the longest dimension of a particle may have little effect on sieve results (Kwan et al., 1999). For example, if a clast is a rectangular cuboid, and the aperture on the sieve is big enough to fit the smallest side through, then sieving has failed at accurately representing grain size (Fernlund, 1998; Kwan et al., 1999). Perhaps most significantly for this study, separate sampling of the increments required to fully explore changes in grain size up through a cm-scale lithofacies (required for analysis of reverse grading) is not feasible.

2.5.2. Image analysis

An alternative approach is to quantify grain size distribution through image analysis. This involves using specialist software such as JMicrovison (Roduit, 2020) to randomly select and measure (the long axis of) individual pumice and lithic clasts, and identify ash grains, in high-quality images of ignimbrite lithofacies. Although potentially influenced by surface breakage of clasts, and limited by the visible orientation of clasts, this non-destructive technique allows for fast and accurate collection of data that can be done remotely.

Image analysis has previously been used in other disciplines, such as engineering, to study the particle shape of coarse aggregates (Kwan et al., 1999), the grain size distribution of sands (Mertens

& Elsen, 2006) and the effects of particle shape on grain size distributions (Arasan et al., 2011). In geology, it has been used to analyse grain size variations in clastic sediments and particle shapes in volcanic debris (Francus, 1998; Buckland et al., 2021). In volcanology image analysis has been used to derive quantitative data on textural features (Giachetti et al., 2011), grain size and grain shape of volcanic deposits (Capaccioni et al., 1997; Riley et al., 2003; Giachetti et al., 2011; Buckland et al., 2021). These studies focused mainly on the 3D characteristics of grains sampled from deposits that have been imaged in the lab. These methods aim to understand how particle shape impacts terminal velocity and estimation of travel distance within ash (Riley et al., 2003), to gain insights into the shape fabric in pyroclastic rock samples (Capaccioni et al., 1997) and to understand the effects of particle shape on grain size analysis (Buckland et al., 2021). Image analysis has not previously been used to characterise the grain size changes and sorting through a reverse graded deposit.

2.6. Deposit aggradation

The flow boundary zone is the surface between the current and the substrate. During deposition, the flow boundary zone must lie at the top of the aggrading deposit. A clast undergoing deposition must cross this zone. Ignimbrite lithofacies are thought to record the processes and conditions over time in the flow boundary zone (Branney & Kokelaar, 2002). As the flow boundary zone rises from the substrate with the aggrading deposit the current may deposit in a progressive or a stepwise fashion (Branney & Kokelaar, 1992; Branney & Kokelaar, 2002).

Progressive aggradation is defined by the deposit surface rising at a constant rate from the base upwards rather than a plug flow that halts en masse. The sedimentary process within a progressively aggrading deposit will occur irrespective of the concentration and transport mechanism of the overriding current. The rate of deposition varies from slow to rapid depending on the conditions of individual PDCs. A progressively aggrading deposit is assembled through time and cannot be representative of the full vertical structure of a current but the conditions through time at the flow boundary. With a continuous supply of material to the flow boundary, the deposit aggrades. (Branney & Kokelaar, 1992; Branney & Kokelaar, 2002; Sulpizio et al., 2014)

Some ignimbrites show vertical changes in chemical composition, lithic clast types and clast sizes, which are thought to show the changes in material supplied to the flow boundary zone over time (Branney & Kokelaar, 2002).

In small-scale PDCs a proposed model for joining of progressive aggradation and *en-masse* deposition assumes most PDC deposits originate from a stratified current (Branney & Kokelaar, 2002; Sulpizio et al., 2014). Current is thought of as a succession of pulses with varying thicknesses. Each pulse can be considered a flow boundary zone with pulses stopping en masse when the resistant forces exceed the driving forces inducing stepwise aggradation (Sulpizio et al., 2014)

Rheology changes resulting from segregation, loading or fabric development could induce sudden frictional interlocking so that the flow boundary jumps upwards preserving the currents' structure (Branney & Kokelaar, 1992; Branney & Kokelaar, 2002; Sulpizio et al., 2014).

In a stratified current, sorting processes such as kinematic sieving (see chapter 2.6.5.) or dispersive pressure (see chapter 2.6.3.) produce a current where the larger clasts are forced to the top of the current and the smaller clasts occupy the base (Bagnold, 1954; Middleton, 1970; Branney & Kokelaar, 2002). During deposition, the large clasts at the top of the current are not being deposited as they are not in contact with the flow boundary at the base of the current (Branney & Kokelaar, 1997; 2002). At the surface of the substrate or aggrading deposit, only the smaller clast which are at the flow boundary can be deposited. In steady conditions, the small material deposited is

continuously replaced and so maintains the deposition of finer material producing a thick non-graded fine-grained deposit not representative of the whole current (Branney & Kokelaar, 2002). As the deposit surface aggrades the larger clasts that have segregated to the top of the current may overpass depositing further downstream. In these conditions, the deposit will aggrade as a massive fine-grained deposit until a critical point is reached where a rheological change due to grain size changes or loading causes the flow boundary to jump (stepwise aggradation), preserving the current's inverse grading (Branney & Kokelaar, 1992; Branney & Kokelaar, 2002; Douillet et al., 2013).

2.6.1. Reverse grading

Segregation in granular currents occurs when particles with similar properties group together in a current. In a current with particles of varying densities, this way of sorting particles could separate particles by grouping together based on density; for example, denser particles may sink to the base of the current whilst others rise. In a current where the density of particles is similar or equal particles may be sorted by their size; this may be large particles to the base and small particles to the top or inversely, small particles to the base while large particles rise to the top (Hill et al., 1999; Choux & Druitt, 2002; Choux et al., 2004).

Inverse grading is often observed in field studies where the basal portion of a deposit shows clear inverse grading overlain by a layer of massive and/or millimetre scale laminated deposits (Sohn & Chough, 1993; Brown et al., 2007; Trofimovs et al., 2008; Smith & Kokelaar, 2013). This is likely a result of sorting within the current, followed by settling of the finer ash on top from the end stages of the PDC when the large lithics and fragments have been ejected and only the finer ash remains to be ejected. It could also result from general ash fall from the cloud produced during the eruption.

Reversely graded ignimbrite facies have been reported at a variety of field locations (Sohn & Chough, 1993; Brown et al., 2007; Trofimovs et al., 2008; Smith & Kokelaar, 2013), but detailed quantification of the grain size characteristics of these distinct deposits has not previously been attempted.

2.6.2. Reverse grading theories

Particle segregation in granular flows is a phenomenon that occurs in many disciplines from volcanology to sedimentology, and from pharmaceuticals to the food industry (Rosato et al., 1987; Savage & Lun, 1988; Ottino & Khakhar, 2000). It has been studied across this variety of disciplines using experimental approaches such as rotating disk/platforms (Cagnoli, 2005; Schnautz et al., 2005), water-filled lock exchange flume (Choux & Druitt, 2002) and chute flow experiments (Savage & Lun, 1988). Studies focusing on particle segregation often refer to dispersive pressure (Bagnold, 1954) or kinematic sieving (Middleton, 1970) as the mechanism of segregation.

2.6.3. Dispersive pressure

One of the first attempts to explain reverse grading in granular flows was the dispersive pressure suggested by Bagnold (1954). Dispersive pressure describes the dilative strains acting upon grains during grain flow. Dispersive pressure arises in dry, granular-type debris flows because of shear deformations in the granular material, which consists of particles. As the flow shears, collisions between particles produce accelerations of the granular fluid perpendicular to the flow direction. The pressure associated with the dilatative strains (the dispersive pressure) raises the centre of mass

of the flow, changing the normal pressure, and therefore the shear resistance, of the flow on the ground (Bagnold, 1954; Buser & Bartelt, 2011).

Bagnold tested this theory using two experiments. The first experiment (Fig. 2.1) uses spherical grains of paraffin wax and lead stearate with a consistent diameter of 0.132 cm, the same density as the water used, in the annular space between an inner stationary drum and an outer concentric rotating drum. In this experiment uniform shear strain rate and uniform grain dispersion was ensured by using a small ratio of radial difference/mean radius. Dispersive pressure was measured as excess pressure in the annular space and recorded using a manometer over a range of rotating speeds (Bagnold, 1954).

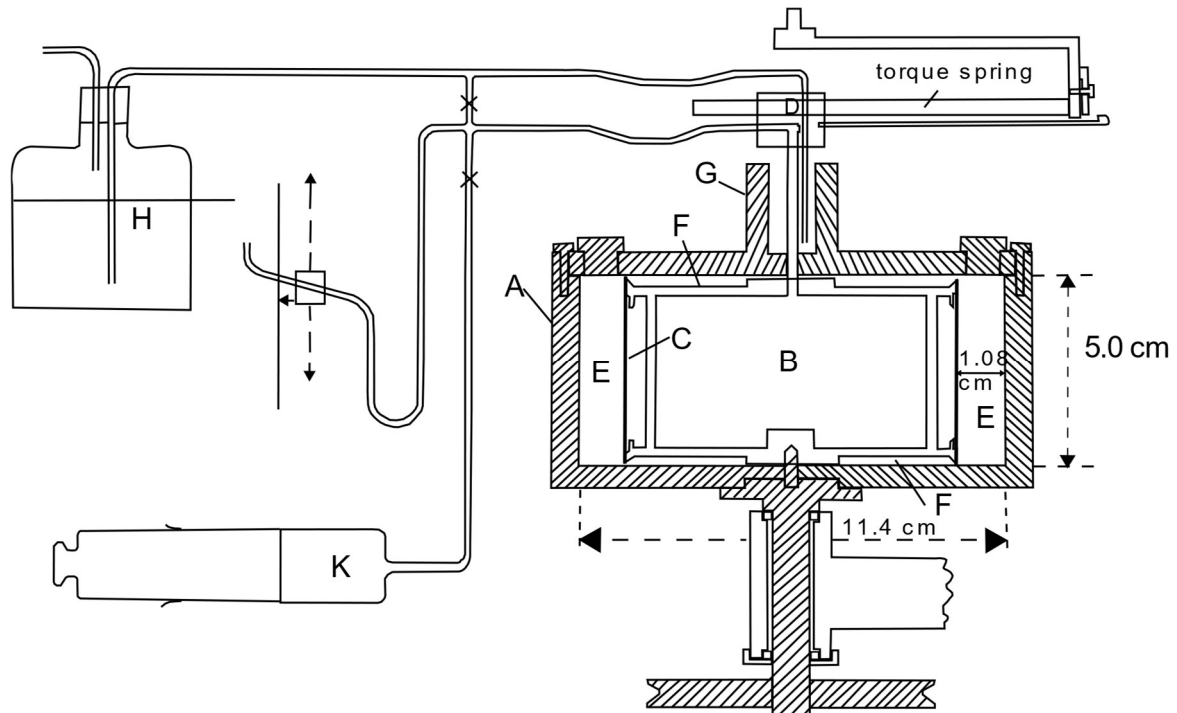


Figure 2.1 The outer drum A, solidly built of Perspex and brass, could be rotated through change-wheels at a series of known speeds ranging from 0-25 to 8-6 rev/sec. The periphery C of the inner drum B, permanently filled with water, consisted of sheet rubber sealed to the drum flanges. Attached to the head D was a calibrated spring for torque measurement. The end-spaces FF, was filled with water up to a convenient level in the open stand-pipe G. This level was reproduced in the wide reservoir H. A pump, K, enabled air bubbles to be driven out of the whole apparatus when needed. (rotating parts shown in hatched) (Bagnold, 1954).

In the second experiment (Fig. 2.2), dry quartz sand with a mean diameter of 0.035 mm is allowed to flow down a simple flume. By raising the reservoir gate, at a given distance a sand flow of any required height could be started and then stopped by closing the gate. The angle of the flume was kept constant at 33° and the distance to the sliding gate was 5ft. The changing variable used was the flow height (Bagnold, 1954).

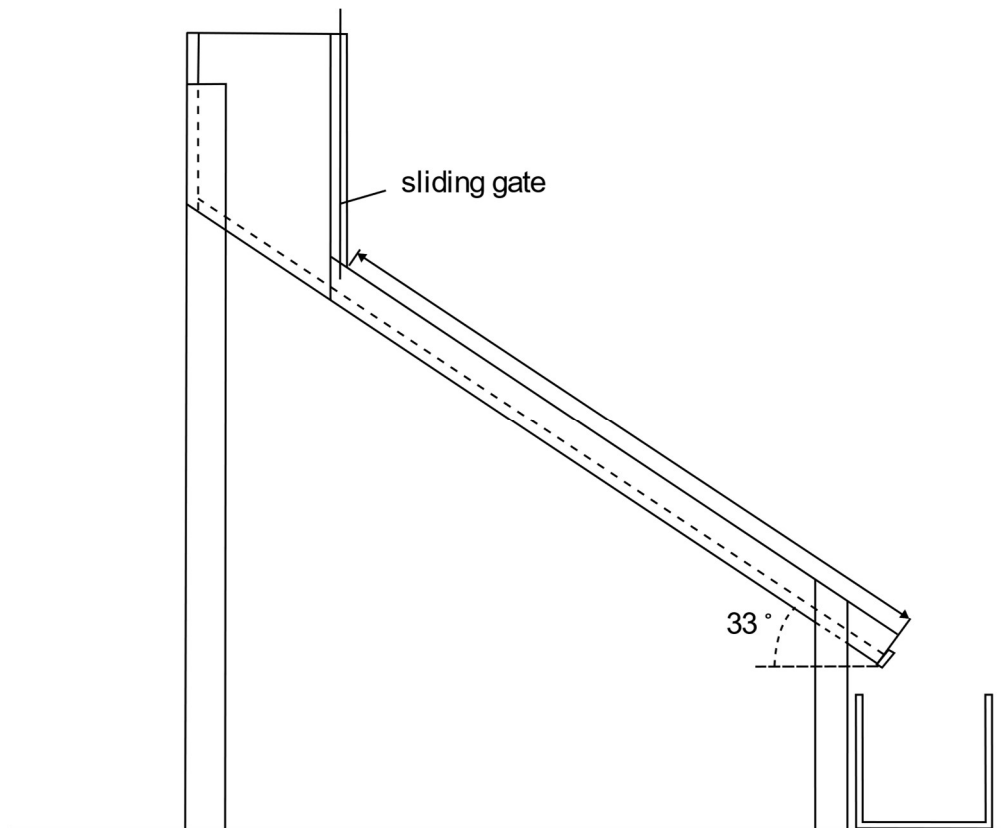


Figure 2.2 Flume used in the second experiment with a length of 5ft and a constant angle of 33°, and a sliding gate that can be opened at various heights to create sand flows of the required heights (Bagnold, 1954).

The dispersive pressure model used an analogue experiment to quantify dispersive pressure acting upon particles and showed experimentally that dispersive pressure (P) can be expressed by

$$P = f(C)\sigma D^2 \left(\frac{dU}{dy}\right)^2$$

where σ is the density of particles, D is their diameter, dU/dy is the velocity gradient or shear strain rate, and $f(C)$ is a positive function of the particle concentration (Bagnold, 1954; Legros, 2002). The findings of Bagnold (1954) show that with increasing grain size the pressure experienced by the particle will also increase the pressure experienced by the grain. With the assumption that pressure is kept constant within the grain flow, something else must be lowered to keep the pressure of the large grain in equilibrium. As such the larger grains will drift towards areas of low shear strain, and the smaller particles to areas of high strain.

This theory assumes that the density of the grains and interstitial fluid is uniform, the dispersion is in a state of uniform shear strain, and that the shear strain and kinetic energy of the system must somehow remain constant (Bagnold, 1954). This realistically cannot be applied to pyroclastic density currents which are known to be dynamic and unsteady with a large range in clast size and density (Sparks, 1976; Cas & Wright, 1987; Druitt, 1998). Legros (2002) shows that particle weight is only overcome by the upward directed dispersive pressure for lighter particles, that the particle must be less dense than the bulk density of the flow to rise and therefore dispersive pressure cannot explain the migration upwards of large dense particles. Thus, there must be an alternative method of particle sorting in a granular flow.

2.6.4. Gravitational settling

Ignimbrites commonly show reverse grading of low-density pumice clasts and normal grading of high-density lithic clasts (Sparks, 1976; Smith & Kokelaar, 2013). Therefore, it seems probable that grading is largely the result of the density contrast of individual fragments within pyroclastic density currents, with the matrix often denser than the large pumice clast (Sparks, 1976). Lithics have a much greater density than the matrix (Cas & Wright, 1987) and it is proposed that the principal mechanism of normal grading is gravitational settling (Sparks, 1976). Sparks (1976) also notes that reverse grading of lithics was seen in thinner deposits and that erosion removes much of the unconsolidated ignimbrites at the top, suggesting large lithic clasts may be lost here possibly skewing the data.

2.6.5. Kinematic sieving

In more recent times, kinematic sieving (Middleton, 1970; Shinbrot & Muzzio, 1998) has become the widely accepted process of creating a reverse graded deposit, sometimes referred to as the Muesli effect or the Brazil-Nut effect (Möbius et al., 2001). Kinematic sieving is explained by small particles percolating through gaps created by the movement of larger particles below that then fill the voids underneath preventing the larger particles from falling back down (Middleton, 1970; Rosato et al., 1987; Shinbrot & Muzzio, 1998; Cagnoli, 2005; Marks et al., 2012; Staron & Phillips, 2015). Bagnold's (1954) results are applicable to a steady, uniform, simple shear flow of neutrally buoyant grains of equal size, which are unrealistic constraints in natural environments. He also neglected random velocity fluctuations of grains (Sohn & Chough, 1993). Alternatively the kinematic sieving gravity-driven process only requires a grain size difference for particle segregation to occur without neglecting the particles density or flow conditions (Sohn & Chough, 1993; Sohn, 1997).

Grain size increase will result in a segregation rate increase (Möbius et al., 2001), and larger grains are subject to greater kinetic energy during the oscillation of beds. The greater activity produced by these larger grains will produce larger gaps for smaller particles to infiltrate and boost the larger grain upwards (Möbius et al., 2001). Furthermore, changes in density in either direction will increase the rate at which a particle is likely to segregate. In the gravity-driven model, a heavier particle should be more likely to fall than a lighter particle of the same size and vice versa due to the gravitational potential acting upon the particle.

In addition to density, the shape will also have an impact on percolation velocities. For spherical particles with uniform density kinematic sorting will likely lead to a deposit where the largest particles are always on top and the smallest particles are always at the base. However with non-uniform shaped particles, this may not always be the case, Fernlund (1998) and Kwan et al. (1999) showed that in a sieve the smallest dimension on a particle will determine its likelihood to pass through. PDCs are known to have particles of varying size and shape (Cas & Wright, 1987) and so it remains possible that during kinematic sieving, as long as a gap is larger than the smallest dimension of a larger particle it may fall through; however, this is reliant on the larger particle being in the correct orientation, and therefore, this will not occur as often as small particles percolating through.

Sohn and Chough (1993) show that the amount and velocity of percolation depends on the total strain, the relative sizes of the small particles to the large particles and the rate of strain. The most important factor in the rate of percolation is the relative size of the diameter of small grains (d_s), to the diameter of large particles (D_l). In materials with a grain size difference of $d_s/D_l \leq 0.25$, percolation occurs instantly. When d_s is similar to D_l the sieving of grains will not take place as easily. However, the mechanism of grain percolation operates with the probability of a hole forming in which a grain can fall into, and the chances of this happening are much greater for smaller particles.

As long as there are grains of different sizes, segregation has the tendency to occur, thus inversely graded deposits can still be produced in even similarly sized particles. (Scott & Bridgwater, 1975; Savage & Lun, 1988; Sohn & Chough, 1993).

2.6.5.1. Kinematic squeezing

Towards the rigid impermeable bed percolation velocities become negative (Savage & Lun, 1988), and thus there must be additional mechanisms of transferring particles between the lower layers. In this lower region of the current, it is suggested that there is a moving layer of highly concentrated bedload material termed a traction carpet, developed beneath and driven by an overlying turbulent current (Sohn, 1997). Traction carpets are split into two regions; the lower frictional region comprised of non-vibrating grains maintaining continuous contact with each other, and the upper collisional zone dominated by particle collisions. In the collisional region percolation of smaller particles is promoted by active grain interactions, (Savage & Lun, 1988; Sohn, 1997). However, within the frictional region, high particle concentration hinders kinematic sieving. Additionally escaping pore fluid may support or elutriate finer particles upwards (Sohn, 1997).

The term 'squeeze expulsion' or 'kinematic squeezing' refers to the squeezing of larger particles upwards from the frictional zone at the base of a current (Savage & Lun, 1988; Sohn, 1997; Branney & Kokelaar, 2002; Le Roux, 2003) (Fig. 2.3). It is possible that through squeeze expulsion, upwards movement of large particles may occur. This is not as common as percolation and grain segregation in the lower region of the traction carpet is hindered by the minimal movement of particles (Savage & Lun, 1988; Sohn, 1997).

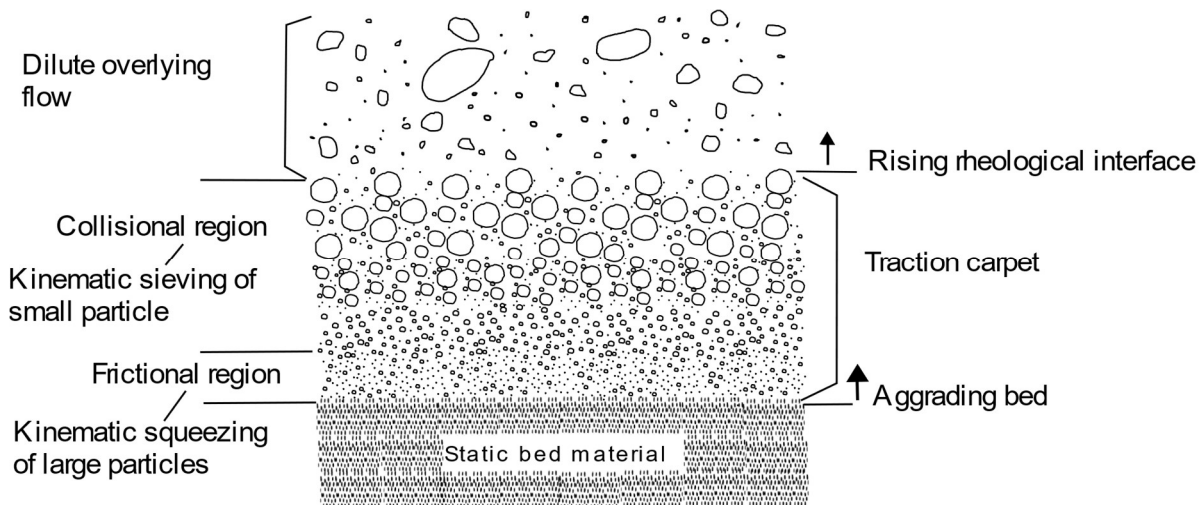


Figure 2.3 Deposition in a traction carpet via gradual aggradation (Sohn, 1997)

Pyroclastic density currents are examples of a polydisperse granular current, with a range of particle sizes from ash under 2 mm, lapilli between 2 and 64 mm, and blocks or bombs over 64 mm (Cas & Wright, 1987). They can often contain a wide range of densities, with pumices usually around 1 g/cm³ or less and lithics up to 3 g/cm³ (Cas & Wright, 1987; Choux et al., 2004). As a result, the experiments that model pyroclastic density currents should reflect this to make the results as comparable to real-world PDCs as possible e.g. Savage and Lun (1988); Choux and Druitt (2002). For instant segregation the d_s/D_l value must be less than 0.25 (Sohn & Chough, 1993). Using this ratio a 2 mm clast will segregate instantly from any clast over 8 mm, whilst an 8 mm clast will segregate instantly from any clast over 32 mm. These examples cover only a small range of grain sizes seen in currents which range from a few micrometres to several meters (Cas & Wright, 1987) giving a high probability of particle segregation in a pyroclastic density current.

2.7. Modelling

Investigation of grain size sorting has often been the subject of granular material studies (Bagnold, 1954; Hand, 1997; Möbius et al., 2001; Choux & Druitt, 2002; Choux et al., 2004). A variety of techniques has been used in previous studies to model granular currents including unfluidized 'dry' currents (Bagnold, 1954; Savage & Lun, 1988), static experiments using shaking or rotating of granular material (Cagnoli, 2005; Schnautz et al., 2005), and using fluidisation (Choux & Druitt, 2002).

Static experiments involve vibrating beds with large 'intruder' particles with varying densities and observing their movement relative to the fine matrix (Shinbrot & Muzzio, 1998; Cagnoli, 2005). These experiments set out to investigate the "Brazil-nut or Muesli effect" during which they recorded that large particles introduced into a finer matrix, termed 'intruder' particles, would rise to the top of the bed as expected. According to the muesli effect, coarse light particles should rise to the top of an intermediate matrix and dense particles should sink due to the increased gravitational potential acting upon them. However, it was observed that coarse dense particles also rose to the top of the beds. Observations of high-speed video footage would conclude that during oscillation of the bed, greater inertia experienced by heavier grains causes them to lift off the bed allowing for smaller particles to infiltrate the gaps underneath preventing backtracking. This inertia model would allow for dense clasts to rise along with the lighter clasts above the fine matrix (Shinbrot & Muzzio, 1998; Cagnoli, 2005).

Dry flume experiments are completed by allowing granular material to flow down an inclined plane to investigate the current behaviours exhibited, and the behaviours of different sized clasts such as grading and runout distances (Bagnold, 1954; Bartali et al., 2020).

More recently gas fluidisation has been used to model PDCs in flumes (Rowley et al., 2014; Smith et al., 2018; Smith et al., 2020). In this gas fluidisation method, long-lived high pore pressure can be simulated through continuous gas fluidisation (Rowley et al., 2014). Fluidisation is achieved by injecting gas vertically into a granular bed, creating a condition whereby the drag exerted by the gas counterbalances the weight of the particles, at which point intergranular friction is lost and the bed behaves in a liquid-like manner (Gilbertson et al., 2008; Rowley et al., 2014). The velocity at which this occurs is termed the minimum fluidization (U_{mf}) velocity. When the gas flux through the sediment is less than the U_{mf} the sediment is partially fluidized and termed aerated (Smith et al., 2018). Volcanic ash that forms the matrix of many ignimbrites belongs to Group A of Geldart's Classification (Geldart, 1973), where it expands homogeneously when fluidized at gas velocities above U_{mf} until gas bubbles form. The gas velocity at which bubbles form is shown as U_{mb} . Previous works using gas fluidisation have used glass ballotini beads measuring $\sim 63 \mu\text{m}$ (Smith et al., 2018; Smith et al., 2020) and $75 \pm 15 \mu\text{m}$ (Rowley et al., 2014). In these previous experiments data was collected on current behaviour, depositional behaviour, and the effect of variable aeration. There is yet to be sufficient data collected on the depositional behaviour of polydisperse sediments and on reverse grading within deposits.

2.7.1. Bedforms

Bedforms record the conditions of a current at the time of deposition. Examination of bedforms in areas of reverse grading will provide a critical insight into the conditions needed to create inversely graded deposits.

Bedforms related to PDCs can be described as massive, planar, shallow, and steep backset (Smith et al., 2020). Massive beds are beds that remain constant throughout, planar beds are described as having angles of $<2^\circ$ relative to the substrate, shallow backsets can be defined by a low angle of repose ($<\theta_{dyn}$), and steep backsets are defined as having a high angle of repose ($>\theta_{dyn}$) (Smith et al., 2020). Backset beds are examples of regressive bedforms; regressive bedforms have often been observed in the field (Douillet et al., 2013; Douillet et al., 2019) and have sometimes been reported to have reverse grading (Brown & Branney, 2004a). Regressive bedforms are aggrading structures that have upstream migration of the crest due to rapid deposition (Cas & Wright, 1987; Douillet et al., 2013; Douillet et al., 2019).

Each of these bedforms represents a change in conditions in the current. Massive beds remain constant throughout and are interpreted to represent steady conditions within a current (Branney & Kokelaar, 1992; Branney & Kokelaar, 2002). Planar beds are typically among the first to be deposited in thick high velocity currents with high Froude numbers (Fr 3-5) and low friction (Smith et al., 2020). As a current's velocity decreases and friction increases, regressive bedforms will begin to deposit. Experimental analysis from Smith et al. (2020) shows that shallow backsets form at Froude numbers of Fr 2-3, and steep backsets at Fr 0.59-2.

3. Quantifying reverse grading in ignimbrites with image analysis

3.1 Introduction

Reversely graded ignimbrite facies have been reported at a variety of field locations (Sohn & Chough, 1993; Brown et al., 2007; Trofimovs et al., 2008; Smith & Kokelaar, 2013), but detailed quantification of the grain size characteristics of these distinct deposits has not previously been attempted.

Traditionally, sampling and sieving techniques have been used to quantify the grain size distribution of pumice, lithics and ash in ignimbrite lithofacies (Sparks, 1973; Sparks, 1976; Walker, 1980). This requires excavating a representative sample from the lithofacies and sieving the materials which can be done in the field or in a laboratory setting. Obtaining a grain size distribution from sieving usually involves separating a sample using sieves and weighing the material collected from each size range. The largest clasts from outcrops are usually measured in the field, as they may be too large for transport.

Sieving allows for the analysis of large amounts of material and (in theory) provides measurements of whole clasts, rather than just the visible area of clasts at the surface. However, sieving ignimbrite facies is not ideal. This level of sampling is destructive to the outcrop and detrimental from a geoconservation and geoethical standpoint. Perhaps most significantly for this study, separate sampling of the increments required to fully explore changes in grain size up through a cm-scale lithofacies (required for analysis of reverse grading) is not feasible. See chapter 2.5.1. for more information

An alternative approach is to quantify grain size distribution through image analysis. This involves using specialist software such as JMicrovison (Roduit, 2020) to randomly select and measure (the long axis of) individual pumice and lithic clasts, and identify ash grains, in high-quality images of ignimbrite lithofacies. Although potentially influenced by surface breakage of clasts, and limited by the visible orientation of clasts, this non-destructive technique allows for fast and accurate collection of data that can be done remotely.

Image analysis has previously been used in other disciplines, such as engineering, to study particle shape of coarse aggregates (Kwan et al., 1999), the grain size distribution of sands (Mertens & Elsen, 2006), and effects of particle shape on grain size distributions (Arasan et al., 2011). In geology, it has been used to analyse grain size variations in clastic sediments and particle shapes in volcanic debris (Francus, 1998; Buckland et al., 2021). In volcanology image analysis has been used to derive quantitative data on textural features (Giachetti et al., 2011), grain size and grain shape of volcanic deposits (Capaccioni et al., 1997; Riley et al., 2003; Giachetti et al., 2011; Buckland et al., 2021). These studies focused mainly on the 3D characteristics of grains in samples collected from field deposits and photographed in laboratories. Using methods that aim to understand how particle shape impacts terminal velocity and estimation of travel distance within ash (Riley et al., 2003), to gain insights into the shape fabric in pyroclastic rock samples (Capaccioni et al., 1997) and to understand the effects of particle shape on grain size analysis (Buckland et al., 2021). Image analysis has not previously been used to characterise the grain size changes and sorting through a reverse graded deposit.

Grain size data collected from deposits provides insight into important flow characteristics. Changes in grain size within a deposit can tell us about current capacity during flow. During a waxing phase larger clasts may be introduced into a current, however, they may also be indicative of a waning current as the current loses energy it is no longer able to support larger clasts and will begin to

deposit its load (Branney & Kokelaar, 2002). Detailed recording of grain size and grain type across a deposit (logging) may allow the observer to interpret flow conditions. Grain size data is also used to infer source parameters such as eruption column height, eruption rate and volume (Burden et al., 2011; Bonadonna et al., 2013; Buckland et al., 2021). In addition to flow characteristics, grain size data can provide information on sorting and grading of clasts, which can reveal depositional behaviours exhibited by PDCs. Vertical grain size changes within a deposit can be used to interpret changing conditions during the flow such as waxing and waning of a current or source dynamics over time ('unsteadiness' through time, Branney and Kokelaar, 2002). Lateral changes reflect non-uniformity (Branney and Kokelaar, 2002) in space and time, including maximum travel distances of clast sizes which can be used to inform us of current capacity and eruption strength.

Grain size distribution can be used to give a more detailed analysis on the current behaviour of different grain sizes within currents, by analysing sorting patterns within an ignimbrite, and then using modelling techniques to recreate these deposits. Analogue modelling can be used to create currents and interpret what conditions are needed to produce a variety of deposits (Rowley et al., 2014; Smith et al., 2018; Smith et al., 2020). By understanding these conditions, we are able to more accurately model PDCs which in turn will assist in creating hazard mitigation strategies for people in volcanic regions.

Volcanologists often provide descriptions of ignimbrites based on qualitative descriptions collected in the field. These qualitative descriptions consist of stratigraphic logs and sketches, which are used to record detailed accounts of key features based on observations. In these observations, volcanologists may record the largest clast sizes and different clast types, and provide estimations and interpretations of the outcrop. The image analysis technique allows us to quantitatively check whether these estimations are correct.

3.1.1 Aims

This section of the thesis aims to use image analysis to quantify the characteristics of reverse grading in ignimbrites. This data will allow for an improved, quantitative understanding of these stratigraphic structures, and will also be used to compare against the quantitative bedform data generated in the laboratory experiments (Chapter 5) for a fuller understanding of how representative the experiments are.

3.1.2 Objectives

The aim of this chapter will be achieved through the following three objectives:

1. To examine how clast size and sorting changes up through reverse-graded ignimbrite facies.
2. To assess the effectiveness of image analysis as a non-destructive method of collecting quantitative data from volcanic outcrops.

3.2 Methods

Using JMicrovison, an image analysis software, data on grain size distribution, largest clast size and sorting will be collected for six ignimbrites to quantitatively characterise reverse graded facies.

3.2.1 Image selection

Images were selected based on meeting the following criteria: (1) must show reverse grading in an ignimbrite; (2) must have a clearly defined scale and (3) must be a high enough resolution to accurately measure clast size down to 2 mm (to allow identification of ash). To make the

measurements as accurate as possible on smaller clasts a minimum resolution of 3 pixels is required on the edge of a clast to accurately measure its boundaries (Lindqvist & Åkesson, 2001) . In addition to these properties, a general description of the image was also required, including location, field observations and field interpretation of the deposit.

3.2.2 Image Analysis

In each image, reverse-graded ignimbrite packages were delineated into 5 horizontal sections of equal thickness. The marked-up image is then uploaded to image analysis software JMicrovison (Roduit, 2020). Using the area editor tool, the 5 sections are mapped out and named i, ii, iii, iv and v, where i is the lowest subsection and v is the highest section. For example, package A1 would be marked as A1i, A1ii etc. By separating the package into 5 subsections, grain size changes can be tracked upwards through the package allowing for a detailed analysis of the reverse grading.

Using the scale on the photo, the software is calibrated. Measurements are accurate to 0.1 mm. The point counter tool allows for the selection of clasts at random within the defined areas. Each time the tool lands on a different clast the long axis is measured using the 1D measurement tool and the type of clast is recorded. This is repeated 50 times for each of the 5 subdivisions. Following this, to investigate how outliers are impacting the results, the 10 largest pumice clasts and the 10 largest lithic clasts (selected by eye) in each subdivision were measured. An average of the 10 largest clast measurements results was calculated to observe any trends up the stratigraphy.

3.2.3 Data Analysis

Each clast measurement taken in the JMicrovison software is recorded in Microsoft Excel, along with a clast number and a clast type (pumice, lithic or ash), identification of clast type was completed by analysing the texture of a clast in higher resolution photos. Along with identifying the predominant colour of the pumices within each image, when the definition on the clast was low colour could be used to assist in identification. Everything below 2 mm was labelled ash. Each package subdivision is sorted into grain size fraction bins (based on the phi scale, Table 1) using the histogram function to allow grain size distribution to be analysed. Data collected for analysis is available in Appendix I.

Table 3.1 Bins used to analyse data in Excel along with conversions from mm to phi and microns.

microns	mm	phi
1000	1	>0
2000	2	-1
4000	4	-2
8000	8	-3
16000	16	-4
32000	32	-5
64000	64	-6
128000	128	-7
256000	256	-8

Gradistat, a particle size analysis programme for unconsolidated sediments (Blott & Pye, 2001), is used to quantitatively analyse the sorting patterns exhibited in the deposits (Table 3.2). By inputting

the grain sizes and their frequencies into the programme, the logarithmic method of moments for sorting (σ_ϕ) is calculated using the following equations:

Mean
$$\bar{x}_\phi = \frac{\sum f m_\phi}{100}$$

Standard deviation
$$\sigma_\phi = \sqrt{\frac{\sum f (m_\phi - \bar{x}_\phi)^2}{100}}$$

Table 3.2 Sorting value parameters used by the Gradistat for the logarithmic method of moments (Blott & Pye, 2001)

Sorting (σ_ϕ)	
Very well sorted	<0.35
Well sorted	0.35-0.50
Moderately well sorted	0.50-0.70
Moderately sorted	0.70-1.00
Poorly sorted	1.00-2.00
Very poorly sorted	2.00-4.00
Extremely poorly sorted	>4.00

3.3 Images used for analysis

This study utilised 6 high-resolution images of reverse graded ignimbrite deposits with various grain sizes, ranging from deposits containing fine lapilli to deposits containing coarse lapilli and blocks. These images were chosen based on their resolution, and clear presence of reverse grading. Additionally, each image displayed different characteristics including grain size and grain type; i.e., some were predominantly pumice and ash and some showed increased lithic composition.

In some images the deposits are not uniform; they may thin out or thicken in some areas, and some may be eroded on the sides or due to the positioning of the deposit and the camera may not be able to show the deposit fully across the photograph. In such cases the linework that divides the deposits into subsections accounts for the differences in height across the deposit making them sub-parallel, this is to ensure that each subsection is equal in area.

3.3.1 Packages 1 and 2

In proximal exposures of the 273 ka Poris Formation at the Diego Hernandez wall of Las Canadas Caldera, Tenerife, ignimbrite packages containing reversely graded pumices with weak normal grading of lithics are observed within the lower part of the succession (Smith & Kokelaar, 2013). Two packages were chosen for analysis (named 1 and 2). Both packages 1 and 2 show a complete reverse graded sequence; each package is marked by a sharp contact between the lighter (pumice clast-rich) top and the darker (finer-grained) base. Note that the apparent curvature of the packages (due to

outcrop form and photo angle) is accounted for by the subdivisions being drafted parallel to these contacts.

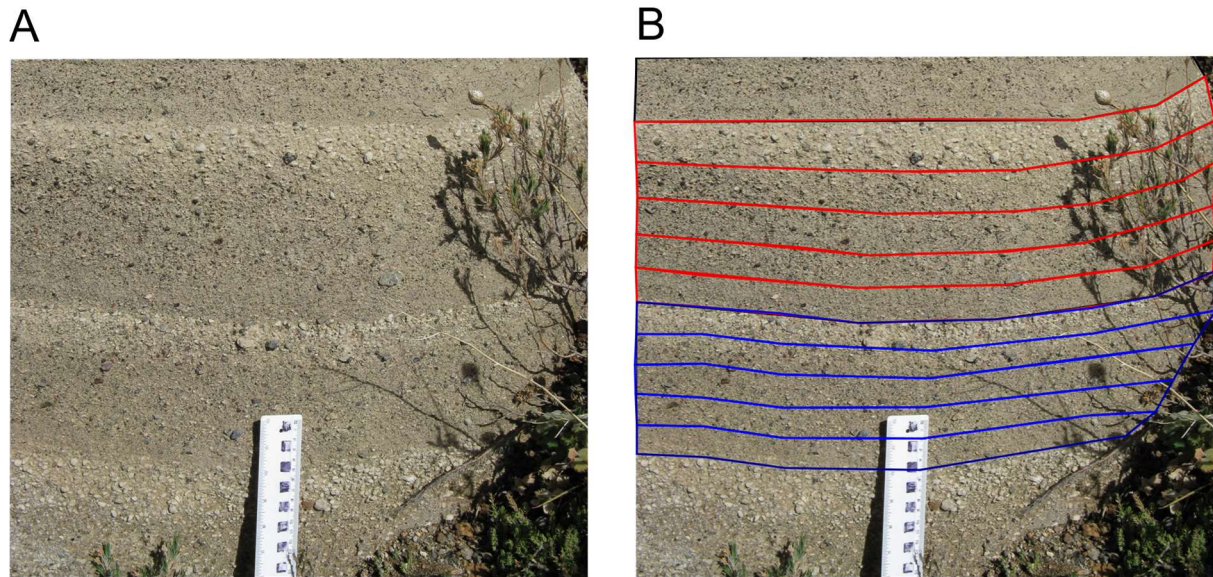


Figure 3.1 Packages 1 (blue) and 2 (red), showing reversely graded ignimbrite in the Poris Formation, Tenerife (A) and marked up for analysis (B). Note that this image contains two packages for analysis (1i, 1ii, iii, iv, Av and 2i, 2ii, iii, iv, Av). Photo courtesy of N. Dowey.

3.3.2 Package 3

Reverse graded pumice rich deposit originally interpreted as showing reversely graded pumices and normal grading of lithics, the resolution on this image was slightly lower than the previous image, although ash was still identifiable and clasts down to 2 mm were still able to be accurately measured. The top of the deposit for package 3 is not seen within this image; however, the remainder of the deposit still shows grading, coarsening upwards from the base.

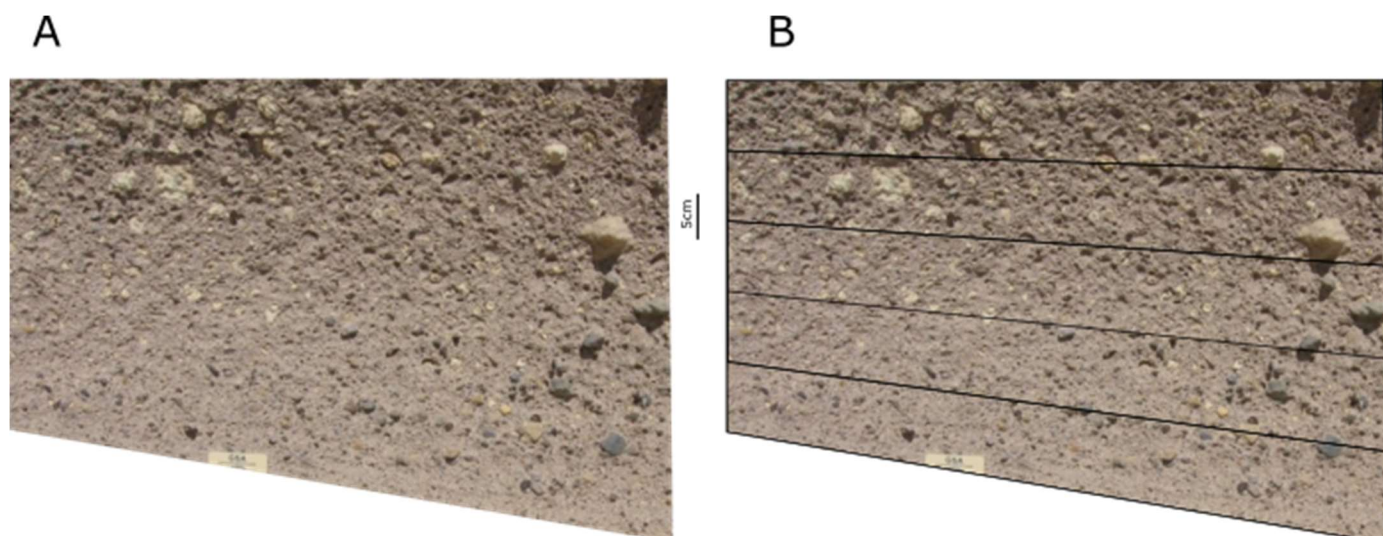


Figure 3.2 Package 3, ignimbrite from Bandas Del Sur, Tenerife, (left) and marked up for analysis (3i, 3ii, etc) (right) Resolution = 923x692 (± 1.25 mm). Photos courtesy of Rebecca Williams.

3.3.3 Package 4

This package shows very fine-grained lapilli and ash at the base grading up into coarse lapilli. The top of this package cannot be seen in the photo. The uneven linework on the photograph is due to the deposit being thicker on the right-hand side than on the left; the linework accounts for this to ensure all subsections are equal.

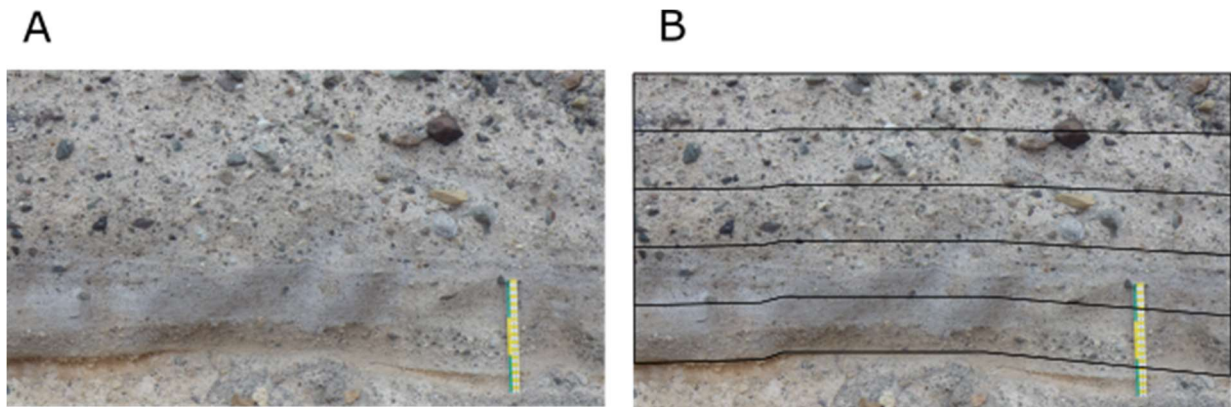


Figure 3.3 Package 4 ignimbrite located in Bandas Del Sur, Tenerife (left). Same image, but with linework added to map packages into five sections of equal thickness (right). Resolution = 4608x2592 (± 0.33 mm). Photo courtesy of Rich Brown.

3.3.4 Package 5

Package showing a full reverse graded sequence, grading from fine lapilli and ash at the base to very coarse lapilli at the top. This deposit was formed on an uneven surface and is marked at the top by an erosional contact. The image was cropped to remove the unnecessary packages above and below. The uneven nature of this package requires the linework to be kinked in the centre to keep each subsection's area as equal as possible.

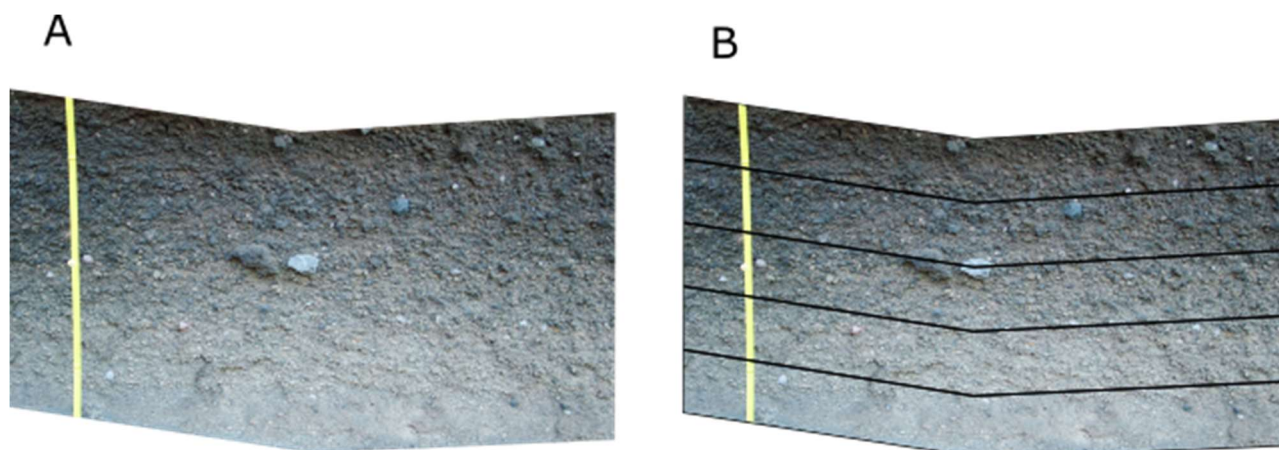


Figure 3.4 Package 5 reversely graded ignimbrite located in Bandas Del Sur, Tenerife (left). Same image, but with linework added to map packages into five sections of equal thickness (right). Resolution = 2848x2316 (± 0.47 mm). Photo courtesy of Rich Brown.

3.3.5 Package 6

Package with a wide range of grain sizes ranging from ash (under 2 mm) to blocks (over 64 mm). The base of this package is curved, and the top cannot be seen in the image. The visible deposit remains clearly reverse graded and thus remains a useful deposit to examine.

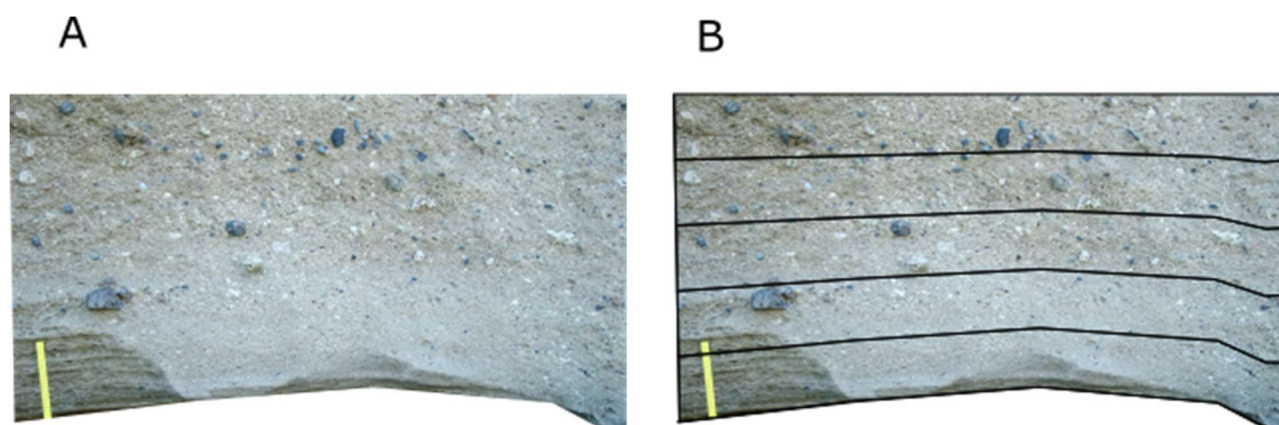


Figure 3.5 Package 6 ignimbrite from Bandas Del Sur, Tenerife (left). Same image, but with linework added to map packages into five sections of equal thickness (right). Resolution = 2848x2316 (± 0.90 mm). Photo courtesy of Rich Brown.

3.4 Results

Data from ignimbrites collected through image analysis allows for a detailed quantitative analysis of vertical changes in grain size through reverse graded packages, providing a greater insight into how

reverse grading can be characterised within real-world ignimbrites. Variation within the composition and grain size of these deposits allows for a better comparison with deposits that will be created using laboratory experiments.

3.4.1 Package 1

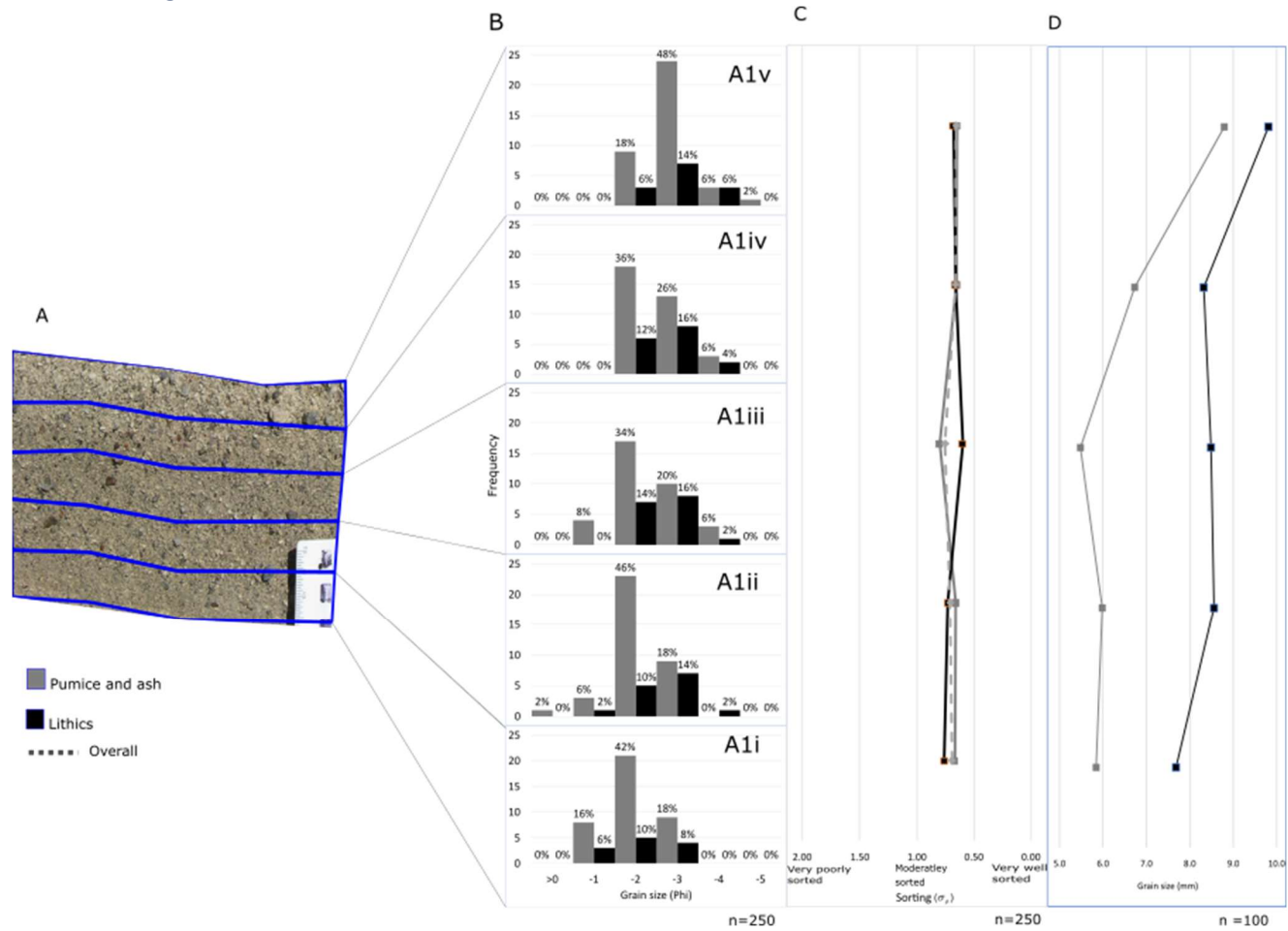


Figure 3.6 (a) Lithofacies package 1 with five equal subsections (2.7 cm tall) marked in red, accompanied by (b) grain size distribution charts for each subsection (1i, 1ii, 1iii, 1iv and 1v). (c) sorting values calculated using Gradistat within each subsection of package 1. (d) Mean average grain size of the 10 largest (qualitatively selected) pumice and lithic clasts.

3.4.2 Package 2

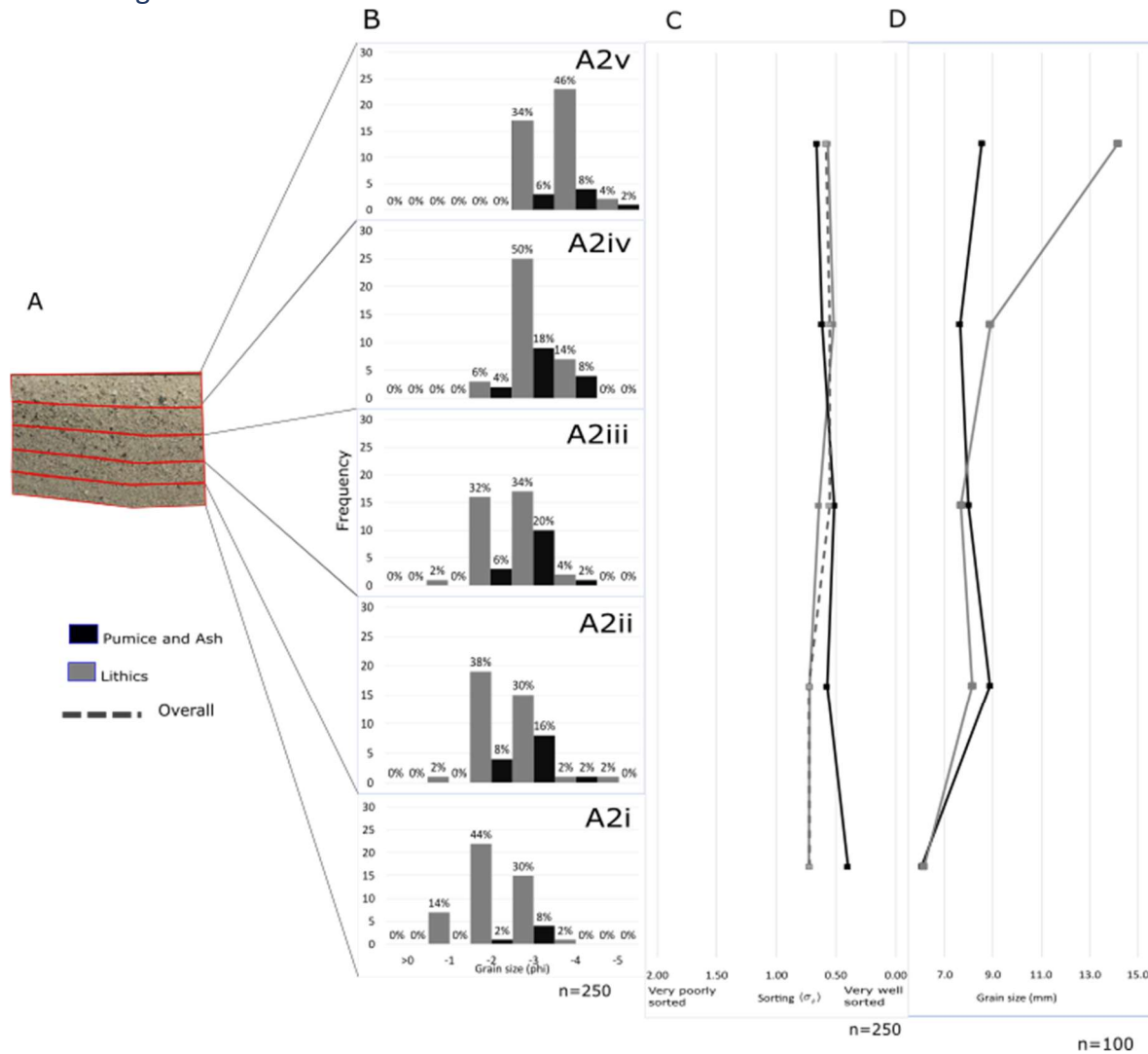


Figure 3.7 (a) Lithofacies package 2 with five equal subsections (3.4 cm tall) marked in red, accompanied by (b) grain size distribution charts for each subsection (2i, 2ii, 2iii, 2iv and 2v). (c) sorting values calculated using Gradistat within each subsection of package 2, (d) Mean average grain size of the 10 largest (qualitatively selected) pumice and lithic clasts.

3.4.3 Package 3

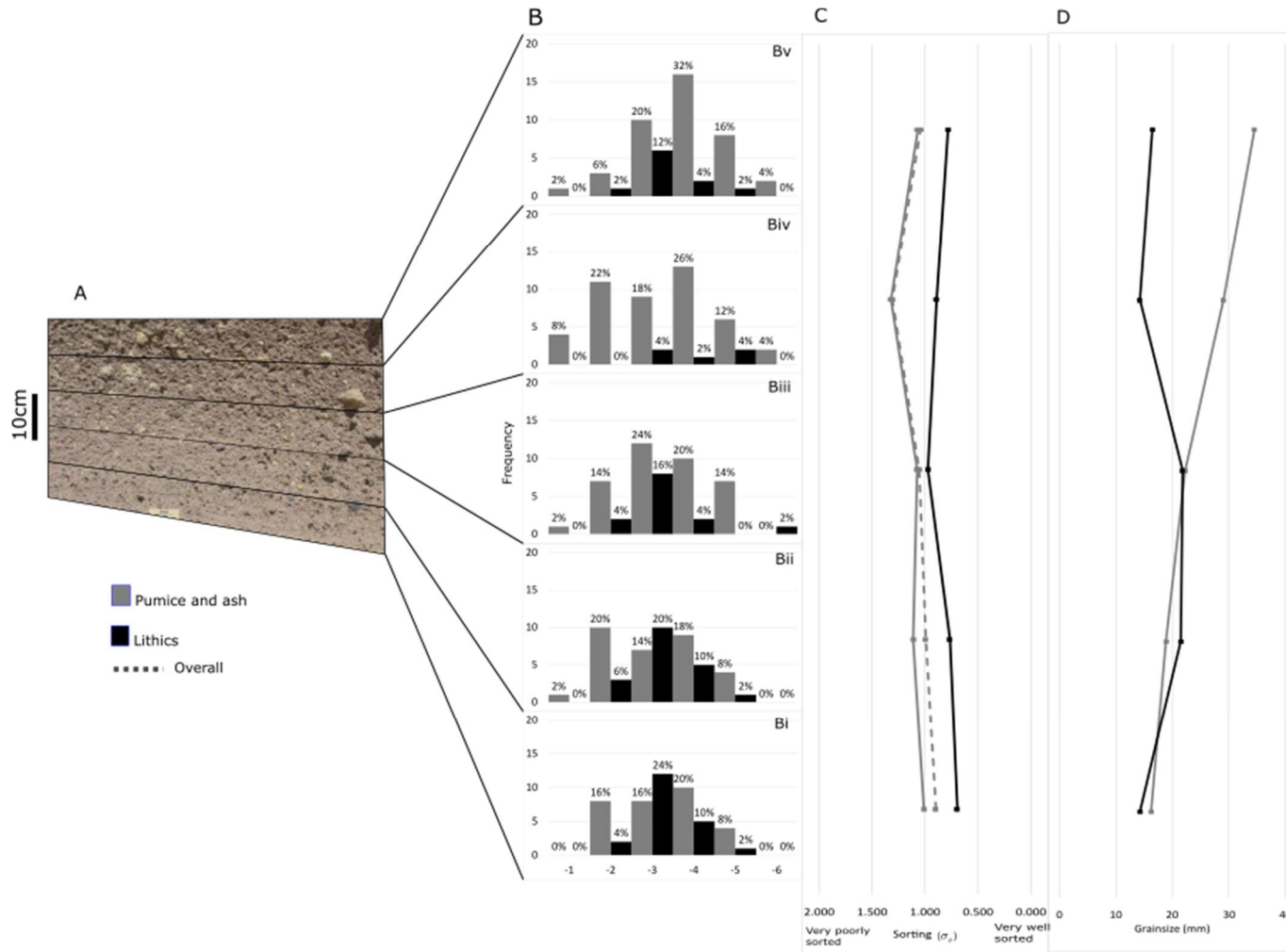


Figure 3.8 (a) Lithofacies package 3 with five equal subsections marked in Black, accompanied by (b) grain size distribution charts for each subsection (3i, 3ii, 3iii, 3iv and 3v). (c) sorting values calculated using Gradistat within each subsection of package 3, (d) Mean average grain size of the 10 largest (qualitatively selected) pumice and lithic clasts.

3.4.4 Package 4

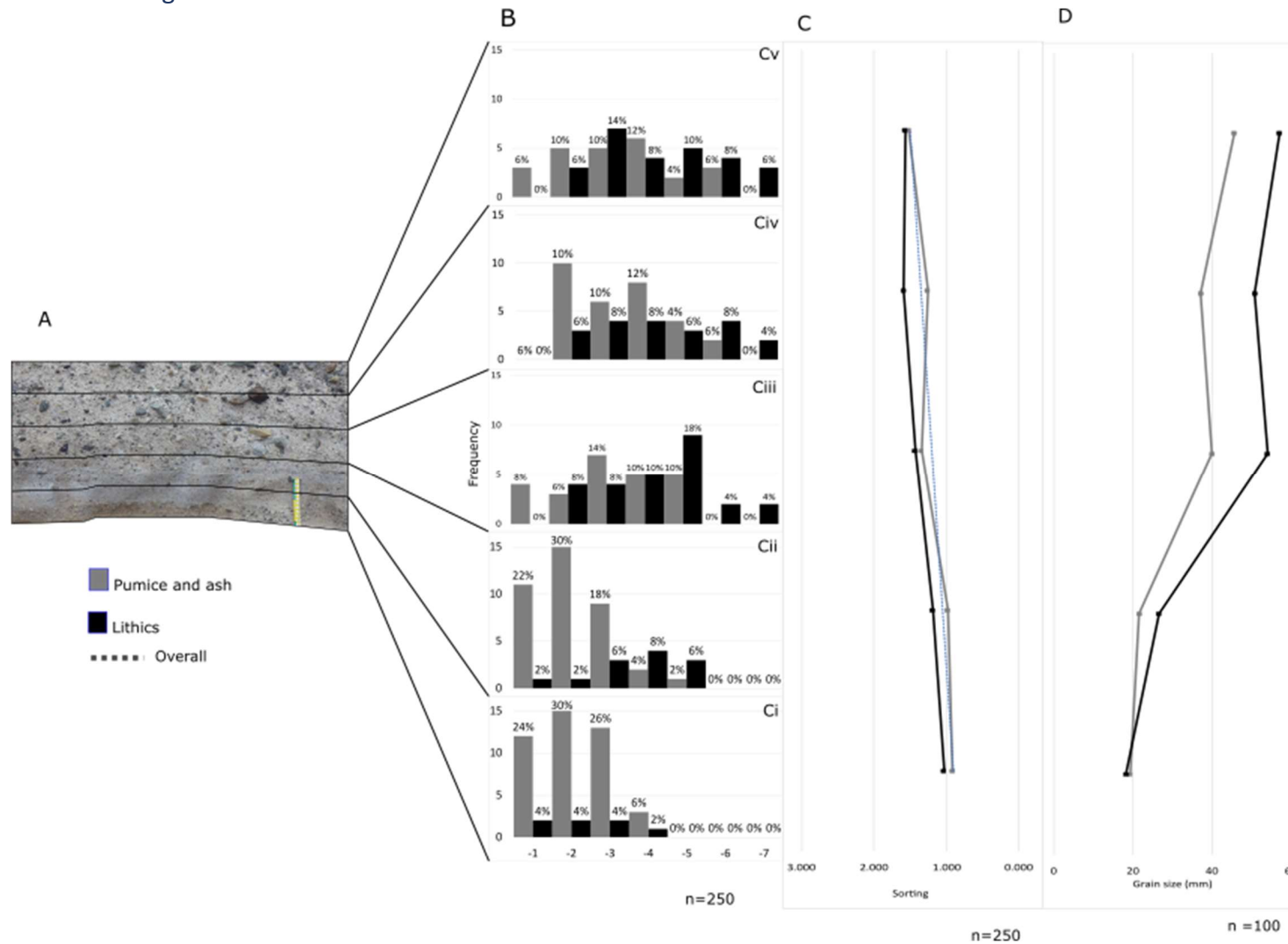


Figure 3.9 (a) Lithofacies package 4 with five equal subsections marked in Black, accompanied by (b) grain size distribution charts for each subsection (4i, 4ii, 4iii, 4iv and 4v). (c) sorting values calculated using Gradistat within each subsection of package 4, (d) Mean average grain size of the 10 largest (qualitatively selected) pumice and lithic clasts.

3.4.5 Package 5

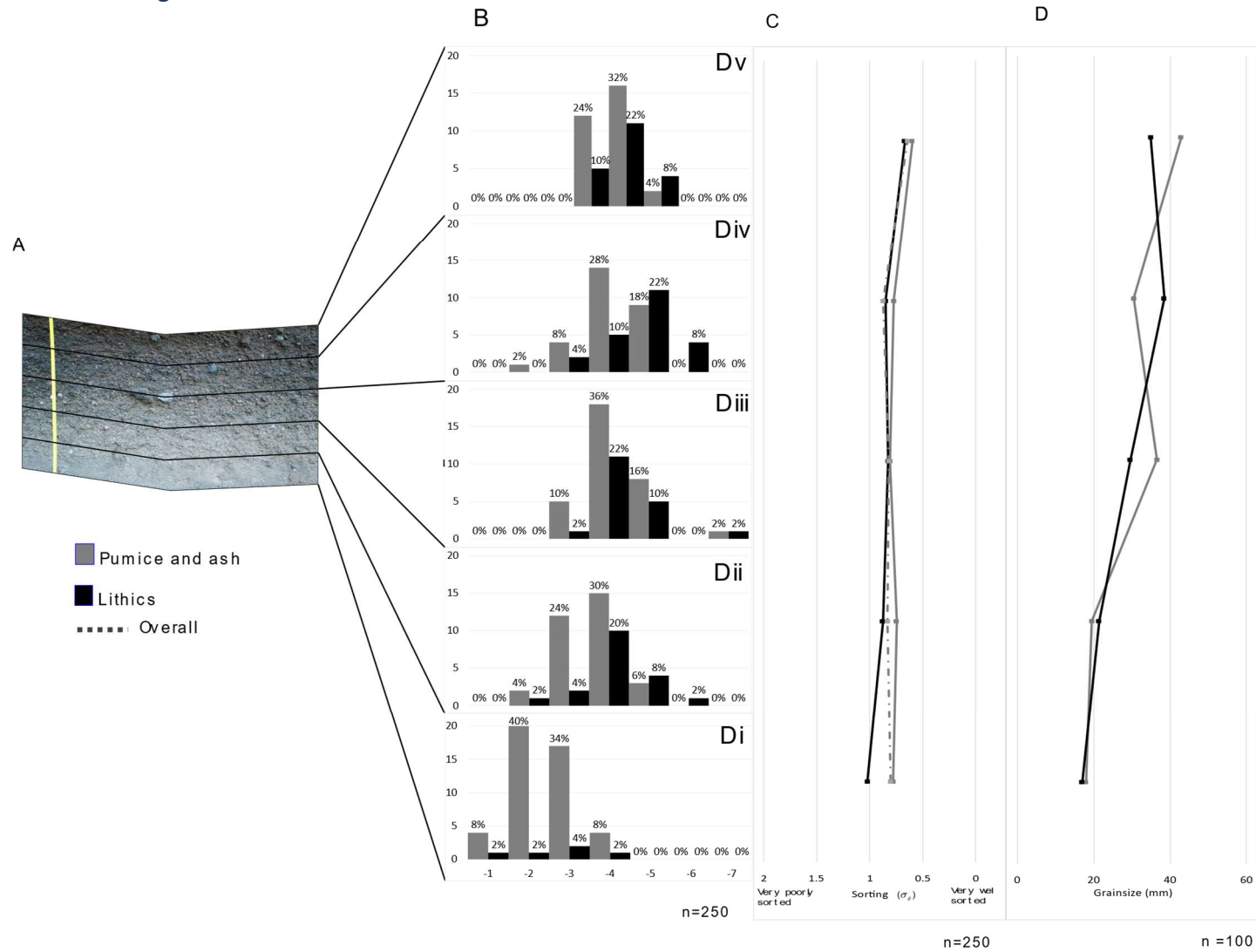


Figure 3.10 (a) Lithofacies package 5 with five equal subsections marked in black, accompanied by (b) grain size distribution charts for each subsection (Di, Dii, Diii, Div and Dv). (c) sorting values calculated using Gradistat within each subsection of package 5, (d) Mean average grain size of the 10 largest (qualitatively selected) pumice and lithic clasts.

3.4.6 Package 6

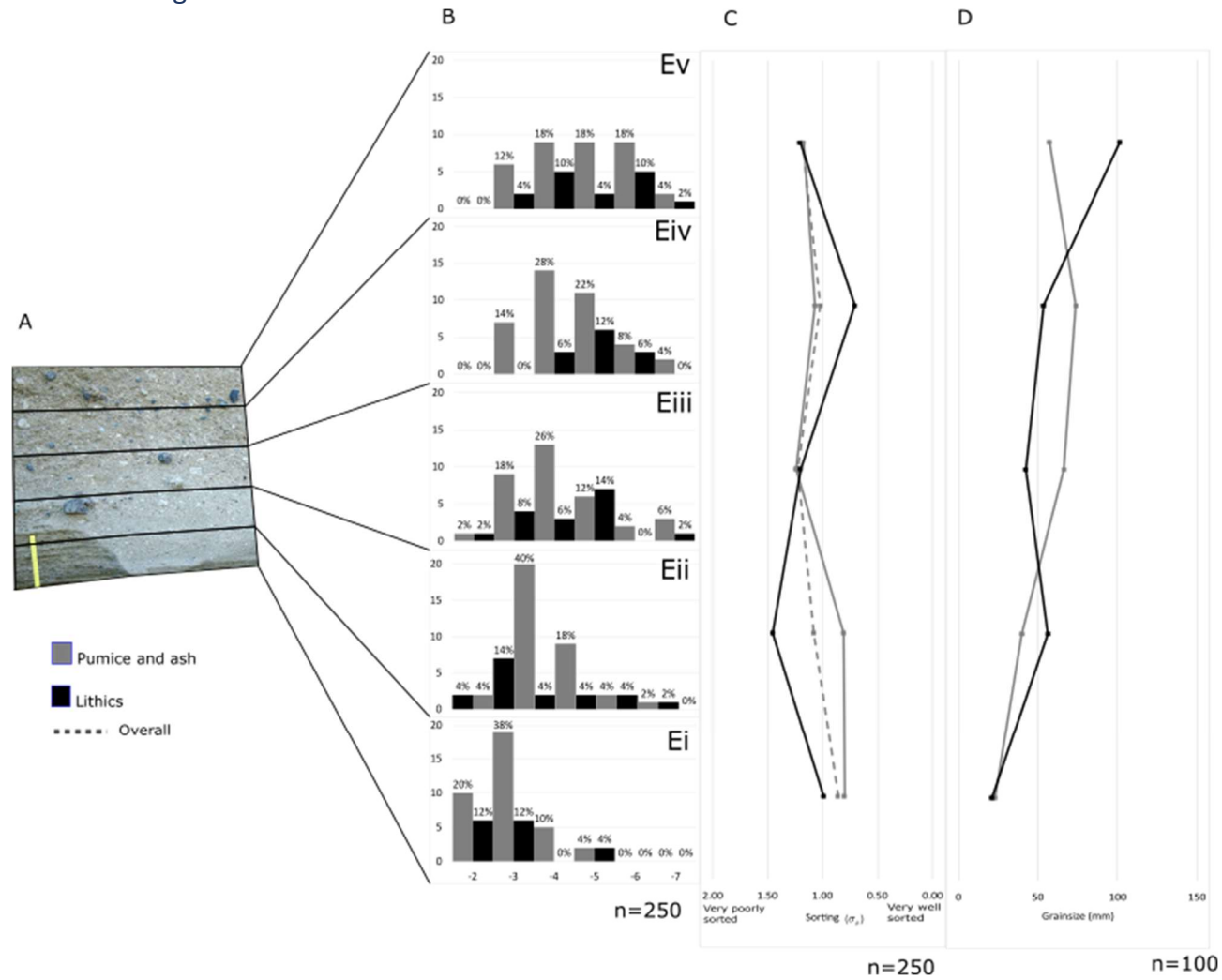


Figure 3.11 (a) Lithofacies package 6 with five equal subsections marked in black, accompanied by (b) grain size distribution charts for each subsection (Ei, Eii, Eiii, Eiv and Ev). (c) sorting values calculated using Gradistat within each subsection of package 6, (d) Mean average grain size of the 10 largest (qualitatively selected) pumice and lithic clasts.

Analysis of package 1 confirms a trend of reverse grading in both pumice and lithics (Figure 3.6b). 1i grain size is predominantly 2-4 mm (-2phi) with 52% of clasts in that size range (42% pumices, 10% lithics) with a rather even distribution of clasts between -1 and -3phi. In A1ii, the total percentage of clasts under 2 mm reduces from 22% to 12% and is just 8% in 1iii between 1iv and A1v. Clasts over 2 mm were not recorded. In the uppermost part of this package (1v), 76% of clasts have a long axis larger than 4 mm, compared to just 26% at the base (1i). The average grain size in 1v (5.9 mm) is 1.96 times larger than in 1i (3.0 mm). A t-test confirms that this is a significant difference with a P-value of 6.7×10^{-9} , over 99.99% significant.

Sorting values for Package 1 are all between $0.5 \sigma_\phi$ and $1 \sigma_\phi$, pumice and ash range between $0.649 \sigma_\phi$ and $0.800 \sigma_\phi$ and lithics range between $0.599 \sigma_\phi$ and $0.759 \sigma_\phi$, showing this to be a moderately sorted deposit, with both pumice and lithics sharing similar values throughout.

In package 1, the largest pumice clasts display a coarsening upwards trend. The largest clasts are 1.5 times larger in 1v (8.8 mm) than 1i (5.8 mm). The largest lithic clasts also display a coarsening upwards trend. Lithics are 1.3 times larger in 1v (9.8 mm) than 1i (7.7 mm), but the relationship between clast size and height in the deposit does not appear to be as strong as in the pumices.

The quantitative data portrayed in Figure 3.7 shows that package 2 exhibits a distinct gradational coarsening of clast upwards. Clasts within the 2-4 mm (-2phi) bracket are dominant in 1i with 46% of all clasts within this subsection belonging to that size range. 2ii is slightly coarser with 92% of clasts in the 2-4 and 4-8 mm brackets (both 46%), with the same gradational increase into 2iii. Between 2iii and 2iv there is a jump in clast size, increasing from just 2% of clasts larger than 8 mm (-3 phi) in 2i to 60% of clasts over 8 mm in 2v. The overall average grain size in 2v is 2.5 times greater than in 2i (3.8 mm and 9.6 mm respectively), an increase of over 99.99% significance (t-test).

The average grain size of the 10 largest pumices displays a very strong relationship between grain size and package subsections where the largest pumices in 2v are 2.3 times larger than those in 2i (14.2 mm, 6.2 mm respectively). With lithics like in package 1 displaying a weaker trend in grading where clasts are 1.4 times larger in 2v than 2i (8.5 mm and 6.0 mm respectively). The sorting pattern shows this to be moderately well sorted, with value ranges of $0.522 \sigma_\phi$ to $0.727 \sigma_\phi$ for pumice and $0.400 \sigma_\phi$ to $0.661 \sigma_\phi$ for lithics, suggesting grain sizes have been segregated somewhat evenly over the deposit.

Package 3 (Figure 3.8) displays a deposit with weak grading from base to top with a 1.4x increase in grain size from 3i to 3v. the total percentage of clast larger than -3phi is 40% of 3i compared to 68% in 3v, where the largest clast sizes only make up a maximum of 4% of a single subsection (3iv, 3v)

Sorting values indicate an overall poorly sorted deposit, with pumices being poor poorly sorted ($1.08 \sigma_\phi$ to $1.323 \sigma_\phi$) and lithics being moderate to moderately poorly sorted ($0.698 \sigma_\phi$ to $0.973 \sigma_\phi$)

The average of the 10 largest pumices and lithics increased by 2.1x and 1.2x respectively. The pumices relationship between the top 10 largest clast size and height within the deposit is almost linear whereas the lithics appears somewhat random with no obvious relationship despite an overall increase.

Package 4 demonstrates an ignimbrite rich in lithics which make up 36% of the total deposit. The deposit is matrix supported and visibly segregated in the photo. The data depicted in Figure 3.9

supports this with a large increase in grain sizes between -5 and -7phi from 0% in 4i to 36% in 4v with an overall grain size increase of 4.9x from 3.9 mm in 4i to 19.1 mm in 4v.

Sorting values show that this deposit becomes gradually more poorly sorted starting at a value of $0.913 \sigma_{\phi}$ for pumice and $1.030 \sigma_{\phi}$ for lithics at the base and reaching values of $1.518 \sigma_{\phi}$ for pumice and $1.568 \sigma_{\phi}$ for lithics at the top of the package, these values remaining within the poorly sorted range of 1.00-2.00 σ_{ϕ} (Blott & Pye, 2001),

The 10 largest clasts also show a significant increase of 3.1x for lithics and 2.4x for pumice. With this deposit being matrix supported as the size of the larger clast increases the sorting decreases as it incorporates a larger distribution of grain sizes.

Package 5 (figure 3.10) is a lithic-rich lapilli tuff, which is clearly reverse graded, with the average grain size in 5v of 4.8 times greater than 5i with grain sizes of 4.4 mm in 5i and 21 mm in 5v with 68% of clast equal to or larger than -5 phi in 5v compared to 0% in 5i.

Sorting values indicate that this deposit changes from moderately sorted at the base with values between $0.7 \sigma_{\phi}$ and $1.00 \sigma_{\phi}$ to moderately well sorted at the top with values between $0.5 \sigma_{\phi}$ and $0.7 \sigma_{\phi}$.

This trend is also visible in the average 10 largest clasts of each section with pumices experiencing an increase of 2.4x and lithics by 2x. This deposit also is moderately well sorted with sorting values between $0.5 \sigma_{\phi}$ and $1 \sigma_{\phi}$.

Package 6 (figure 3.11) presents a very poorly sorted, pumice and ash-rich lapilli tuff with 78% of the deposit being pumice and ash. It is a coarse deposit and as with the other coarser deposits (Packages 4 and 5), it has a large grain size increase with an average grain size in 6v 3.9 times greater than the average grain size in 6i from 6.5 mm average in 6i to 19.2 mm in 6v.

Sorting values for this deposit range from moderately sorted ($0.707 \sigma_{\phi}$) to poorly sorted ($1.452 \sigma_{\phi}$), with lithics showing the larger variation. When compared to the top 10 largest clasts it would appear that the sudden and large increase in the size of larger clasts have skewed the results within the subsections 6ii and 6v, whereas the pumice appears to vary less and seems unimpacted by the largest clast size.

The average of the 10 largest pumices and lithics in each section also display a large increase in size with a 2.5x increase for pumices and a 4.8x increase in size for lithics. Although the lithics are reversely graded there is an anomaly in 6ii with a large increase from 20.9 mm in 6i to 56.3 mm in 6ii and down to 42.2 mm in 6iii. This sudden increase in grain size range is reflected in the sorting where the deposit becomes much more poorly sorted than the rest of the deposit.

3.4.7 Composition

A composition analysis of the 6 ignimbrite packages was conducted by combining all the data for each package and plotting onto a ternary diagram (Fig 3.12) using Veusz (Sanders, 2008) to observe variation within the concentration of lithics, pumice and ash within the deposits, in order to assist interpretation of results collected through grain size analysis. The ternary plot shows that each of the ignimbrites lies within a similar range with none of the deposits exceeding 40% lithic fragments.

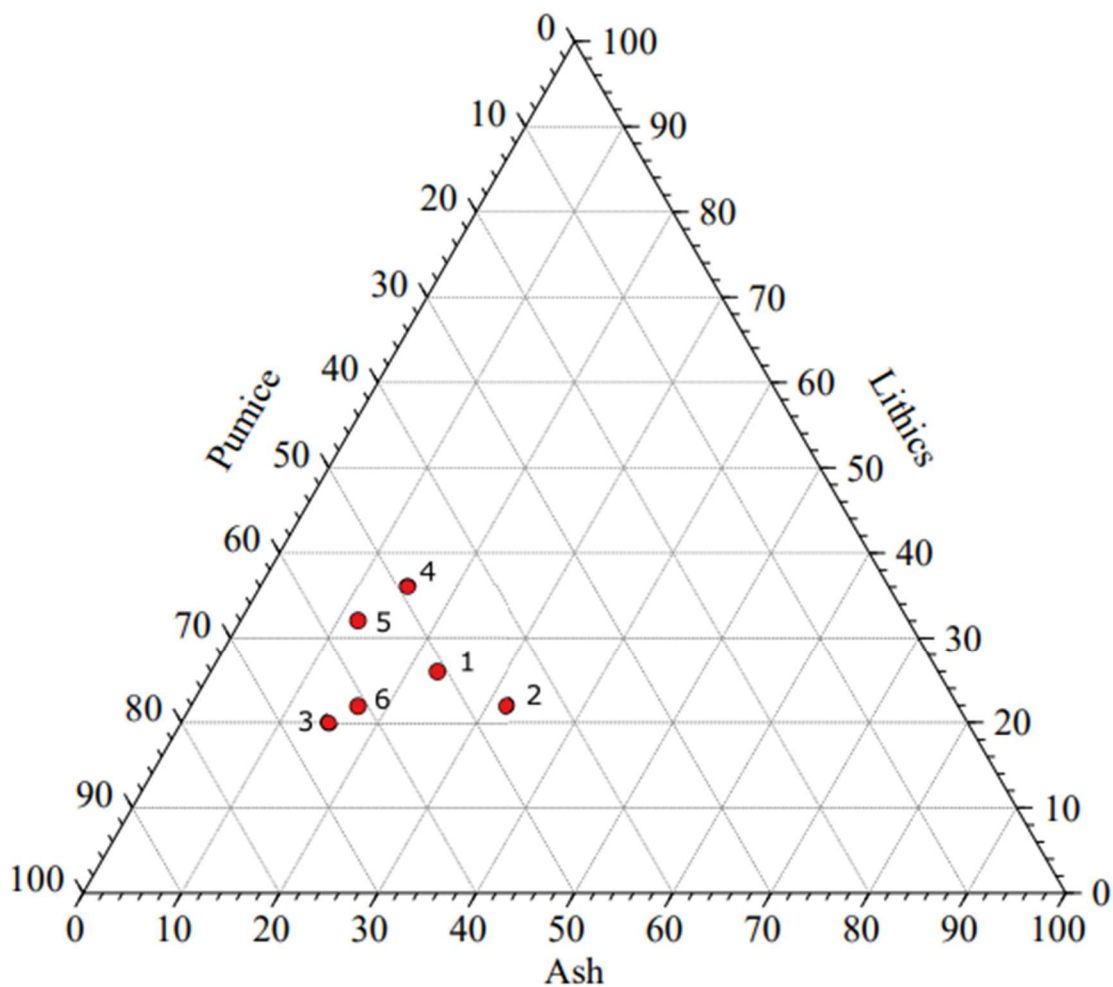


Figure 3.12 Ternary plot showing the composition of pumice, ash and lithics for the images used.

3.5 Discussion

3.5.1 How is reverse grading characterised?

3.5.1.1 General characteristics

In all the images of reversely graded ignimbrites in this study, pumices display strong reverse grading. On average, the largest pumice clasts are 120% larger at the top (v section) compared to the base (i section). Lithics do not appear to follow the same trend. Some packages show strong grading of lithics (e.g., 4 and 5) while some show no trend (Image 3), or weak grading (Image 2). Previous studies have shown that in fluidised and unfluidized granular currents denser clasts tend to fall to the base of deposits (Möbius et al., 2001; Choux & Druitt, 2002; Choux et al., 2004; Schnautz et al., 2005), thus it would be expected that the deposits of ignimbrites show the same characteristics. However, the lithic clasts (which are denser than pumices) are reverse graded in these deposits, opposing the findings of these studies and the field interpretations (Smith & Kokelaar, 2013). The lack of reverse grading in lithics in Package B suggests that density does play a role in reverse grading if conditions do not support these denser clasts.

3.5.1.2 Grain size distribution

Sparks (1976) suggests that only coarse clasts are graded and the matrix or clasts under 0.5 mm remain constant throughout. The grain size distribution charts displayed in the figures would suggest that this is sometimes true as clasts under 2 mm can be found through all subsections in deposits 1,2,3 and 4. However this cannot be a “rule”, as shown in package 5 where clasts under 2 mm were not recorded in the top two subsections. The data does however suggest that there is a relationship between particle size and grading with coarser deposits displaying more intense grading, as seen in Packages 4, 5 and 6 which are all much coarser than the other packages and an average overall grain size increase of 354.7% compared to a 94.6% for the finer deposits (deposits 1, 2 and 3). In deposits 4, 5 and 6 the grain size ranges from ash to blockss. In all these examples the coarser clasts show the largest grading with very few larger clasts recorded in the lowest subsections, whereas the top subsections show at least 30% of all clasts over 16 mm in all 3 coarser deposits, however, the smaller clasts < 2 mm remain present throughout (with the exception of deposit 5). Although grading seems more present among the larger grain sizes, it is still present within smaller grain sizes, appearing to support Sparks (1976); however, as results could not be collected on clasts below 0.5 mm this cannot be investigated. The sorting data also suggests a moderate relationship with grain size and sorting, with packages 4 and 6 both showing poorly sorted deposits and overall coarser grain size in comparison to packages 1, 2, and 3 which show moderate to moderately well-sorted deposits and finer grain sizes. Package 5 does not fit this description as it shows a coarser deposit with moderate sorting.

3.5.1.3 Sorting

Ignimbrites have often been characterised as poor to very poorly sorted through qualitative analyses (Druitt, 1998; Branney & Kokelaar, 2002; Brown & Andrews, 2015), which show that deposits vary between moderately well sorted and poorly sorted as shown by the sorting values collected, which range from $0.5 \sigma_{\phi}$ to $1.5 \sigma_{\phi}$.

Ignimbrites 1, 2 and 3 are the finest grained deposits examined, with 1 and 2, the finest of all. Images 1 and 2 present the best sorting of all deposits examined with values ranging between $0.5 \sigma_{\phi}$ and $1.0 \sigma_{\phi}$ displaying a moderate grading of clast size. Image 3 shows weak grading with sorting values between $0.7 \sigma_{\phi}$ and $1.0 \sigma_{\phi}$ for lithic clasts, while pumices have sorting values between $1.0 \sigma_{\phi}$ and $1.4 \sigma_{\phi}$. Image 3 shows little to no grading among lithic clasts and weak grading of pumice clasts.

Ignimbrite 4 presents a coarser deposit than deposits 1, 2 and 3 yet finer than deposits 5 and 6. The sorting values indicate that the deposit become gradually more poorly sorted upwards from $0.9 \sigma_{\phi}$ at the base to $1.5 \sigma_{\phi}$ at the upper section. Deposit 4 presents strong size grading of clasts with a 4.9x increase in clast size from base to top.

Ignimbrite 5 is another coarse deposit with a similar grain size range to Ignimbrite 4. However, ignimbrite 5 shows the opposite trend to ignimbrite 4 where it is poorly sorted at the base with a value of $1.0 \sigma_{\phi}$, and moderately well sorted at the top with a value of $0.5 \sigma_{\phi}$ showing moderate to strong grain size grading upwards.

Deposit 6 is the coarsest of all deposits examined. The sorting values are erratic ranging from $0.7 \sigma_{\phi}$ to $1.5 \sigma_{\phi}$ with moderate to strong grading showing a gradual shift from a small distribution of smaller grain sizes at the base to a wide distribution of grain sizes upwards with increasing concentration of larger clast sizes.

Across finer deposits pumices, ash and lithics display better sorting, in coarser deposits the lithics are more poorly sorted than pumice and ash. The finer deposits are all between 20 and 30% lithic and

deposits 4 and 5 that show poorer sorting for lithic have 30-40% lithics. Package 6 shows erratic sorting values and lies within the 20-30% lithics range possibly suggesting that an increase of larger sized denser lithic clasts has an impact on sorting.

3.5.1.4 *Composition*

composition analysis shows that the ignimbrites fall into a similar range with all deposits composed of between 20% and 36% lithic fragments. This along with the varied sorting and grain size data shows that even among deposits of similar composition the flow dynamics can vary, producing dissimilar deposits. Alternatively, this could suggest that there is data that has not been collected that could identify causes of dissimilarity among similarly pumiceous deposits, such as density of clast, and topography that the PDC deposited on. Furthermore, the lack of deposits with lithic fragments over 40% may suggest that reverse grading in these types of deposits is less common and perhaps a higher concentration of lithic fragments may inhibit the sorting mechanism.

3.5.2 *The effectiveness of image grain size analysis of volcanic outcrops*

When using image analysis, the image only shows the exposed surface of the rock and not the interior. This is unlikely to be representative of the facies as a whole. However, this is also a problem in outcrop sampling. Ignimbrites are inherently variable in space and time; therefore, any sample is unlikely to be truly representative or more representative than the section studied in the images.

Image analysis only shows one view of a clast, which may not be the largest side (ideally required for this form of analysis), or even a whole side at all, it could be a partial section or a corner. As with sieving, a limitation of the image analysis technique is the assumption that the clast is spherical, and the longest axis may not be measured (Kwan et al., 1999; Giachetti et al., 2011).

Image textural analysis to distinguish between pumice and lithics could be subjective; the quality of the observations can depend largely on the interpretative skills of the observer (Francus, 1998). It can be difficult to see some clast edges, and due to this only high-resolution images can be used to make the measurements as accurate as possible on smaller clasts with a minimum resolution of 3 pixels (Lindqvist & Åkesson, 2001). Not only does the image need to be high resolution but it must be face on with the exposure, as if the face is slanted the measurement will be inaccurate.

Image analysis also does not take into account any other notable observations beyond the visible characteristics of the deposit itself, whereas fieldwork can provide much richer data on the deposits such as observing topography (Sohn & Chough, 1993; Smith & Kokelaar, 2013), and provide opportunities to measure characteristics of samples collected in the field (Giannetti & De Casa, 2000; Brown & Branney, 2004b).

However, image analysis measurements are performed objectively (through random point counting) and quickly on image 'samples' carefully chosen by the operator. One can select a single lamina, or any other distinctive sedimentary structure representative of a single sedimentary event. Moreover, specific areas can be selected and points randomly selected within a chosen area in order to provide a representative and unbiased sample (Lindqvist & Åkesson, 2001).

When making observations in the field they are subjective and often qualitative. Although the observer can make some measurements in the field, making 250 measurements per package as in this study is time consuming and thus cannot be done in the field. Furthermore, field measurements are not always possible with some graded packages on a meter scale, and not always accessible. Image analysis on the other hand provides an opportunity to collect accurate quantitative data to

accompany qualitative observations made by the observer in the field. On harder to access deposits a high-quality photograph provides an opportunity to collect quantitative data when it was previously not possible.

The method poses no risk of damaging rocks that need to be analysed, all that is required is a high-resolution photograph. Therefore, it is an ethical option, particularly in geo-conservation heritage areas such as national parks and sites of special scientific interest (SSSIs) where sampling may be strictly forbidden.

Furthermore, the observer does not have to take images themselves; by obtaining permission from other geoscientists samples can be readily collected. Additionally, by using photos from other geoscientists a representative sample from multiple locations can be collected.

3.6 Conclusions

In the reversely graded ignimbrites studied above, both pumice clasts and lithic clasts show a gradual coarsening upwards, with clasts often around twice as large at the top of the deposit compared to the base. Pumice clasts display the greatest level of sorting with a consistent gradual increase in clast size, whereas lithics show this to a lesser extent, with an overall coarsening but with a larger number of outliers in comparison with pumices. The deposits studied show that grading is more evident in coarser ignimbrites than within finer ignimbrites; however, the grading remains significant within finer ignimbrites. The ignimbrites can also be characterised by moderate sorting. The finer deposits are better sorted than the coarser deposits

Through the quantitative data collected, conclusions have been drawn that in some cases, contradict the qualitative interpretations from in the field. Furthermore, through image analysis there is more data that can be collected than with traditional methods. This could allow for potential future works further characterising deposits with textural features and shape analysis, providing high-resolution images and/or 3D imaging.

4. Quantitative analysis of the Muesli effect

4.1. Introduction

This chapter presents a review of published investigations of particle segregation in granular material, and documents new analogue shaking experiments and image analysis that quantitatively analyse the processes of formation, and characteristics, of reverse grading in granular material. Results are compared to image analysis of reverse grading in ignimbrites (Chapter 3) and provide baseline data for flume experiments that investigate whether the muesli effect is a controlling factor for particle sorting in granular currents (Chapter 5).

4.1.1 Aim and objectives

This chapter aims to use analogue experiments to investigate and quantify the processes that lead to reverse grading. This work will address the following objectives:

- To observe how grains move when shaken in an unfluidized environment.
- To quantify how clast size affects particle movement.
- To examine how clast density determines particle movement.

4.2. Background

Particle segregation in granular flows is a phenomenon that occurs in many disciplines, from volcanology to sedimentology and pharmaceuticals to the food industry (Rosato et al., 1987; Savage & Lun, 1988; Ottino & Khakhar, 2000). Studies focusing on particle segregation often refer to dispersive pressure (Bagnold, 1954) or kinematic sieving (Middleton, 1970) as the mechanism of segregation.

4.2.1. Particle segregation theory

4.2.1.1. *Dispersive pressure*

One of the first theories to explain reverse grading was dispersive pressure Bagnold (1954). In the dispersive pressure model, individual grains are subject to dilative strains, it I suggested that larger grains will drift towards areas of low strain found at the free surface of the current, and small grains will drift towards the areas of higher strain at the base of the current. (see chapter 2.6.3.). This theory has many assumptions that do not represent the conditions in pyroclastic density currents. These assumptions include the density of the grains and interstitial fluid are uniform, and that the shear strain and kinetic energy remain constant. This realistically cannot be applied to pyroclastic density currents which are known to be dynamic and unsteady with a large range in clast size and density (Sparks, 1976; Cas & Wright, 1987; Druitt, 1998). Thus, there must be an alternative method of particle sorting in a granular flow.

4.2.1.2. *Kinematic sieving (aka the Muesli Effect)*

Kinematic sieving is a gravity driven process that only requires a grain size difference for particle segregation to occur (Middleton, 1970; Sohn & Chough, 1993; Sohn, 1997). Kinematic sieving is the process by which small particles will percolate through gaps created by large grains moving. Once

the small grains fall through and the voids are filled the larger grains are prevented from falling back down(see chapter 2.6.5.).

4.2.1.3. *Kinematic squeezing*

Kinematic squeezing is the process where grains are squeezed between layers in an area of highly concentrated bedload termed the traction carpet (Savage & Lun, 1988; Sohn, 1997; Branney & Kokelaar, 2002; Le Roux, 2003) see chapter 2.6.5. Through kinematic squeezing, upwards movement of large particles may occur (Fig 4.1); this is not as common as percolation, and grain segregation in the lower region of the traction carpet is hindered by minimal movement of particles (Savage & Lun, 1988; Sohn, 1997). Large particles are exposed to greater pressures and are increasingly likely to be forced upwards or sideways in the frictional zone. Squeeze expulsion often results in lateral movements of grains rather than vertical and thus is not as effective a mechanism of segregation as kinematic sieving (Savage & Lun, 1988; Sohn, 1997).

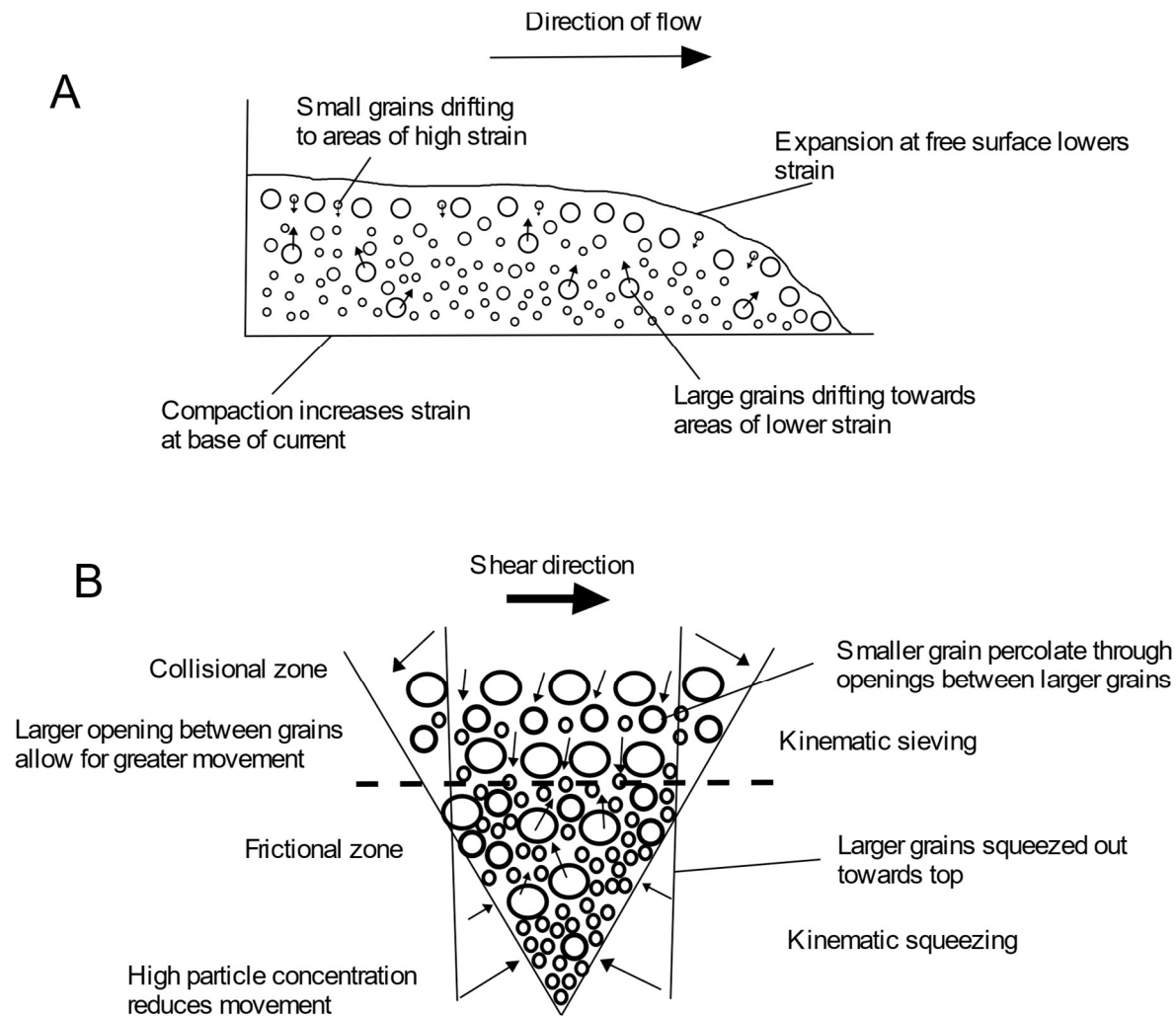


Figure 4.1 (A) Interpreted movement of grains according to dispersive pressure model suggested by Bagnold (1954). (B) Concept of kinematic sorting through sieving in the collisional zone, and squeezing in the compressional zone (Le Roux, 2003).

4.2.2. Applicability to polydisperse volcanic granular currents

Pyroclastic density currents are examples of a polydisperse granular flow, with a range of particle sizes from ash under 2 mm, lapilli between 2 and 64 mm and blocks or bombs over 64 mm (Cas & Wright, 1987). They typically contain a wide range of densities, with pumices usually around 1 g/cm³ or less and

lithics can be up to 3 g/cm^3 (Cas & Wright, 1987; Choux et al., 2004). As a result, experiments that model pyroclastic density currents should reflect this to make the results as comparable to real world PDCs as possible (e.g. Savage and Lun (1988); Choux and Druitt (2002)). The kinematic sorting model requires grain size differences to allow segregation to occur., Segregation may take place with any grain size difference, although the smaller the difference the longer it may take. For instant segregation the d_s/D_l value must be less than 0.25 (Sohn & Chough, 1993); using this ratio a 2 mm clast will segregate instantly from any clast over 8 mm, whilst an 8 mm clast will segregate instantly from any clast over 32 mm. These examples cover only a small range of grain sizes seen in currents which range from a few micrometres to several meters (Cas & Wright, 1987) giving a high probability of particle segregation in a pyroclastic density current.

In more recent years, multiple papers have tackled the muesli effect observing how larger particles move through a field of smaller particles (Shinbrot & Muzzio, 1998; Möbius et al., 2001; Cagnoli, 2005; Schnautz et al., 2005). In these papers, it is observed that a large particle that is lighter than the surrounding matrix (often termed an 'intruder' particle) will rise to the top, whereas a denser intruder will settle to the base of deposits (Cagnoli, 2005; Schnautz et al., 2005), with segregation velocity increasing when clast size increases (Cagnoli, 2005). Furthermore, a reverse of this has also been reported where segregation velocity increases with density, suggesting that inertia plays a role within segregation (Möbius et al., 2001). Experimentation by Möbius et al. (2001) observed dense particles 'jumping' upwards as a result of inertia so that smaller particles may infiltrate beneath, meanwhile, the motion of light objects fluctuates wildly preventing this (Shinbrot & Muzzio, 1998).

Although these studies do characterise the movement of larger particles, they often use only one or very few large clasts per experiment (Shinbrot & Muzzio, 1998; Cagnoli, 2005), and only record the movement of the particles without focusing on the deposits created by the experiment. PDCs and other granular currents often contain a large range of grain sizes (Cas & Wright, 1987), which needs to be reflected better in models that deal with segregation in granular material to increase understanding of how different grain sizes interact during flow. Reverse grading is a common feature of ignimbrites, Due to the dangers posed by PDCs, active currents cannot be observed up close or in real time and as a result, volcanologists must focus on the deposits created by PDCs to investigate current behaviour. By recreating deposits in laboratory experiments, current behaviours can be investigated furthering the understanding of how PDCs move. To investigate whether kinematic sorting is involved in creating reverse graded beds, we must first understand how this process occurs in an unfluidized controlled environment and then investigate how changing grain sizes and density may affect this process. By studying the deposits before and after a bed is agitated, a more complete quantitative and qualitative analysis can be completed on how kinematic sorting creates reverse graded deposits in a granular current. Additionally, examining the deposits in experiments studying the muesli effect will allow for further comparison to those deposits we see in the real world.

4.3. Methods

Analogue modelling is used by premixing materials that are shaken and observed for particle movement. These experiments address the objectives outlined in 4.1.1, providing quantitative data on how clast size and density affects particle movement.

4.3.1. Experimental design

The experiment (Fig. 4.2) involved shaking a particle mixture for a set time and recording both the processes observed and the resultant deposit. For each experiment, a 10 cm deep mixture of pre-mixed material (Table 4.1) was poured into an acrylic container measuring 17 cm x 8 cm (H x W). This was strapped onto a palm sander vibrating at 12000 rpm on a level platform. The material in the container was mixed well by a stirrer for 30 seconds, then vibrated for 2 minutes. Experiments were recorded using a full HD camera (resolution of 4920 x 3264 pixels = 0.6 mm accuracy) at 60 frames per second from a distance of 10 cm. Immediately following experiments, high resolution photos (8000 x 6000 pixels/ 0.1 mm accuracy) were taken of the deposit.

A set of trial experiments were run to identify both the optimal amount of material and optimal recording conditions for detailed analysis. A minimum of 10 cm of material in the container was found to be optimal as it allows for a detailed analysis, with each subsection a minimum of 2 cm to record the full range of grain sizes (the largest grains are 1.5 cm). Cameras were placed 10 cm from the sidewall to allow for full coverage of the deposit while retaining sufficient resolution to observe particle movement. Trials found that 2 minutes of shaking allowed for movement across all grain sizes in both dense and non-dense experiments.

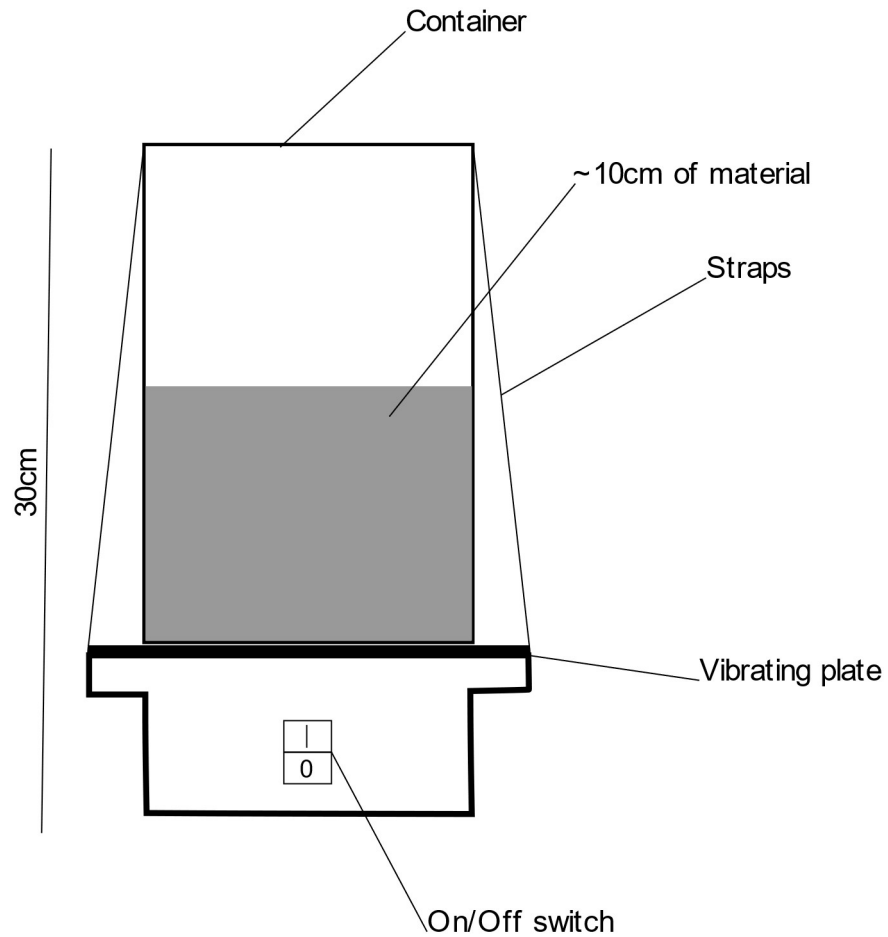


Figure 4.2 Sketch of the experimental setup used for the shaking experiments

4.3.2. Materials

Two sets of materials were used to investigate particle movement: mixtures of particles with similar densities but different sizes (type 1 experiments) and mixtures of particles with both different densities and different sizes (type 2 experiments) (Table 4.1).

The type 1 mixtures comprised semolina, couscous, and giant couscous: materials with different grain sizes but broadly similar densities ($\sim 1 \text{ g/cm}^3$). Three different experiments were conducted with varying percentages by weight of the three materials (Tables 4.2 and 4.3).

The type 2 mixtures comprised materials with varying grain sizes and density including poppy seeds, oats, raisins, hazelnuts, and Brazil nuts (Table 4.1). In these mixtures, the oats, hazelnuts, and Brazil nuts represent relatively low density pumice, and the poppy seeds and raisins represent higher-density lithic fragments.

Density was measured using the Archimedes method. In this method the material is weighed using scales to provide a mass accurate to $\pm 0.01 \text{ g}$. 10 ml of water is placed into a measuring cylinder with $\pm 0.05 \text{ ml}$ accuracy. The weighed material is placed into the measuring cylinder and the displacement is measured providing a volume. The mass was then divided by the volume to calculate the density.

Table 4.1 Densities for the materials used in the shaking experiments

	Material	Density (g/cm³)	Size range (mm)	Size range (phi)
Type 1 experiments	Semolina	1.09	0.2-0.6	2 to >0
	Couscous	1.08	1-3	>0 to -1
	Giant Couscous	1.00	2.4-4.5	-1 to -2
Type 2 experiments	Poppy seeds	2.61	0.5-0.8	1 to >0
	Oats	0.79	0.5-9	1 to -4
	Raisins	1.56	4-11	-2 to -4
	Hazelnuts	1.11	9-13	-4
	Brazil nuts	1.11	11-15	-4

4.3.3. Parameters and experimental runs

Mixtures are described by the percentage weight of each grain size. For type 1 experiments, mixes of similar density materials represent a fines rich deposit (fines rich mix), a medium well-mixed deposit (medium mix), and a coarser deposit (coarse rich mix). A uniform mix with equal amounts of all three components was also run (Table 4.2).

For the type 2 experiments, mixtures were based on weight percentage of each material. The different mixes represent a pumice rich deposit (lower density mix), a mixed deposit (medium mix), and a lithic rich deposit (higher density mix) (Table 4.3). At the end of each experiment the materials were separated using sieves with 0.5, 1, 2, 4, and 8 mm apertures in order to prepare the next mixture.

Table 4.2 Different compositions of semolina, couscous, and giant couscous used in similar density experiment.

	% Semolina	% Couscous	% Giant couscous
Type 1 uniform mix	33.3	33.3	33.3
Type 1 fines rich mix	50	40	10
Type 1 medium mix	40	50	10
Type 1 coarse rich mix	10	40	50

Table 4.3 Composition of poppy seeds, oats, raisins, and nuts used in different density experiments

	% Poppy seeds	% Oats	% Raisins	% Nuts
Type 2 lower density	50	20	20	10
Type 2 mixed	25	25	25	25
Type 3 higher density mix	20	50	20	10

4.3.4. Analysis

Using photos taken before and after shaking, image analysis was performed using JMicrovision (Roudit, 2020) to characterise grain size distribution through the deposit following the same method outlined in Chapter 3.2. Gradistat (Blott & Pye, 2001) was used to analyse the sorting patterns exhibited in the deposits. These were then compared to the results of the image analysis of the ignimbrite photos in Chapter 3.2. Video frames collected from a recording of the experiment were inserted into ImageJ to record the distance moved over time calculating the velocity at which different materials percolated or rose during shaking. All raw video files are available as a supplementary dataset at :

[<https://www.youtube.com/playlist?list=PLR9QBAIPJ3f4Kh19mHuU4ZvnO0pKFelQg>]. Photos of deposits from each experiment are available as a supplementary dataset at: [<https://www.flickr.com/photos/198477086@N07/albums/with/72177720308992452>]

4.4. Results

4.4.1. Type 1 experiments (different sizes, similar density)

Type 1 uniform mix (Table 4.2) used equal amounts of the similar density materials - 33% fine grains (semolina), 33% medium grains (couscous) and 33% coarse grains (giant couscous). The before image (Fig. 4.3A) displays a poorly sorted deposit with minor reverse grading. This is reflected in the grain size distribution charts (Fig. 4.3B) which show the base to be very fine and the other subsections displaying very similar characteristics to each other. The upper 4 subsections of 4.3A show a majority of grains at >0 and -1 phi (2 mm and under), and a varying number of larger grains displaying a slight but insignificant coarsening upwards trend. After 2 minutes of shaking reverse grading is much more pronounced, with a very fine basal section and a coarse rich top (Fig. 4.3E). The grain size distribution charts (Fig. 4.3D) display a gradual increase in grain size, where 98% of the basal subsection of the deposit comprises grains below -1 phi (2 mm), whilst in the uppermost subsection 74% of grains are over 2 mm. The sorting values (Fig.4.3C) indicate a gradual move from well sorted at the basal subsection with a value of $0.4 \sigma_\phi$ to poorly sorted at the uppermost subsection at $1.18 \sigma_\phi$. The two lowermost subsections are predominantly a single grain size (>0 Phi) leading to well/moderate sorting shown here. Upwards through the deposit there is less segregation between the larger grain sizes, and as a result, the upper 3 subsections display poorer sorting.

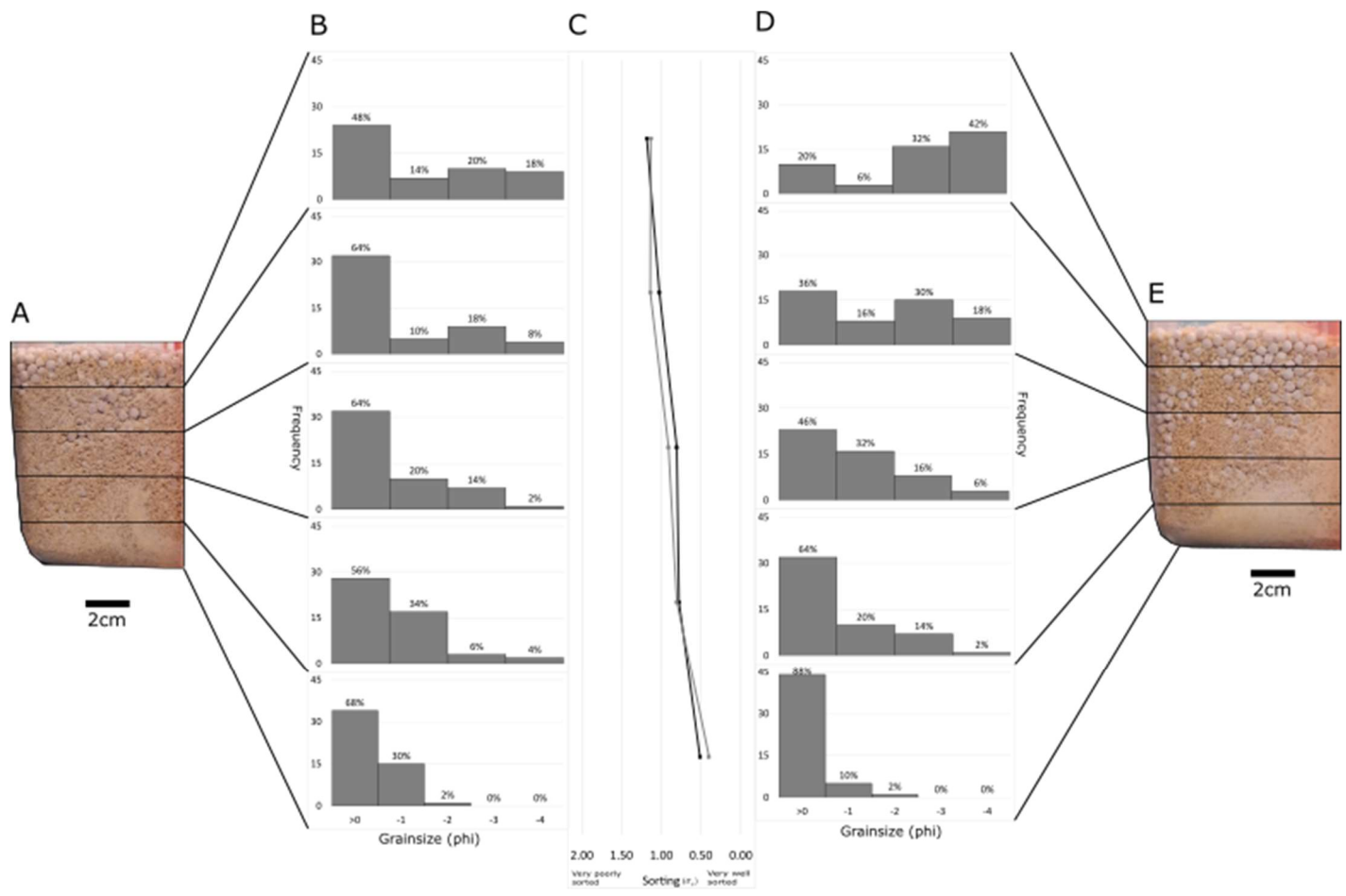


Figure 4.3 Grain size distribution of Type 1 uniform mix (with equal amounts of giant couscous, couscous, and semolina) before and after 2 minutes of shaking at 12000 rpm. (A) Type 1 uniform mix before shaking occurred, split into five equal subsections, (B) Grain size distribution of each deposit subsection before shaking, (C) Sorting values for the 5 subsections before (black) and after (grey) shaking, calculated using Gradistat, (D) Grain size distribution of each deposit subsection after shaking, (E) Type 1 uniform mix after shaking.

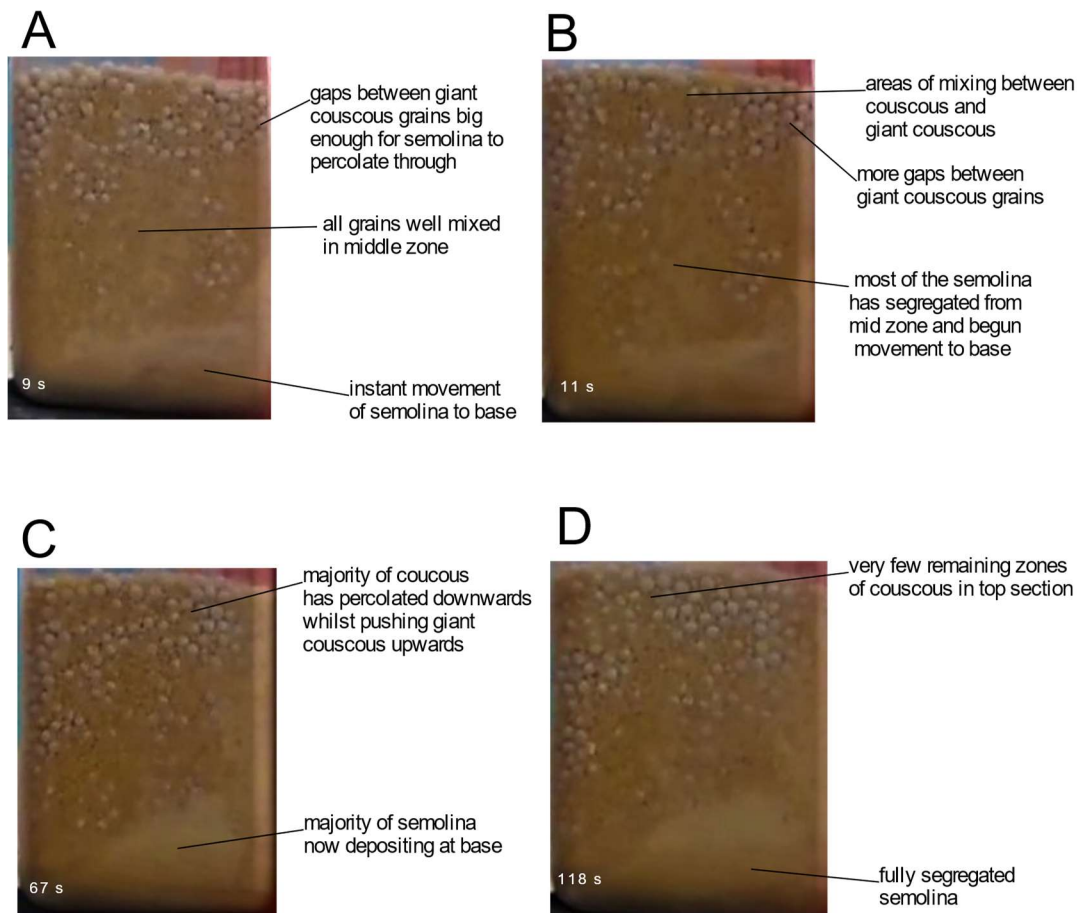


Figure 4.4 Video frames taken from type 1 uniform mix with equal parts couscous, semolina, and giant couscous. The numbers in the bottom left corner of frames are time in seconds since shaking began. **A** Instant percolation of finer material leads to almost full segregation of finest material from the deposit. **B** Larger couscous begins to vibrate increasingly, areas of couscous in between larger grains (highlighted in red) begin to shrink. **C** Medium sized grains now segregating from the largest grains, areas between the larger grain (highlighted in red) shrinking as grains percolate downwards, increasing level of fine material at the base as rapid segregation continues. **D** Areas between the largest grains disappeared as the medium sized grains percolated through, full segregation of finest material. (see supplementary [video 4.1](#))

Video frames in Figure 4.4 allow for observation of particle movement during the experiment. 4.4.A shows the experiment after 9 seconds of shaking. Here the fine grains appear to have fully segregated from the coarse grains and have almost segregated from the medium grains. Small gaps can be seen between grains near the top of the section large enough to fit fine grains and some medium sized grains but too small for the coarse grains. Just 2 seconds later in Figure 4.4B, the number of gaps between the coarse grains has increased and medium grains started to percolate through. There is still a large amount of mixing within the two grain sizes. In Figure 4.4C the amount of medium grains mixed in with the coarse grains has significantly decreased as the particles percolate downwards through opening gaps. Between 11 and 67 seconds there is a large reduction in the amount of couscous visible within the top section of the deposit as it has percolated through gaps opening below. By 118 seconds, the top of the section is almost exclusively coarse grains with the middle displaying a degree of mixing between coarse and medium grains, and the base remains fully segregated.

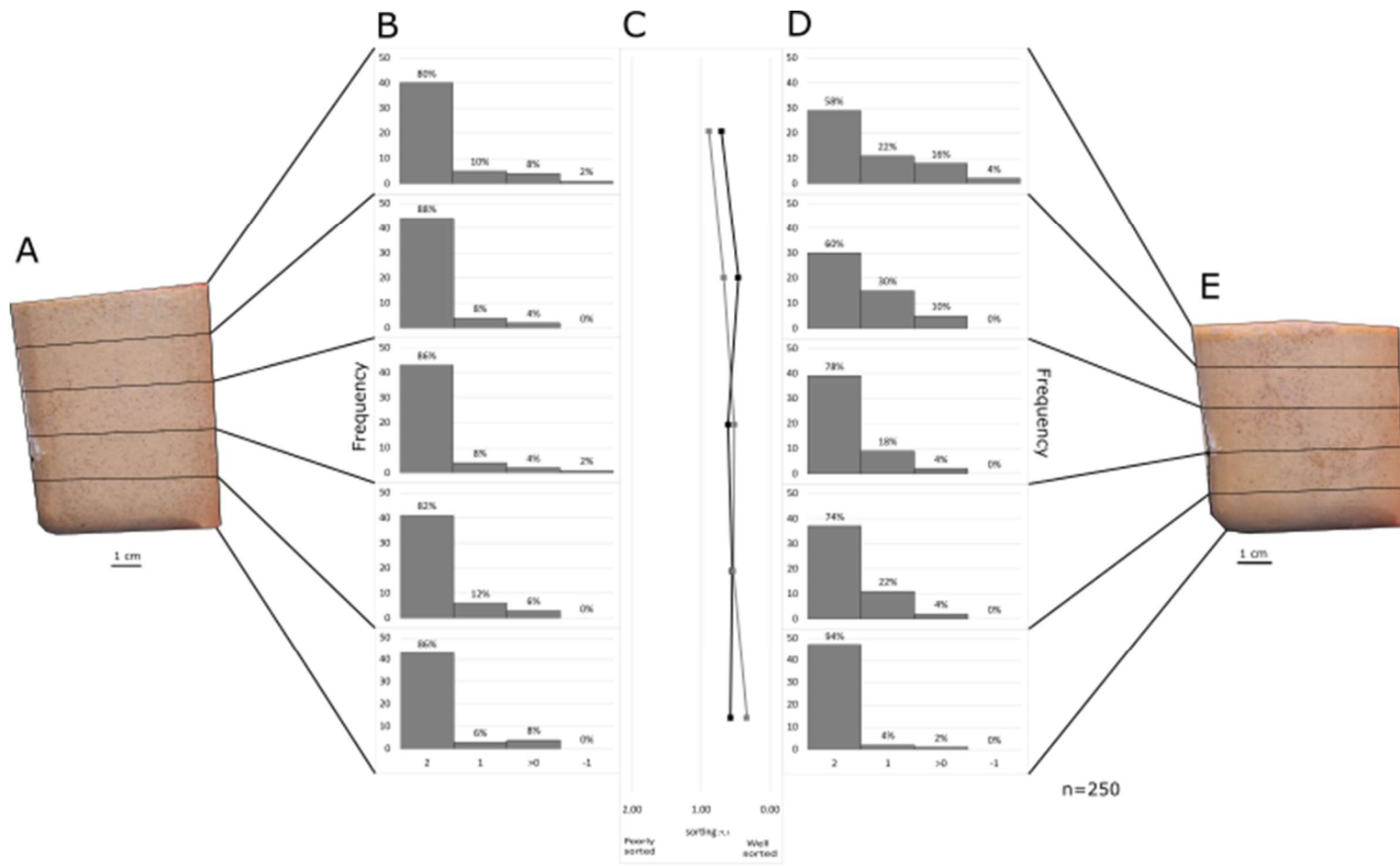


Figure 4.5 Grain size distribution of Type 1 fines rich mix (with 50% semolina, 40% couscous and 10% giant couscous) before and after 2 minutes of shaking at 12000 rpm. (A) Type 1 fines rich mix before shaking occurred, split into five equal subsections, (B) Grain size distribution of each deposit subsection before shaking, (C) Sorting values for the 5 subsections before (black) and after (grey) shaking, calculated using Gradistat, (D) Grain size distribution of each deposit subsection after shaking, (E) Type 1 fines rich mix after shaking.

Type 1 fines rich mixture uses a majority (50%) of the finest grain size available (0.2-0.6 mm) simulating a fine ash-rich deposit. Before shaking (Fig 4.5A) the fine grains are nearly evenly distributed across the mixture, with the finest material accounting for between 80 and 88% across all subsections before shaking (Fig.4.5B). This appears to be due to the fine grains obscuring the larger grains from vision. After 2 minutes of shaking (Fig. 4.5E), there is a visible change in the uppermost subsection, whereby medium and coarse grains have appeared at the top, whilst in the mid 3 subsections (2nd basal to 2nd upper subsection) an increased presence of medium sized grains is recorded. Data displayed in the grain size distribution charts after shaking (Fig 4.5D) shows a gentle grading pattern has emerged with the medium sized grains with a grain size of 1-3 mm (0 to -1 phi) rising from only 2% at the basal subsection to 22% at the uppermost subsection. Sorting values (Fig. 4.5C) indicate well to moderate sorting throughout all subsections. The basal section is shown to be the most well sorted with a sorting value of 0.34 σ_ϕ whilst the uppermost section is the least well sorted at 0.89 σ_ϕ .

Type 1 medium rich experiments (Figure 4.6) use a mix of 40% fine grains (semolina), 50% medium grains (couscous) and 10% coarse grains (giant couscous), simulating a lapilli-tuff deposit. Before shaking (Fig. 4.6A), the mixture showed no grading of particles with all 5 subsections displaying similar grain size distributions (Fig. 4.6B) with both basal subsection and uppermost subsections showing a predominance of fine grains (66% in basal, 68% in uppermost subsection). After 2 minutes of shaking (Fig. 4.6E), almost all the fine grains have moved down to the base where the finest grains (2 Phi) (Fig. 4.6B and 4.6D) account for 38% of the total subsection. Additionally a group of large grains has also appeared in the basal subsection while the medium sized grains account for very little of the basal subsection. The mid 3 subsections, i.e., the 2nd lowest to the 2nd highest, show a majority of medium sized grains between 0 and -1 Phi accounting for 36-56% of the total area within these sections. The coarse grains appeared to gather at the base and the top whilst being sparsely spread throughout the mid sections. Average grain sizes collected for each subsection show the top section to be 86% larger than the base with an average grain size of 2.5 mm compared to 1.3 mm, likely due to the lack of the finest particles (under 1 mm) at the top which only accounts for 12% of grains at the top compared to 48% at the base. Sorting values (Fig. 4.6C) for all subsections show poor sorting with the basal section the most poorly sorted with a value of 1.73 σ_ϕ , that gradually becomes better up to the 2nd uppermost subsection where the sorting is moderate (0.86 σ_ϕ), before becoming poor again.

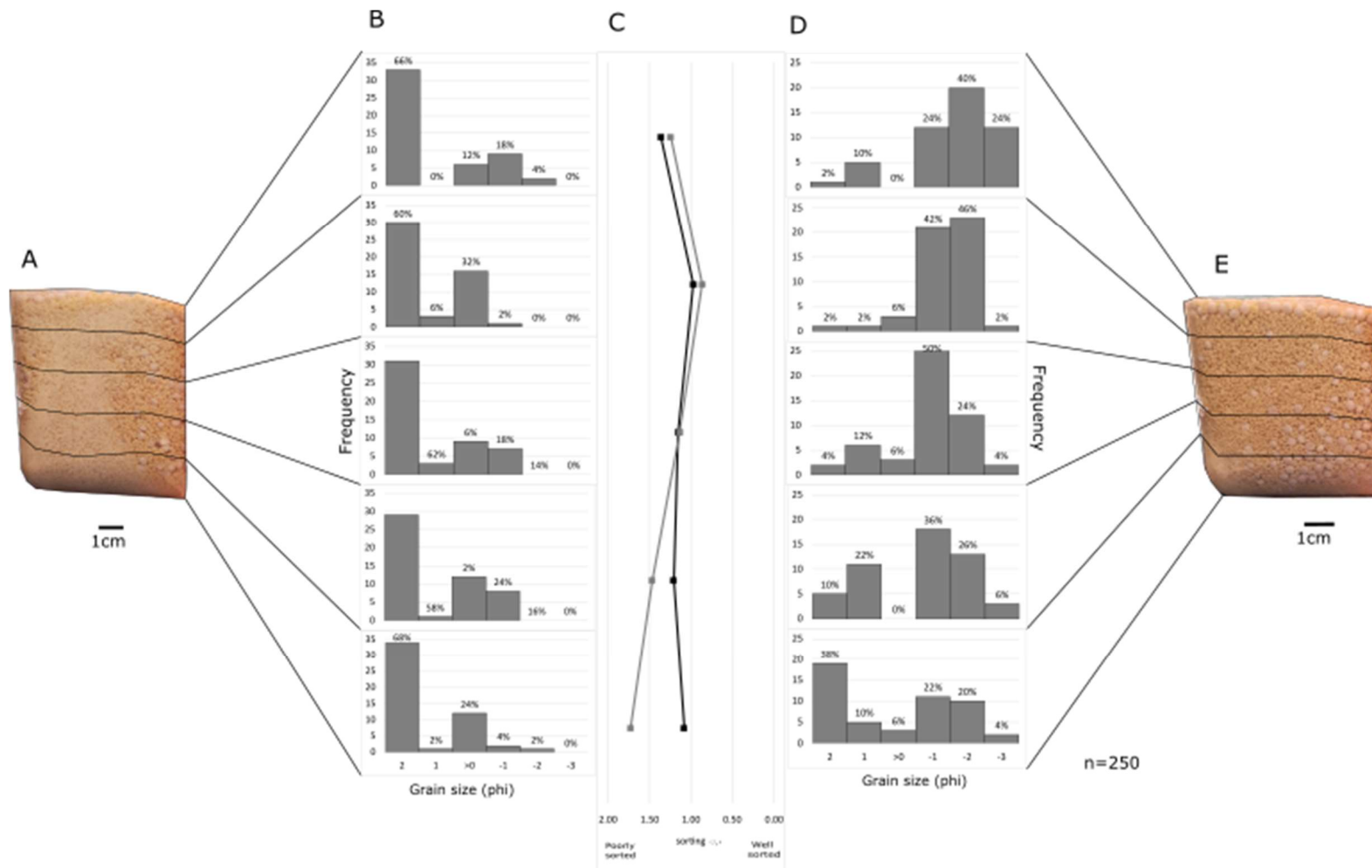


Figure 4.6. Grain size distribution of Type 1 medium rich mix (using a mix of 40% semolina, 50% couscous and 10% giant couscous) before and after 2 minutes of shaking at 12000 rpm. (A) Type 1 fines rich mix before shaking occurred, split into five equal subsections, (B) Grain size distribution of each deposit subsection before shaking, (C) Sorting values for the 5 subsections before (black) and after (grey) shaking, calculated using Gradistat, (D) Grain size distribution of each deposit subsection after shaking, (E) Type 1 medium rich mix after shaking.

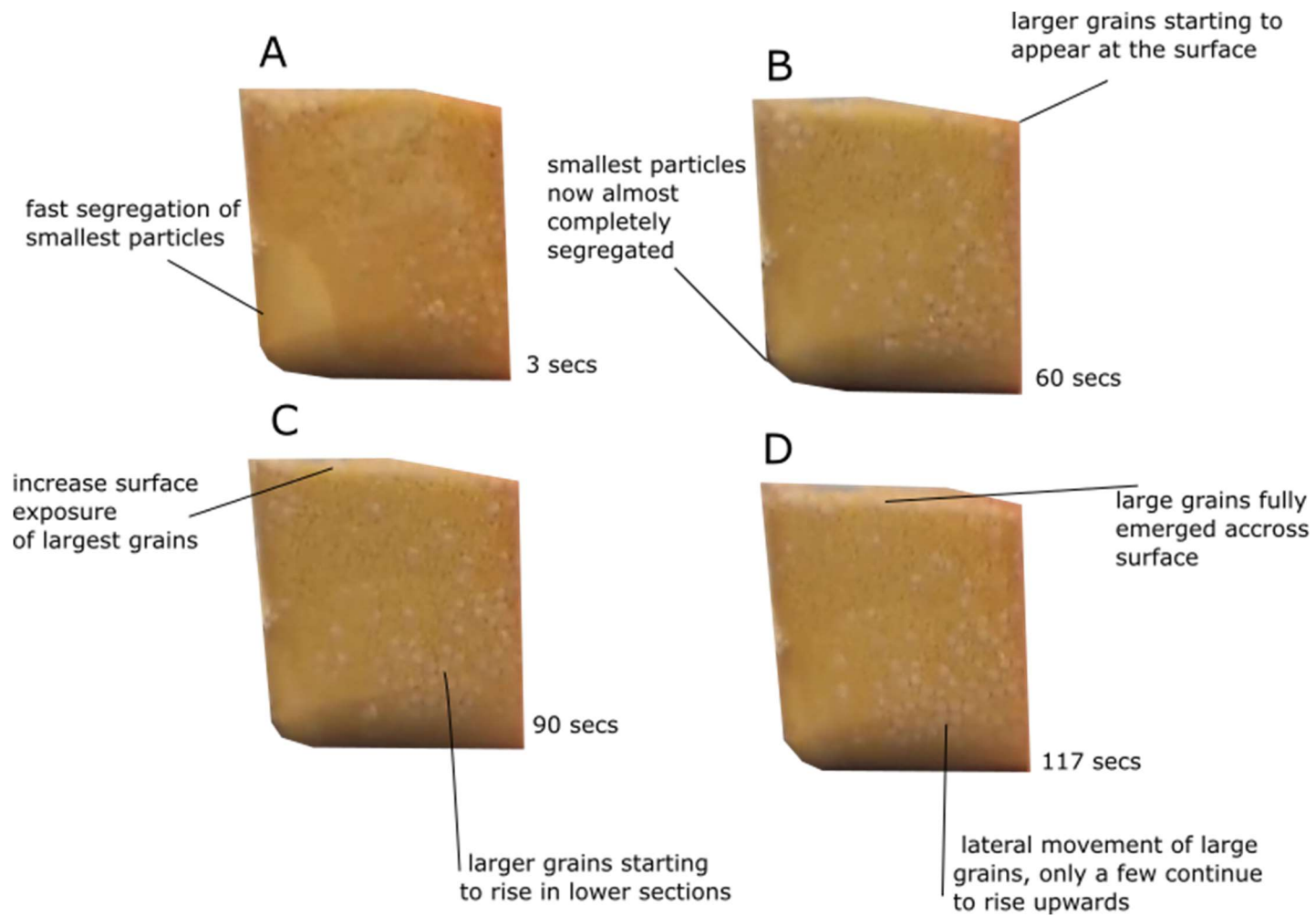


Figure 4.7 Video frames taken from type 1 medium rich mix (using a mix of 40% semolina, 50% couscous and 10% giant couscous). The numbers in bottom right corner of frames are time in seconds since shaking began. **(A)** segregation of the smallest particles begins. **(B)** small particles continue to percolate down, now majority lie at the base, and coarse grains begin to rise through the mixture and emerge at the surface. **(C)** coarse grains rise in lower sections with increased exposure at the surface **(D)** surface now littered with the coarse grains, throughout the mid and base layers, large grains are moving more laterally than vertically. (see supplementary [video 4.3](#))

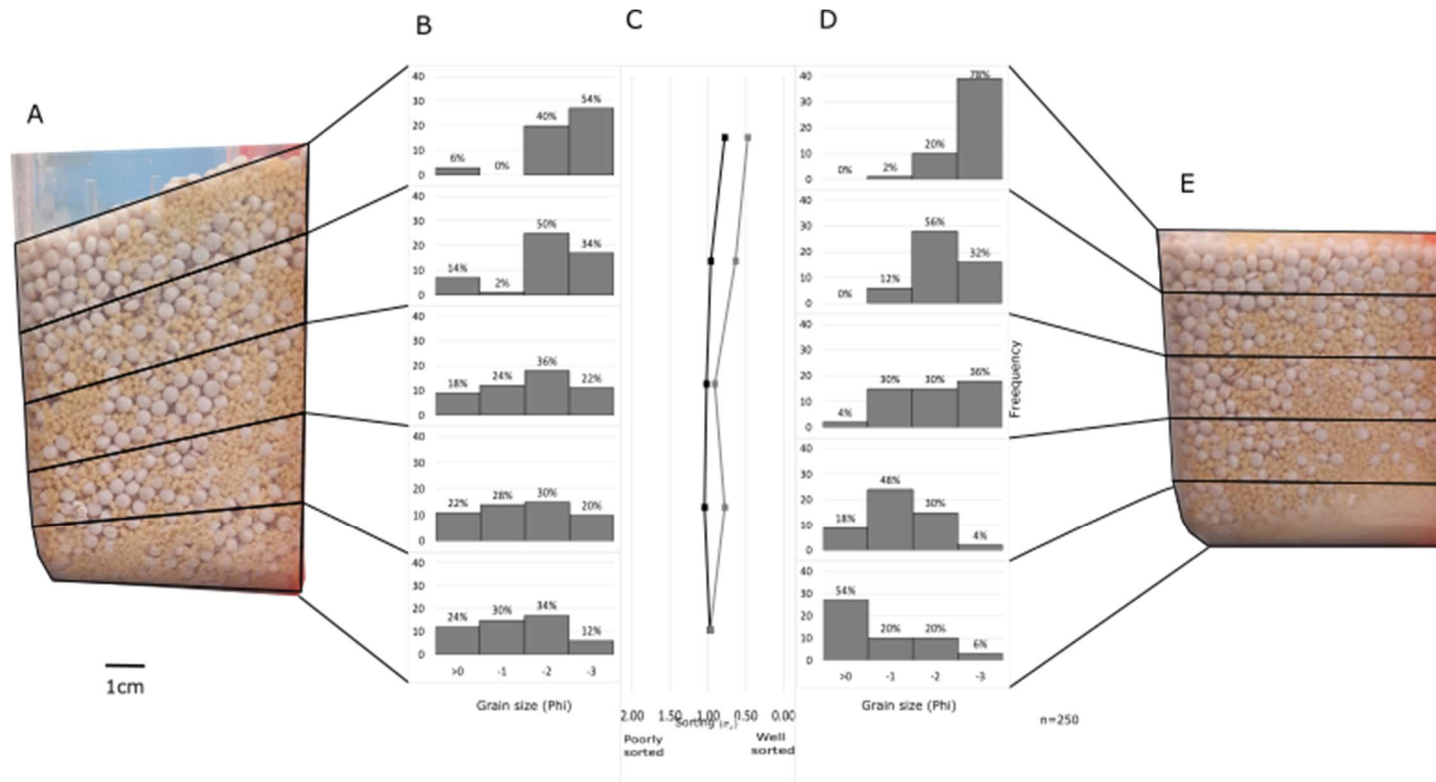


Figure 4.8 Grain size distribution of Type 1 coarse rich mix (using a mix of 10% semolina, 40% couscous and 50% giant couscous) before and after 2 minutes of shaking at 12000 rpm. (A) Type 1 fines rich mix before shaking occurred, split into five equal subsections, (B) Grain size distribution of each deposit subsection before shaking, (C) Sorting values for the 5 subsections before (black) and after (grey) shaking, calculated using Gradistat, (D) Grain size distribution of each deposit subsection after shaking, (E) Type 1 coarse rich mix after shaking.

Video frames (Figure 4.7) collected from the experiment show that the segregation of the finest particles began as soon as shaking began and was practically completed within the first minute. In the first 90 seconds, the larger couscous grains show an overall vertical movement towards the surface., In the final 30 seconds the majority of these larger grains move more laterally than vertically.

Type 1 coarse rich experiments (Fig. 4.8) representing coarse lapilli-tuff use a mixture of 10% fine grains (semolina), 40% medium grains (couscous) and 50% coarse grains (giant couscous). Before shaking this deposit is shown to be a well-mixed deposit with a coarse top (Fig. 4.8A). Following 2 minutes of shaking however this deposit is now reverse graded, with each subsection upwards being slightly coarser than the one below. This is shown quantitatively in the grain size distribution graphs (Figure 4.8D) where the percentage of the smallest grain size available reduces from 54% to 0% from base to top. Meanwhile the coarsest size has increased from 6% to 78%. The grain size distribution charts for both before and after shaking show that before shaking the finest grain sizes were spread out across all subsections, however, after 2 minutes of shaking the finest grain sizes are only present between the base and the middle of the deposit with a majority in the basal subsection, a total of 71% of all >0 phi grains.

4.4.2. Type 2 experiments (different sizes, different densities)

Type 2 fines rich experiment (Fig. 4.9) uses mostly denser material (using a mix of 50% poppy seeds, 20% oats, 20% raisins and 10% nuts). Before shaking (Fig. 4.9A), this deposit shows no grading with each subsection showing broadly similar characteristics with a majority of fines, mostly around 55% of each subsection (Fig. 4.19B), representative of the mixture used. Following 2 minutes of shaking, the deposit (Fig 4.9E) shows reverse graded characteristics, most notably a very fine basal subsection and an abundance of larger grains at the uppermost section with average grain size for both subsections at 0.8 and 2.2 mm respectively.

Following 2 minutes of shaking, grains are segregated by both size and density, with denser grains showing to have a greater downwards movement than light particles of the same size. Figure 4.9A shows small dense (poppy seeds) grains to be well spread across all 5 subsections. Before shaking the basal subsection and uppermost subsection contain 34% and 36% of dense grains under 1 mm respectively, however after shaking this changes to 60% in the basal subsection and 12% in the uppermost subsection showing a large downwards movement in small dense grains.

Following shaking, the uppermost subsection shows an abundance of both medium and coarse grains larger than -2 Phi (4 mm) of which there appears to be a lack of in the mixture before any shaking took place increasing from 26% to 54%. The medium grains also appear to be graded in accordance with size as well, with an average grain size of oats for both subsections at 1.2 and 2 mm at the base and top respectively.

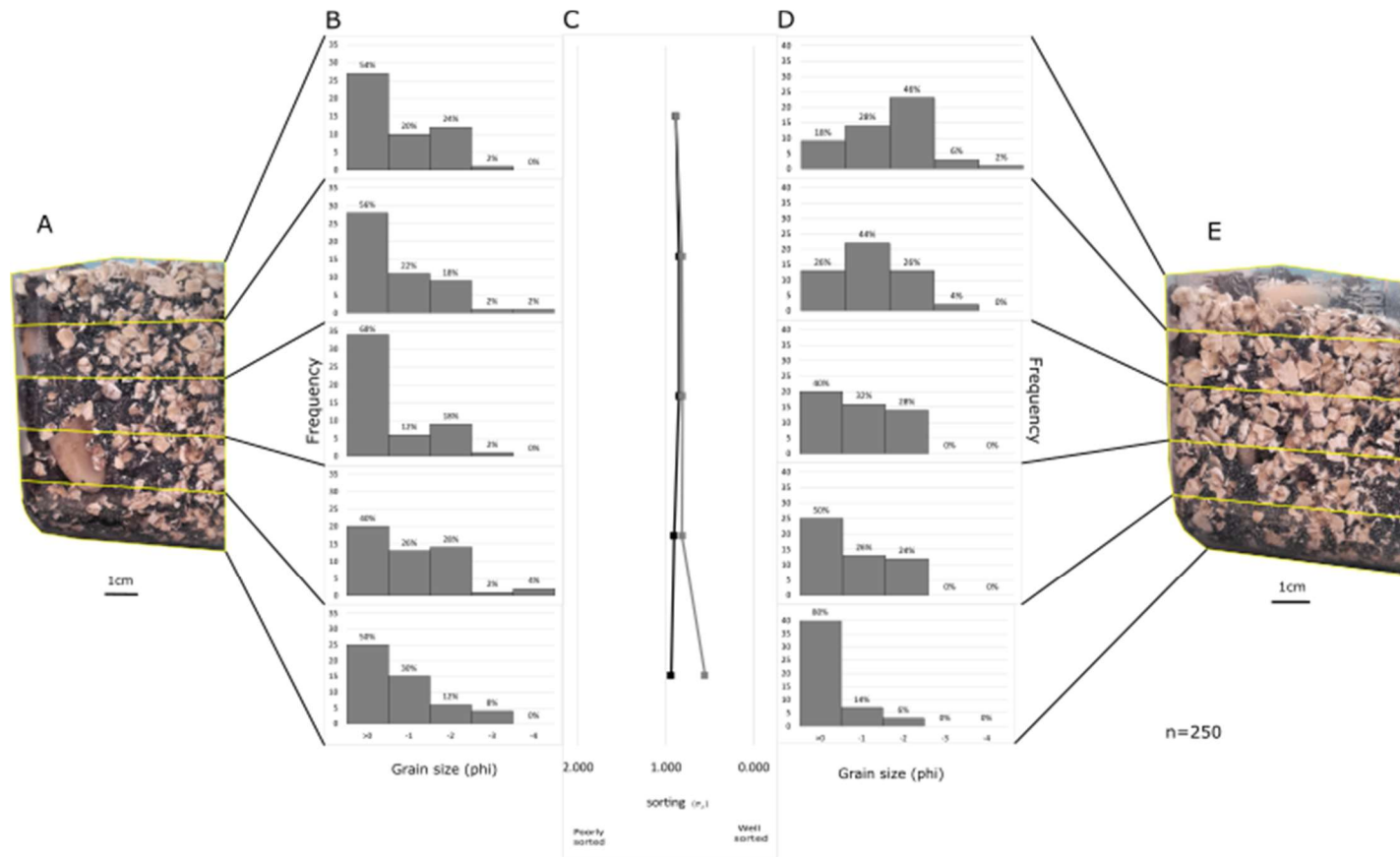


Figure 4.9 Grain size distribution of Type 2 fines rich mix (using a mix of 50% poppy seeds, 20% oats, 20% raisins and 10% nuts) before and after 2 minutes of shaking at 12000 rpm. (A) Type 1 fines rich mix before shaking occurred, split into five equal subsections, (B) Grain size distribution of each deposit subsection before shaking, (C) Sorting values for the 5 subsections before (black) and after (grey) shaking, calculated using Gradistat, (D) Grain size distribution of each deposit subsection after shaking, (E) Type 2 fines rich mix after shaking.

Type 2 uniform mix uses equal amounts of fine grains (poppy seeds), medium grains (oats), coarse dense grains (raisins) and coarse light grains (nuts). In this experiment the fine grains (poppy seeds) and coarse dense (raisins) represent lithic fragments due to their higher densities (2.61 g/cm^3 for poppy seeds and 1.56 g/cm^3 for raisins) and the oats and nuts with densities of 0.76 g/cm^3 and 1.11 g/cm^3 respectively, represent pumice fragments. Before shaking the mix shows no grading upwards as shown in the grain size distribution charts in Figure 4.10B where the finest material accounts for between 50 and 70 % of all clasts measured in all 5 subsections. After two minutes of shaking, grain size grading is now visible on the photo of the deposits, and this is supported by the grain size distribution charts which shows a 52% decrease in the two smallest grain sizes and a 36% increase in the two largest grain sizes from the base to the top of the deposit. In addition, the flat-shaped medium grains (oats) have also reversely graded from an average size of 2.1 mm at the base to 4.3 mm at the top. Furthermore, the top of the deposit after shaking shows that both the higher density coarse grains and the lower density coarse grains have emerged at the top. Some of the lighter grains have settled above the denser grains while some coarse light grains have not been able to rise past the coarse dense grains to the surface. Additionally, at the base small dense grains have shown a large migration downwards, from covering most subsections before shaking to having a large concentration in the basal two subsections after shaking.

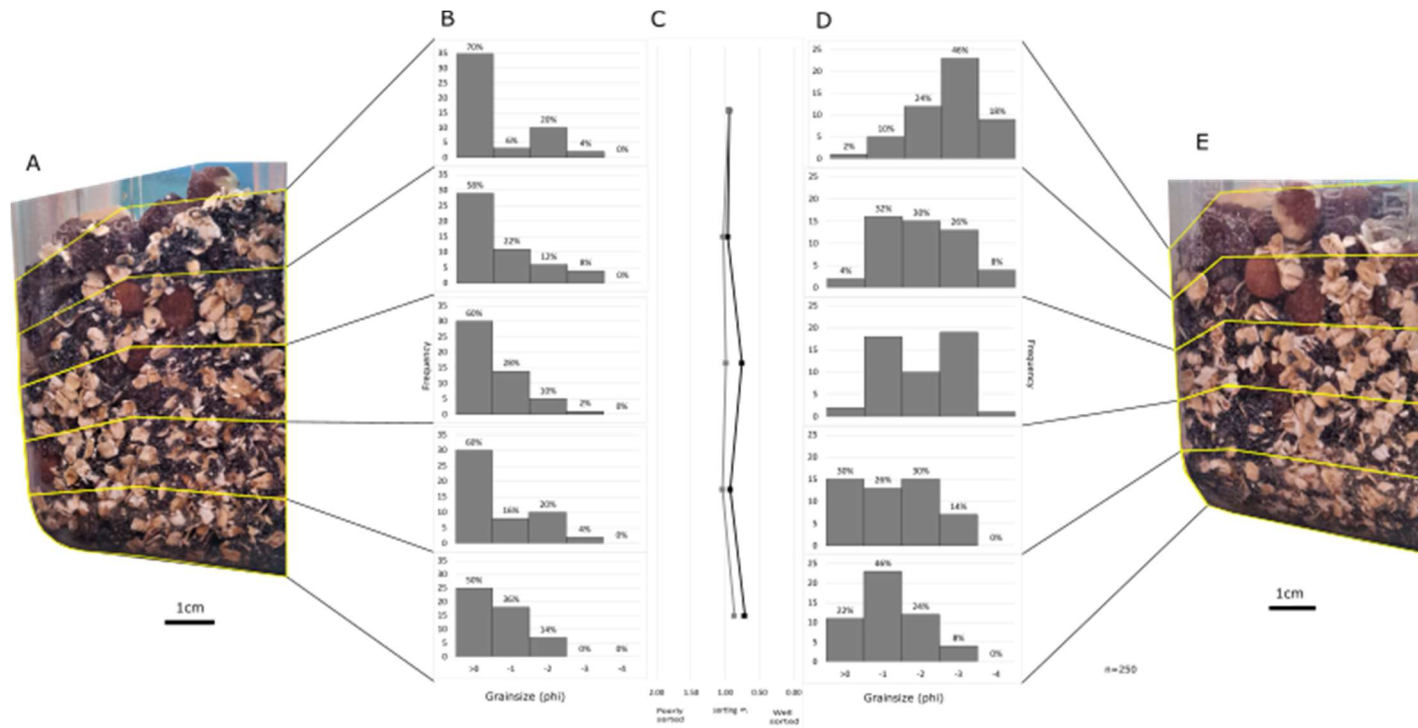


Figure 4.10 Grain size distribution of Type 2 uniform mix (using a mix of 25% poppy seeds, 25% oats, 25% raisins and 25% nuts) before and after 2 minutes of shaking at 12000 rpm. (A) Type 1 fines rich mix before shaking occurred, split into five equal subsections, (B) Grain size distribution of each deposit subsection before shaking, (C) Sorting values for the 5 subsections before (black) and after (grey) shaking, calculated using Gradistat, (D) Grain size distribution of each deposit subsection after shaking, (E) Type 2 uniform mix after shaking.

The downwards movement of smaller particles is captured using video collected during the experimentation. In Fig. 4.11 a movement of the higher density fine grains and smallest medium grains can be observed moving downwards to the lower left corner of the container over a period of 3.8 seconds. In these frames both light and dense particles are moving downwards at a fast rate. The dense fine grains percolated at a velocity of 18.5 mm/s meanwhile the fine oats percolated at 11.9 mm/s. In Fig.4.11 the process causing this movement is displayed. In 4.11A a gap between two larger particles is opening up while a pile of smaller particles rests above, at some stage between 4.11A and 4.11B the gap has opened fractionally more allowing the smaller particles to fall through as displayed in 4.11B.

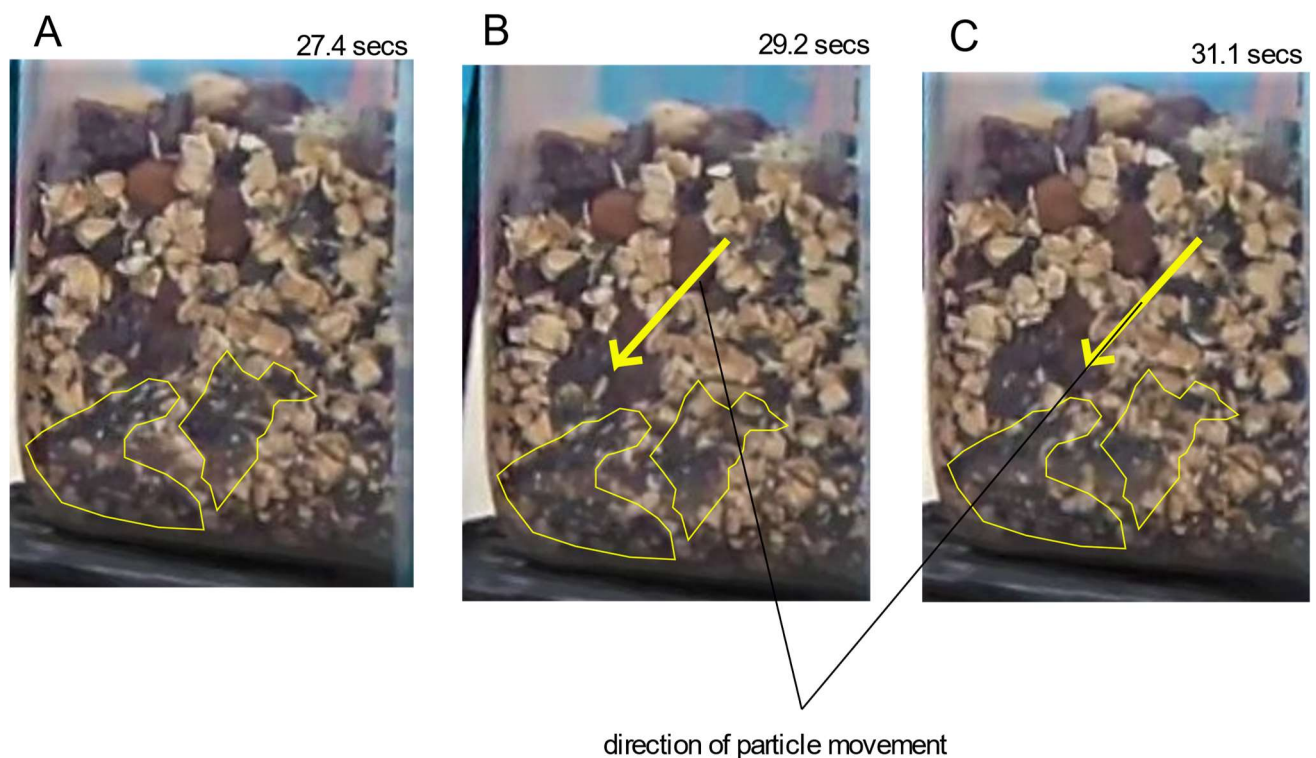


Figure 4.11 Frames of video footage showing the movement of small oats and poppy seeds in type 2 uniform mix. Yellow boundary marks the original spread of small grains in A with the same area overlain on B and C showing the difference in particle spread. Time in seconds is noted in the top right corner of each frame. (see supplementary [video 4.6](#))

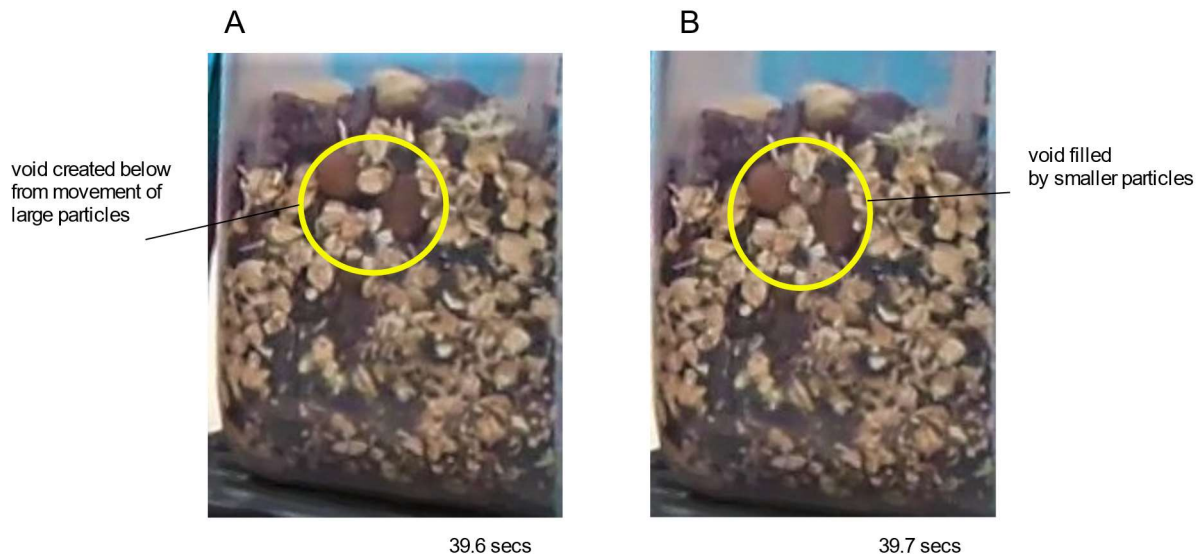


Figure 4.12 (A) video frame showing a gap created by the movement of two large grains with a pile of smaller grains resting on top. (B) a void opens slightly allowing the pile of smaller particles to fall and fill the gap created. Time in seconds is noted in the bottom right of each frame. (see supplementary [video 4.6](#))

Frames captured from type 2 uniform mix (Fig. 4.12) display how segregation occurs in the muesli effect. Figure 4.12A shows two large grains that have moved apart from each other creating a void between them, a pile of smaller grains are resting above this void. In the next frame, Fig. 4.12B the large grains have now moved far enough apart for the smaller grains to fall through and fill in the void created in Fig. 4.12A.

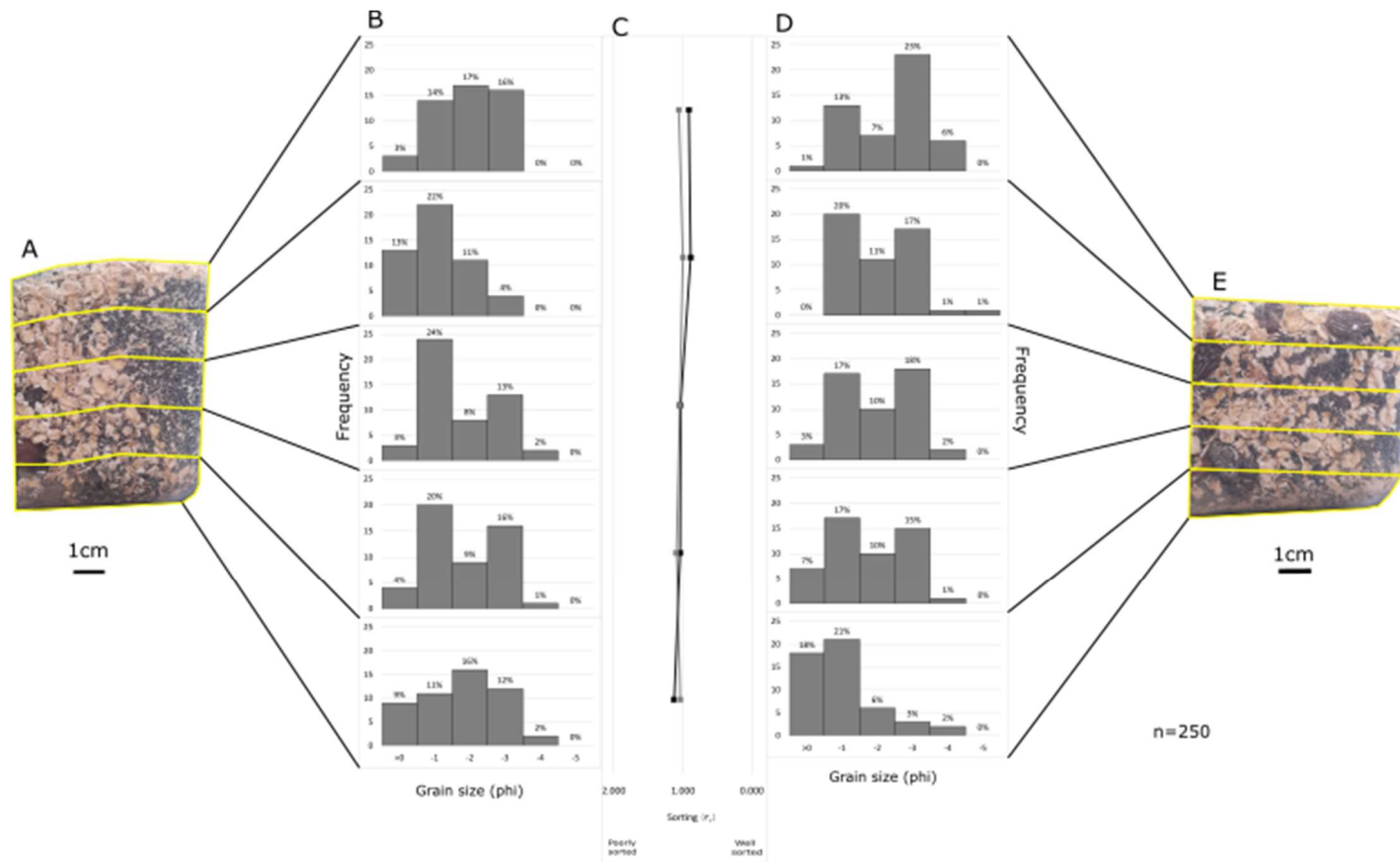


Figure 4.13 Grain size distribution of Type 2 medium rich mix (using a mix of 20% poppy seeds, 50% oats, 20% raisins and 10% nuts) before and after 2 minutes of shaking at 12000 rpm. (A) Type 1 fines rich mix before shaking occurred, split into five equal subsections, (B) Grain size distribution of each deposit subsection before shaking, (C) Sorting values for the 5 subsections before (black) and after (grey) shaking, calculated using Gradistat, (D) Grain size distribution of each deposit subsection after shaking, (E) Type 2 medium rich mix after shaking.

The different density medium rich experiment (Fig. 4.13) uses the coarsest mix of materials and a majority of lighter particles. Before shaking, the majority of the fine material is concentrated near the middle subsections of the mixture whilst the rest of the grains appear to be poorly sorted throughout. This is evident in the middle and second to top subsection where grains under 2 mm account for 54% and 70% of the total grains within each section respectively (Fig. 4.13B). This changes greatly following 2 minutes of shaking with grains under 2 mm only accounting for 40% of each of the respective subsections (Fig. 4.13D). Meanwhile, the base of the deposit has accumulated most of the smaller grains now accounting for 78% of the grain compared to 40% before. Whilst the uppermost subsection experienced the opposite where the number of grains over 8 mm has increased by 26%. The mid sections of the package after shaking (Fig 4.13E) show a high concentration of medium grains (oats) of 54-61% of the total subsections; within these subsections where there is little other material to interact with the medium grains have segregated amongst other medium grains according to size. This is shown by the size of the medium grains at the basal subsection averaging 1.8 mm compared to 5.5 mm at the uppermost section. Coarse dense grains show a greater upwards movement than the coarse light grains from before to after shaking in the medium rich experiments. Coarse dense grains are most prominent in the upper 2 subsections after shaking while the coarse light grains can no longer be seen. They are likely obscured by smaller grains.

Rates of movement for different grain types were determined by using ImageJ recording the distance travelled and time taken to calculate the rate. Data collected shows that the average speed of percolation for a small dense grain (poppy seed) was 18.5 mm/s, while a light grain (oat) would percolate at 11.9 mm/s. Additionally, the speed at which a large dense grain (raisin) would uplift was at 0.08 mm/s whereas a large light grain (nut) would uplift at 0.11 mm/s.

4.5. Discussion

Experiments demonstrate that the bigger the grain size difference the more likely grains are to segregate. All experiments also show that grain sizes with small diameter differences would eventually begin to segregate but at a much slower rate than grains with larger diameter differences. When different densities are used in addition to grain size grading, density grading is also introduced where clasts of the same size will separate due to density differences.

4.5.1. Impact of grain size of segregation

For the type 1 experiments, the average diameter of semolina/fine grains (D_f), couscous/medium grains (D_m) and giant cous cous/coarse grains (D_c) was 0.3 mm, 1.8 mm, and 4.2 mm respectively. Using d_s/D_l as defined by Sohn and Chough (1993) where, $d_s/D_l \leq 0.25$ instant segregation should occur.

Table 4.4 diameter differences D_s/D_l across all grains used in Type 1 experiments

Small grain diameter	Large grain diameter	d_s/D_l range
Semolina (0.3 mm)	Couscous (1.8 mm)	0.07
Semolina (0.3 mm)	Giant couscous (4.2 mm)	0.16
Couscous (1.8 mm)	Giant couscous (4.2 mm)	0.42

Each experiment showed that the fine grains began segregation from the coarse grains ($D_f/D_c = 0.07$) instantly and were almost completely segregated after 11 seconds of shaking, consistent with previously established percolation velocities of the fine grains between the coarse grains (Sohn and Chough, 1993). However, segregation of the fine grains from the medium grains ($D_f/D_m = 0.16$) was not instantaneous taking up to around 60 seconds to fully segregate. These grains should have segregated instantly as they were below the threshold limit (<0.25) which suggests that there is a range of rate of segregation below this limit linked to the diameter difference value.

The medium grains took 10 seconds to start segregating from the coarse grains ($D_m/D_c 0.42$) and they remained partially mixed at the end of the 2 minutes. This is consistent with the diameter difference being above the threshold value (<0.25) for instant segregation. However, even amongst similar sized particles segregation can occur and so as long as smaller particles exist they will eventually percolate through (Sohn & Chough, 1993) as evident in Fig. 4.7 which shows medium grains falling through gaps below the coarse grains, creating a reversely graded package with the finest grains at the base, medium grains on top, with a zone of mixing between fine and medium grains above and the coarsest grains at the top.

As also outlined in Sohn and Chough (1993), when compaction in the lower deposit begins there is limited opportunity for grain movement except by squeeze expulsion. This however was not witnessed within this experiment. Medium grains in the lower sections did not rise after the fine grains had percolated through, whilst the fine grains may begin to interlock with very little movement. When this happens there are no gaps opening above for a larger particle to be pushed up despite the forces being acted upon the grain outlined in the squeeze expulsion theory. In the experiment that used a majority of medium grains (type 1 medium rich mix), accounting for 50% of the whole mixture, segregation of the smallest grains (25 % of the mix) was fast (9 seconds), however, there was limited segregation of the larger grains (25 % of the mix). This may be due to the low concentration of the larger grains; it is the space between the large grains that enables percolation of the smaller grains and when the larger grains are more widely spaced, they are not in contact with each other and thus do not create pore spaces. Instead, when there are fewer coarse grains, they are matrix supported by the smaller grains and so there are fewer pore spaces available for percolation. This could perhaps suggest that in currents with lower concentrations of larger particles percolation as a means of sorting particles is not as efficient and leads to deposits that are not as well graded.

4.5.2. Role of density in segregation

In the different density experiments, a range of sizes shapes and densities of particles as experiments were used to consider how density affects the grain sorting and segregation. For the different density experiments the diameter of fine grains (poppy seeds) (D_f), medium grains (oats) (D_m) and coarse-light grains (nuts)(D_{cl}) and coarse-dense grains (raisins) (D_{cd}) was 0.5-0.8 mm, 0.5-9 mm, 4-11 mm and 9-15 mm respectively.

Table 4.5 diameter differences d_s/D_l across all grains used in Type 2 experiments

Small grain diameter ranges	Large grain diameter ranges	d_s/D_l range
-----------------------------	-----------------------------	-----------------

Poppy seeds (0.5-0.8 mm)	Oats (0.5-9 mm)	1-0.07
Poppy seeds (0.5-0.8 mm)	Nuts (4-11 mm)	0.07-0.04
Poppy seeds (0.5-0.8 mm)	Raisins (9-15 mm)	0.16-0.06
Oats (0.5-9 mm)	Nuts (4-11 mm)	0.8-0.06
Oats (0.5-9 mm)	Raisins (9-15 mm)	0.6-0.05

The finest grains began segregating from coarsest grains ($D_f/D_{cl} = 0.07$) instantly, consistent with the similar density experiments (d_s/D_l is ≤ 0.16). The medium grains segregated well from the coarse grains, whilst the finest medium grains fully segregated from the coarse grains with a diameter difference of 0.06 to 0.05, and the coarsest medium grains did not fully segregate from the coarse grains with a diameter difference of 0.8-0.6. Meanwhile the coarse light and coarse dense grains remained at the top with the coarse light partially segregated above the coarse dense.

The size segregation in the type 2 experiments has been shown to be so dominant that even among single clast types, size segregation is occurring. This is evident with medium grains in the Type 2 experiments which are shown to be reversely graded in the final deposit. The average size of the medium grains are larger in the top subsection than at the base. ranging from oats having an average grain size 0.8 mm larger at the top compared to the base in the fines rich experiment, and 3.7 mm larger at the top in the medium rich experiment.

In these experiments, coarse dense grains (raisins) and coarse light grains (nuts) had size ranges of 4-11 mm and 9-15 mm respectively. The coarse dense grains were 0.45 g/cm^3 denser than the coarse light grains. In all the different density mixtures, following the 2 minutes of shaking both coarse dense grains and coarse light grains had risen to the top of the deposit, tending to show that the coarse light grains would be on top of the coarse dense grains. This suggests that the importance of density of a particle is nearly as great as the importance of size. When there is little difference in grain size, the density become the dominant factor. Analysis of segregation rates revealed that there was a minor difference in the rate at which coarse grains moved, while raisins were uplifted at a rate of 0.08 mm/s , and nuts were uplifted at 0.11 mm/s .

In each experiment using the muesli (different density experiments) the dense, fine grains (poppy seeds) were well mixed and distributed throughout the mixture. Analysis of the video footage shows that the majority of the dense fine grains have percolated down through gaps created by the movement of medium sized grains (dense fine grains and medium grains with size ranges of 0.5-0.8 mm and 0.5-9 mm and densities of 2.61 g/cm^3 and 0.79 g/cm^3 respectively). Comparisons between the percolation rates of medium grains measuring between 0.5 and 0.8 mm and the fine grains reveal differences in percolation rates. The dense fine grains percolated at a velocity of 18.5 mm/s meanwhile the fine oats percolated at 11.9 mm/s . Whilst both the dense and light grains measuring between 0.5 and 0.8 separated from the coarser grains, their final resting position was the dense grains at the base with the lighter grains on top with partial mixing between the two. This suggests that the size of the particle is still the most important factor in segregation as both light and dense are segregated according to grain size. When there is no size difference the density of the grain becomes the important factor in segregation.

In these experiments, we find that for segregation to begin instantly, the diameter difference between large and small grains must be $d_s/D_l < 0.16$ for materials with the same density. Whereas for denser small particles this may be as low as 0.16 but probably closer to the critical value of ≤ 0.25 determined by Sohn and Chough (1993). The exact critical threshold for instant segregation for the

small dense clasts could not be determined due to the large size ranges in the material. Additionally, we find that the critical value for segregation is modified based on size and shape.

4.5.3. Impact of shape on segregation

Oats are tabular, not spherical, meaning they have a shorter axis that can measure less than 0.5 mm (the diameter of the smallest grains). When the grains move during shaking, if they approach a gap large enough to fit the smallest axis through they will be likely to fall through (Fernlund, 1998) giving them the ability to fall into smaller gaps where the fine grains are expected to percolate through. Grains with a spherical shape have higher mobility than angular clasts, along with local bridging of particles, this allows for a high initial rate of segregation of fine spherical particles. As the bridges collapse and the fine particles form a more stable structure with low void spaces, the rate of segregation for spherical particles will reduce. whereas for angular clasts the lower mobility slows down the segregation in the initial phase. Due to their shape, angular particles will have higher void spaces as the settling structure changes allowing for a continued relatively high segregation rate in comparison to the later phase of spherical particle movement (Jha et al., 2008; Shimosaka et al., 2013). In the type 2 experiments, it was observed that the dense fine grains (poppy seeds, spherical) were the first to settle at the base followed by the medium grains measuring less than 0.8 mm (oats, angular). These results agree with the conclusions of Jha et al. (2008) that the spherical grains have the higher initial percolation velocity. However, with the added density difference it remains unclear whether the shape or density played the biggest role in the segregation rate.

Sorting among the tabular shaped medium grains in the type 2 experiments show that among particles of a similar shape, segregation occurs similarly to that of spherical grains in type 1 experiments. with grains sorting according to size with no shape or density difference, size becomes the only remaining factor in segregation.

4.5.4. Sorting

Sorting values across the type 1 experiments tend to remain between 0.5 and 1.0 which is defined as moderate to moderately well sorted, except for medium rich mix which ranges from 0.78 to 1.73, described as poorly sorted. The uniform mix and fines rich mix both show a trend of better sorting at the base gradually increasing to poorly sorted at the uppermost subsection. However, the medium and coarse rich mixes both show to be most poorly sorted at the base.

Type 2 experiments all share values between 0.8 and 1.1 (moderate to poor sorting) with the base of the fines rich mix showing a lower value indicating better sorting. All type 2 experiments show marginally better sorting at the base than the top, with the fines rich mix showing the largest differences (0.82), and the medium rich mix showing the smallest difference (0.019).

Both type 1 and type 2 experiments indicate that packages with a larger concentration of finer grains are sorted better than those with coarser grains. Packages rich in medium grains show overall poorer sorting than other packages suggesting lower levels of segregation in medium rich mixtures.

Type 2 experiments showed poorer sorting within the mid subsections which were dominated by medium sized grains. Along with the poor sorting in medium rich experiments this would suggest that medium sized angular grains have a negative impact on segregation.

The Type 1 medium rich experiment is the poorest sorted and shows poor grading. Fines rich mix results are the best sorted throughout, but grading is hardest to see, By eye it appears to be uniform throughout, however, digital analysis shows regular grain size increases. Type 1 coarse becomes

increasingly well sorted upwards and shows the best grading of all type one experiments. Type 1 uniform mix shows moderate to poor sorting throughout but also shows good grading.

Type 2 medium rich mix showed the poorest grading of the type 2 experiments while the fines rich show the best grading and the uniform mix is similarly graded to the fines rich mix.

When the same image data analysis techniques were used to characterise deposits of real ignimbrites a range of sorting values from $0.5 \sigma_\phi$ to $1.5 \sigma_\phi$ (moderately well sorted to poorly sorted) were recorded. In real ignimbrites, we find that finest grained deposits present as better sorted than coarser deposits with the sorting values ranging between $0.5 \sigma_\phi$ and $1.0 \sigma_\phi$, whereas a slightly coarser grained deposit ranged between $0.7 \sigma_\phi$ and $1.5 \sigma_\phi$. Both fine-grained packages from type 1 and type 2 experiments presented with sorting values between $0.5 \sigma_\phi$ and $1.0 \sigma_\phi$ matching with what is expected of a real ignimbrite. Coarser deposits of real ignimbrites had sorting values between $0.5 \sigma_\phi$ and $1.5 \sigma_\phi$, with some sorting better at the top whilst others sorted better at the base. The type 1 coarse experiment showed that sorting became better upwards, while the type 2 coarse experiment shows that the sorting stays similar throughout the final resting position.

The uniform mix and medium rich mix in the type 1 experiments show sorting values between $0.4 \sigma_\phi$ to $1.2 \sigma_\phi$, and $0.8 \sigma_\phi$ to $1.7 \sigma_\phi$ respectively, which is comparable to deposit 3 in the real ignimbrite deposits which are rich in pumice and ash (80%), which is generally a similar density comparable to the type 1 experiments. Type 2 uniform mix is most comparable to deposit 4 of the real ignimbrites in terms of grain size variations. Both show to be poorly sorted, however, the real ignimbrite shows to be more poorly sorted than the experiment.

Overall, the experimental packages sorting data is fairly similar to the sorting data collected from real ignimbrites, particularly among the finer and coarser packages with small differences across the medium sized grains.

4.6. Conclusions

The experimental deposits created using these shake table experiments have allowed for detailed quantitative and qualitative data on the characteristics of reverse grading created by kinematic sieving. It has allowed for quantification of percolation in mixtures of the same density, analogous to pyroclastic material mixtures comprising ash and pumice lapilli and in mixtures of different densities and grain shapes, analogous to more complex ignimbrites. The experiments have provided data on how changing grain size and increasing density may impact the sorting of grains within a static system and the relationship that has to reverse grading within a deposit. In the next chapter, we explore how mixtures of varying grain size and density are sorted in a dynamic setting, and how this results in variably graded deposits.

5. Experimental analysis of particle sorting in fluidised conditions

5.1 Introduction

Pyroclastic density currents (PDCs) are particle laden currents produced by the gravitational collapse of lava domes, lateral explosion or fallback of eruption columns (Druitt, 1998; Branney & Kokelaar, 2002). Studying of field deposits of PDCs 'ignimbrites' show that most ignimbrites are relatively poorly sorted, typically containing a continuous range of grain sizes from many centimetres down to a few microns (Sparks, 1976). Ignimbrites commonly show reverse grading of low density pumice clasts and normal grading of high density lithic clasts (Sparks, 1976; Smith & Kokelaar, 2013). Therefore, it seems probable that grading is largely the result of the density contrast of individual fragments within the pyroclastic density current, with the matrix often denser than large pumice clasts (Sparks, 1976). Lithics have a much greater density than the matrix (Cas & Wright, 1987) and it is proposed that the principal mechanism of normal grading is gravitational settling (Sparks, 1976). Sparks (1976) also notes that reverse grading of lithics was seen in thinner deposits and that erosion removes much of the unconsolidated ignimbrites at the top, suggesting large lithic clasts may be lost here possibly skewing the data. These interpretations come from observations and interpretation of field deposits, to investigate the transport and deposition mechanisms of PDCs, volcanologists used modelling. Thus far, modelling has suggested that several different processes could be responsible for the reverse grading of ignimbrites. These processes include dispersive pressure, kinematic sorting, waxing and waning. However, these mechanisms have not been tested experimentally in aerated granular currents.

5.1.1 Aims

This chapter aims to investigate whether the muesli effect is responsible for particle sorting within fluidised granular currents.

5.1.2 Objectives

- The aim will be met through the following objectives
- To create reversely graded deposits using a gas fluidised flume
- To characterise the reverse graded deposits created in the flume using image analysis
- To investigate flow boundary behaviour to further understand how reverse graded deposits are made.

5.2 Background

In Chapter 3, six different reversely graded ignimbrites were characterised and we found that across all 6 deposits studied the pumices were 2.2x larger at the top compared to pumices at the base, whereas lithic clasts were 2.3x larger at the top than lithics at the base (excluding deposit 6 which shows a much larger size difference, the average is 1.84x larger). The relative size differences between pumices and lithics within the ignimbrites studied in Chapter 3 suggest that the ability of a clast to segregate is not just affected by grain size. Characterisation of reverse grading revealed that differences in density may affect sorting, with the denser lithic particles experiencing a smaller degree of sorting in comparison to pumices. The image analysis also revealed that deposits can often be described as moderately well to moderately poorly sorted as opposed to the observations often made in the field where deposits are described as poorly or very poorly sorted (Shultz, 1984; Palladino & Valentine, 1995; Brown & Branney, 2004a).

Following the characterisation of ignimbrites, investigation began on characterising and quantifying deposits created through kinematic sieving (Chapter 4). This was completed using mixtures of muesli. The shake table experiments revealed that much like in the ignimbrites, both light and dense

particles were reversely graded, furthermore the lighter grains were also experiencing a greater degree of sorting. The shake table experiments used two sets of experiments, one set where the density of grains was kept equal and another where different density particles were used. We find that in experiments where there was no density difference and only a grain size difference, grains would begin to segregate instantly when they had a diameter difference of D_s (small)/ D_l (large) that was under 0.16, whereas above this threshold grains took longer to segregate. However when grains are the same size but different densities, we find that small dense particles would percolate down faster than small light particles, and for a dense particle the diameter difference of D_s/D_l required was 0.25, the same threshold as proposed by Sohn and Chough (1993). Furthermore, ignimbrite characterisation showed that reversely graded ignimbrites have sorting values ranging between 0.5 and 1.5 and experimental kinematic sorting packages have sorting values ranging from 0.5-1.7. These findings suggested that a relationship between kinematic sorting and reverse grading in ignimbrites could be proposed. However, the static shake table experiments do not reflect a flowing fluidised current as we would expect from a PDC. In order to address this, we needed to investigate the sorting of clasts in a dynamic fluidised flume experiment.

PDCs are too dangerous to be investigated close up during flow, and as a result, they must be investigated by conducting detailed analyses of field deposits and through analogue or computational modelling. Investigation of grain size sorting has often been the subject of granular material studies (Bagnold, 1954; Hand, 1997; Möbius et al., 2001; Choux & Druitt, 2002; Choux et al., 2004). A variety of techniques has been used in previous studies to model granular currents including unfluidized 'dry' currents (Bagnold, 1954; Savage & Lun, 1988), shaking or rotating of granular material (Cagnoli, 2005; Schnautz et al., 2005), and using fluidisation (Choux & Druitt, 2002). More recently gas fluidisation has been used to model PDCs in flumes (Rowley et al., 2014; Smith et al., 2018; Smith et al., 2020). In this gas fluidisation method, long lived high pore pressure can be simulated through continuous gas fluidisation (Rowley et al., 2014). Fluidisation is achieved by injecting gas vertically into a granular bed, creating a condition whereby the drag exerted by the gas counterbalances the weight of the particles, at which point intergranular friction is lost and the bed behaves in a liquid-like manner (Gilbertson et al., 2008; Rowley et al., 2014). The velocity at which this occurs is termed the minimum fluidization (U_{mf}) velocity. When the gas flux through the sediment is less than the U_{mf} the sediment is partially fluidized and termed aerated (Smith et al., 2018). Volcanic ash that forms the matrix of many ignimbrites belongs to Group A of Geldart's Classification (Geldart, 1973), where it expands homogeneously when fluidized at gas velocities above U_{mf} until gas bubbles form (minimum bubbling velocity). The gas velocity at which bubbles form is shown as U_{mb} . Previous works using gas fluidisation have used glass ballotini beads measuring $\sim 63 \mu\text{m}$ (Smith et al., 2018; Smith et al., 2020) and $75 \pm 15 \mu\text{m}$ (Rowley et al., 2014). In these previous experiments data was collected on current behaviour, depositional behaviour, and the effect of variable aeration. There is yet to be data collected on the depositional behaviour of polydisperse sediments focussing on quantifying reverse grading within deposits.

5.3 Methods

5.3.1 Flume set-up

The experimental flume shown in Figure 5.1 is a modified version of the flume used in Smith et al. (2018). In this setup, a hopper sits 0.64 m above a ramp (inclined at 40°) leading into a flume 0.15 m wide and 3.0 m long. The flume is constructed of three separate 1.0 m sections, each with its own compressed air supply fed into the flume via a porous plate. Smith et al. (2018) found that 75 l/min was the minimum amount of air required for U_{mf} at grain sizes of 45-90 μm (the smallest grain size used here). Through trial runs, starting at 75 l/min and building up from there, we found that an air

supply of 100 l/min was able to fluidise a current containing the larger grain sizes (see Table 1). Based on these findings the air supply was set to 100 l/min ($>U_{mf}$) in chamber 1 (proximal, below the hopper), 60 l/min ($<U_{mf}$) in chamber 2 and 0 l/min (unfluidized) in chamber 3 (distal) in all experimental runs. The variable air supply was designed to form an aerated current in the first chamber, which deaerates rapidly into the second chamber promoting deposition in chambers 2 and 3. Gas supply is terminated when a deposit aggrades past the second chamber to prevent significant re-fluidisation of fines in the deposit.

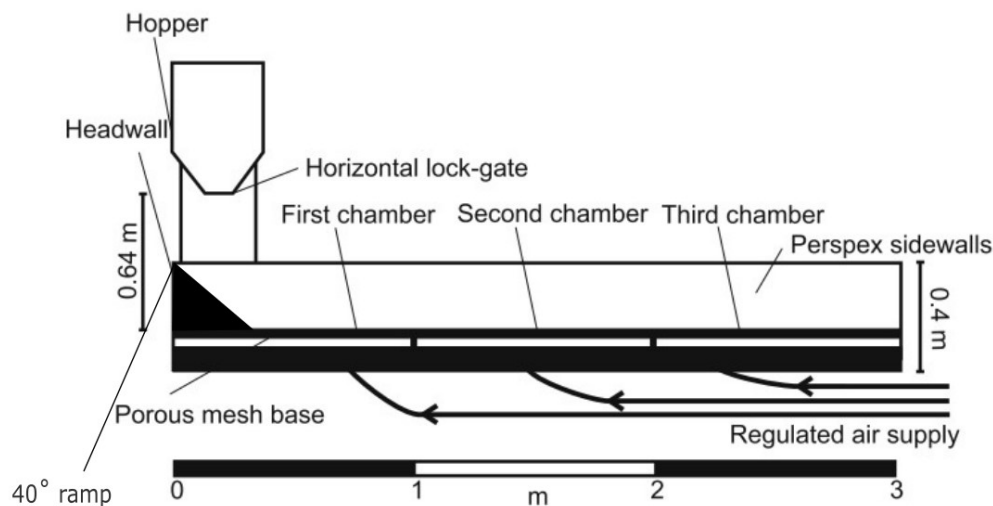


Figure 5.1 longitudinal section of the experimental flume

The experiment uses a hopper to produce a mass flux of $\sim 1.4 \pm 0.2$ kg/s. Material is released onto a 40° ramp installed below the hopper to direct the charge across the flume. The flume base has a 2° downward slope.

5.3.2 Analogue density current material

These experiments were performed using two different types of materials: spherical glass beads of matched particle density but classified grain sizes, and spherical aluminium oxide beads of higher density. Different colours were used for different sized beads to ensure each size range is easily distinguishable from others, and colours are shown in Table 5.1. The beads were sieved before experimentation to ensure the selected size ranges were achieved.

The bulk of each charge (50%+) always comprised 45-90 micron diameter glass beads, the size equivalent to sediment used in previous works (e.g., Rowley et al 2014, Smith et al 2020). This percentage was chosen as it was the lowest percentage of fine particles at which the currents using coarser particles can remain fluidised. A range of mixtures (Table 5.2) with increasing percentages of coarser particles was used to examine how increasing grain size impacts grading. Along with grain size changes, denser particles of aluminium oxide were incorporated into the currents to represent lithic fragments within a PDC to investigate how dense particles behave compared to lighter particles.


Mix 1 is comprised of 45-90 μm beads allowing for comparison to the results collected in Smith et al. (2018) to examine how adding a ramp to the flume affects the behaviour of the current. Each

mixture is premade by weighing out beads using digital scales with an accuracy of ± 0.01 g; the material is mixed before being poured into the hopper and is released at 1.4 ± 0.2 kg/s.

Table 5.1 Types of beads used in flume experiments

Material	Size range (μm)	Median diameter (μm)	Particle Density (g/cm^3)	Bead colour
Glass	45-90	67.5	2.5	White
Glass	125-425	275	2.5	Orange
Glass	425-600	512.5	2.5	Green
Glass	600-800	700	2.5	Purple
Aluminium Oxide	125-425	275	3.0	Black
Aluminium Oxide	425-600	512.5	3.0	Black

Table 5.2 Different mixes of beads used in the flume experiments, colour is used to distinguish between mixes in following tables and figures.

Mix Number	Mix Characteristics by % weight	
1	100% 45 μm -90 μm	Finest  Coarsest
2	80% 45 μm -90 μm 20% 125 μm -425 μm	
3	60% 45 μm -90 μm 20% 125 μm -425 μm 20% 125 μm -425 μm (dense)	
4	80% 45 μm -90 μm 20% 425 μm -600 μm	
5	60% 45 μm -90 μm 20% 125 μm -425 μm 20% 425 μm -600 μm	
6	50% 45 μm -90 μm 30% 125 μm -425 μm 15% 425 μm -600 μm 5% 600 μm -800 μm	
7	60% 45 μm -90 μm 20% 425 μm -600 μm 20% 425 μm -600 μm (dense)	
8	50% 45 μm -90 μm 30% 125 μm -425 μm 20% 425 μm -600 μm 10% 600 μm -800 μm	

5.3.3 Experimental runs

Thirty-one experiments were completed using different mixtures (Table 5.2) to represent increasing grain sizes to investigate how changes in grain size may impact the grading seen in a deposit. Each experiment had a minimum of 3 runs all under identical conditions.

Table 5.3 Experimental runs with mix number (mix numbers are colour coded, matched with those outlined in Table 5.2)

Experiment number	Experimental mix
1	4
2	5
3	5
4	5
5	5
6	5
7	4
8	4
9	6
10	6
11	6
12	8
13	8
14	8
15	8
16	8
17	6
18	1
19	1
20	1
21	2
22	2
23	2
24	7
25	7
26	7
27	7
28	2
29	3
30	3
31	3

5.3.4 Documentation

Experiments were recorded using a full HD (1920 x 1080 p) Go Pro camera at 240 frames per second (fps). Camera recordings were done with 3 different setups, first was encompassing the whole

flume, this way current velocities and mass flux calculations can be collected for each mix. The second setup records the current over 30 cm between 40 cm and 90 cm and the third setup records 30 cm between 70 and 120 cm, both to capture deposit formation. The locations for the last two setups are decided based on where the deposits form in run 1, this way data can be collected following individual packages within the current.

Following each run, high quality photos using a full HD camera were taken along the side wall of the flume and the top of the deposit.

5.3.5 Image Analysis

Following experimentation, analysis of the images was conducted using both qualitative and quantitative analysis. With the exception of a handful of experiments (see below), all deposits were analysed with the following techniques:

Qualitative characterisation of deposit architecture

The architectural characterisation was completed, highlighting important features in the deposit, by annotating stratigraphic patterns and relationships with linework using Inkscape software. Features identified include different types of graded packages and sedimentary bedforms.

Quantitative characterisation of sorting and grading

Reversely graded packages identified were characterised further using JMicrovision to measure grain size and Gradistat to calculate the level of sorting, following the methodology laid out in Chapter 3.2.2 above.

General characteristics

In addition to characterisation within graded packages, distance from the source, height in deposit and type of bedding of each graded package is also recorded and examined to determine common factors between types of grading.

Experiments using only 45 μm -90 μm and 425 μm -600 μm beads were not quantitatively characterised due to the green colour of the coarser 425 μm -600 μm beads not showing well in photos of the deposit, making for a difficult and possibly inaccurate collection of results. In addition, the experiments using 100% 45 μm -90 μm beads only underwent a basic analysis as any internal architecture was invisible to the camera. A general deposit profile and velocity measurements were collected to be used as a baseline for comparison to other mixtures.

5.3.6 Video analysis

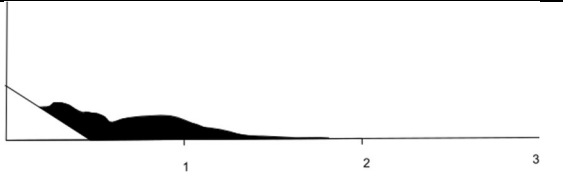

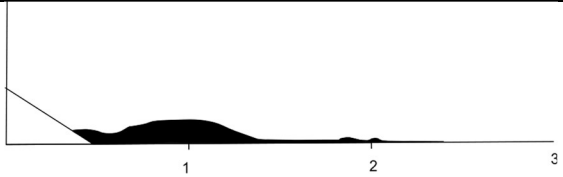
Video footage is examined, recording initial velocities of the current and velocities for different graded packages, calculated by measuring travelled distance using Image J. Additionally, any identifiable particle interactions are recorded to generate a detailed account of how graded packages form under the various experimental conditions. This data is used to analyse any effects of velocity on bedforms and grading. All raw video files are available as a supplementary dataset at : [<https://www.youtube.com/playlist?list=PLR9QBAlPJ3f7BDcuU04b5ns914f54kgcY>]. Photos of deposits from each experiment are available as a supplementary dataset at: [<https://www.flickr.com/photos/198477086@N07/albums/with/72177720308992452>]

5.4 Results

5.4.1 Deposit analysis

Analysis of video footage and photo evidence was used to define typical deposit profiles. Each experimental deposit was sketched highlighting all key features such as reverse graded packages and bedforms. In these sketches it was found that deposits could be characterised by 3 deposit profiles, each profile with distinct characteristics linking to the overall shape of the deposit and internal structure (Table 5.3).

Table 5.4 sketches of deposit of profiles A, B and C with descriptions of key features

	Sketch	Experiment numbers	Description	Notes
A		3,4,7,8,9,10,11,12,13,15,16,17,27,31	Most common deposit profile seen typically reaching between 160-190 cm. Forms thick deposit between 40 and 115 cm then rapidly thins out distally.	The most common type of bedding observed is shallow backset and steep backset bedforms. Average velocity 0.84 m/s
B		1,2,5,6,14,21,23,24,25,26,29,30	Generally, a flatter profile than deposit A, a very fast forming deposit. Deposition during flow is centred around 50-130 cm, deposit then thins out to approx. 1-2 cm before 2 nd peak at 200 cm. Max runout of 220 cm. Deposit often begins remobilizing before all sediment is released from the hopper, leading to a thick deposit of unfluidized grains directly below the hopper on-ramp	Most common type of bedding is planar and shallow backset in thinner deposits, thicker deposits will show steep backsets Average velocity 0.96 m/s
C		18, 19, 20,22,28	The longest currents seen within experiments reaching 235-250 cm. The bulk of the deposit lies between 70 and 140 cm, rapidly thins out beyond bulk with 2 smaller peaks around 180 cm and 200 cm	This deposit formed within the 100% 45-90 micron currents. As all grains are the same size and colour bedding/grading could not be observed Average velocity 1.01 m/s

Average flow front velocities of the currents were calculated for each deposit profile shape; average current velocities differed by small amounts. Profile A had the slowest average current velocity at 0.84 m/s (range 0.62-1.00 m/s), Profile B was faster with an average current velocity of 0.96 m/s (range 0.81-1.11 m/s) and Profile C was marginally the fastest at 1.01 m/s (range 0.83-1.12).

Bedforms were analysed and characterised following Smith et al., 2020 with three bedform-types identified: Planar, Shallow Backset and Steep Backset. Planar bedding is defined by beds that are near parallel to the substrate ($<2^\circ$), shallow backset are those which have shallow stoss sides, and steep backset are those that have steep stoss sides (Fig. 5.2). Profile A – type deposits were predominantly built with backset bedforms (Fig 5.2) whilst profile B was often planar bedding. Profile C has too little bedform data to provide a representable internal structure although the deposit shape and speed may suggest it is most similar to Profile B and is likely planar bedding with shallow backsets.

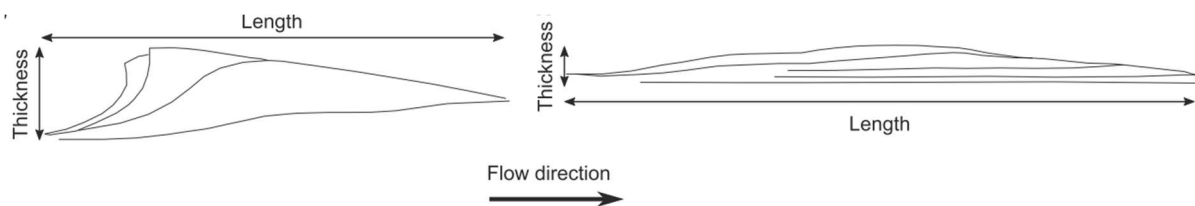


Figure 5.2 Sketches of steep backset bedforms (left) and shallow backset bedforms (right) (Smith et al., 2020)

Grading patterns (as defined by either systematic variations in grain size or grain density) were observed and characterised into three types: no grading, normal grading, and reverse grading. Deposit profile types contained a variety of grading patterns.

5.4.2 Experiments with varied grain size and same density particles

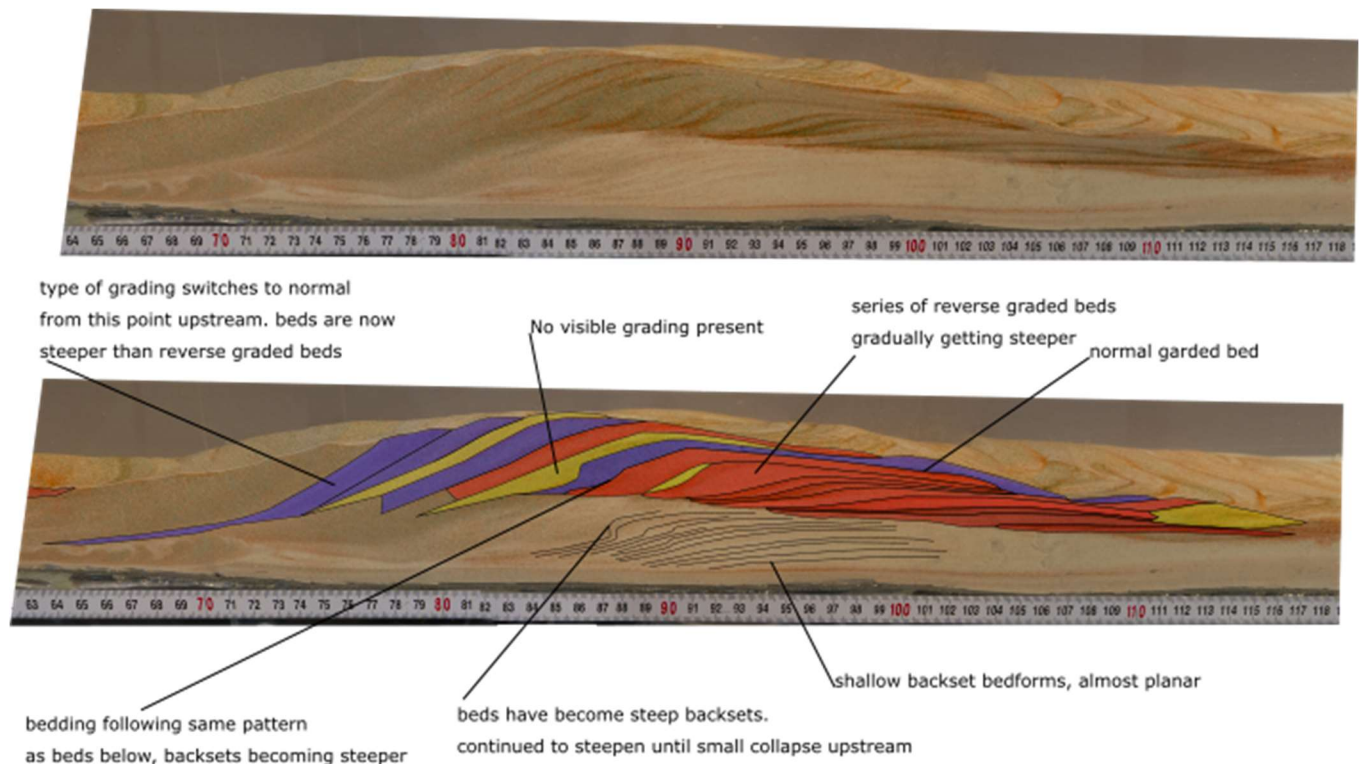


Figure 5.3 A) Profile type B deposit from experimental deposit 4, using Mix 5 (60% 45 μm -90 μm 20% 125 μm -425 μm 20% 425 μm -600 μm). B) Annotations on delineate bedforms and grading patterns visible (red = reverse grading, blue= normal grading, yellow = no grading).

The typical types of grading and bedforms seen within a profile B deposit are presented in Figure 5.3 (using mix 5 Table 5.2). In the lower portion of the deposit, beds are too thin to properly identify or measure any gradational changes, however, the top half of the deposit is constructed of thicker beds where detailed analysis of grading was possible.

The deposit shows that the type of grading changes upstream from reverse graded packages within shallow backset bedforms, to switching between reverse, none and normal grading as the beds become steeper, and finally to normal grading within the steep backset beds. This deposit shows how the grading and bedforms change upstream (Fig 5.3B) where the beds begin as planar beds, but then begin to develop backsets which gradually become steeper until they collapse upstream due to gravity.

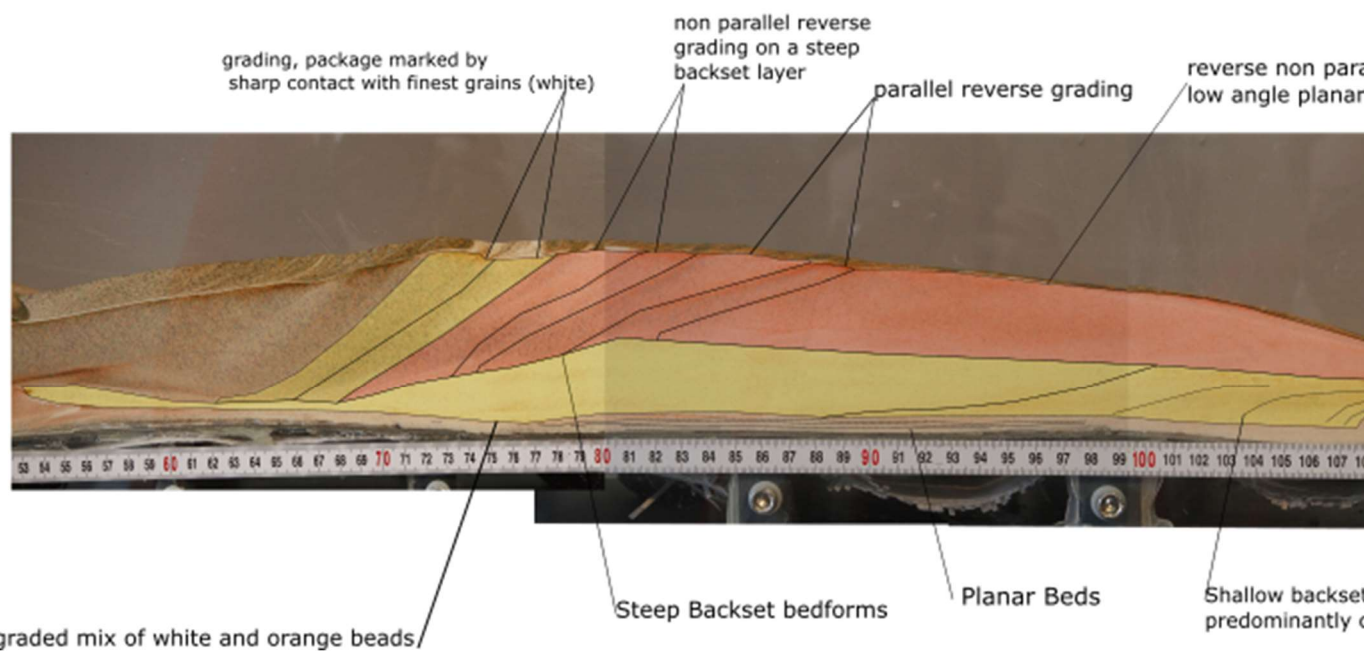


Figure 5.4 (A) Experimental deposit 14 using mix 4 (50% 45-90 μm white beads, 30% 125-425 μm orange beads, 20% 425-600 μm green beads and 10% 600-800 μm purple beads). (B) photograph of experiment 14 deposit with sketch overlain showing types of grading and bedforms present. Red shading indicates reverse grading and yellow shading indicates no grading; this picture shows no normal grading however it was observed more distally in the deposit.

Within deposit 14 (Fig. 5.4) beds are either reversely graded or not graded at all. The further upstream in this deposit, the less prevalent the grading is, moving from strong parallel grading in the shallower beds to non-parallel somewhat weak grading within the steeper beds and eventually no grading in the steepest beds. A rather similar pattern to the deposits shown for mix 2.

Beyond 135 cm the deposit became too thin to clearly see any type of grading, however, from above and the side the deposit appeared to be mostly fines, but when the top layers were brushed away, coarser grains were found beneath showing it to be normally graded.

5.4.3 Experiments with varied grain sizes and different density

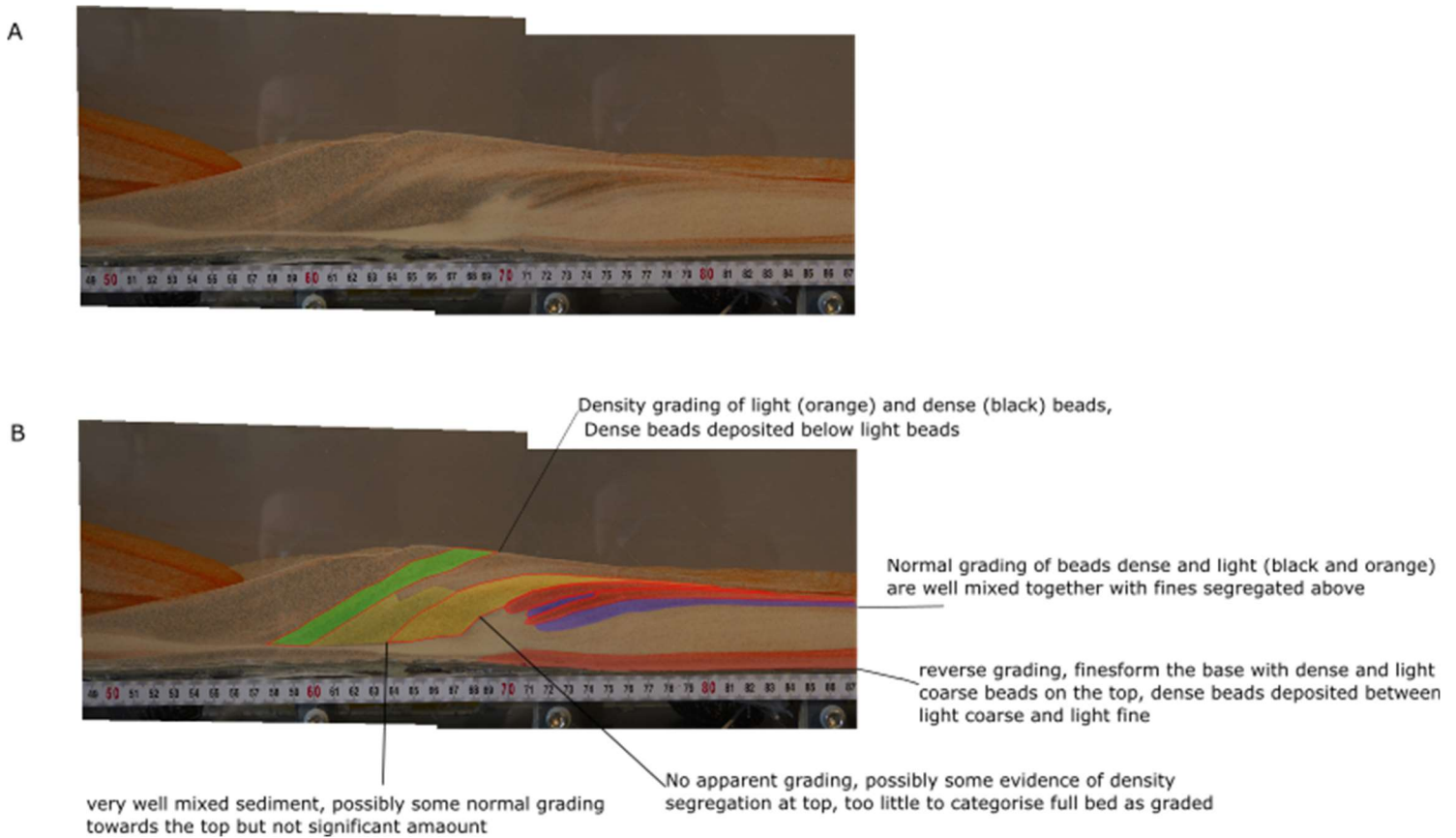


Figure 5.5 (A) Deposit from experiment 31 using a mix of 60% fines (White), 20% medium light beads (Orange), and 20% medium dense beads (Black)

As within the non-dense currents, the deposit from experiment 31 contains normal grading, reverse grading of grain sizes and areas of no grading. However, the addition of denser particles introduces grading by density within beds as demonstrated in the bed highlighted in green in fig. 5.5. Though both the orange and black beads are the same size (125-425 microns) the denser black beads have deposited below the lighter orange beads. These reverse graded beds, highlighted in red in Figure 5.5, shows the separation of the coarser beads, which are 125 μm -425 μm , from the finer beads measuring 45 μm -90 μm . Within these reverse graded beds, there is also the separation of the dense black beads from the lightweight orange beads of the same size where the dense beads are deposited below the light coarse beads and above the fine grains.

5.4.4 Bedforms

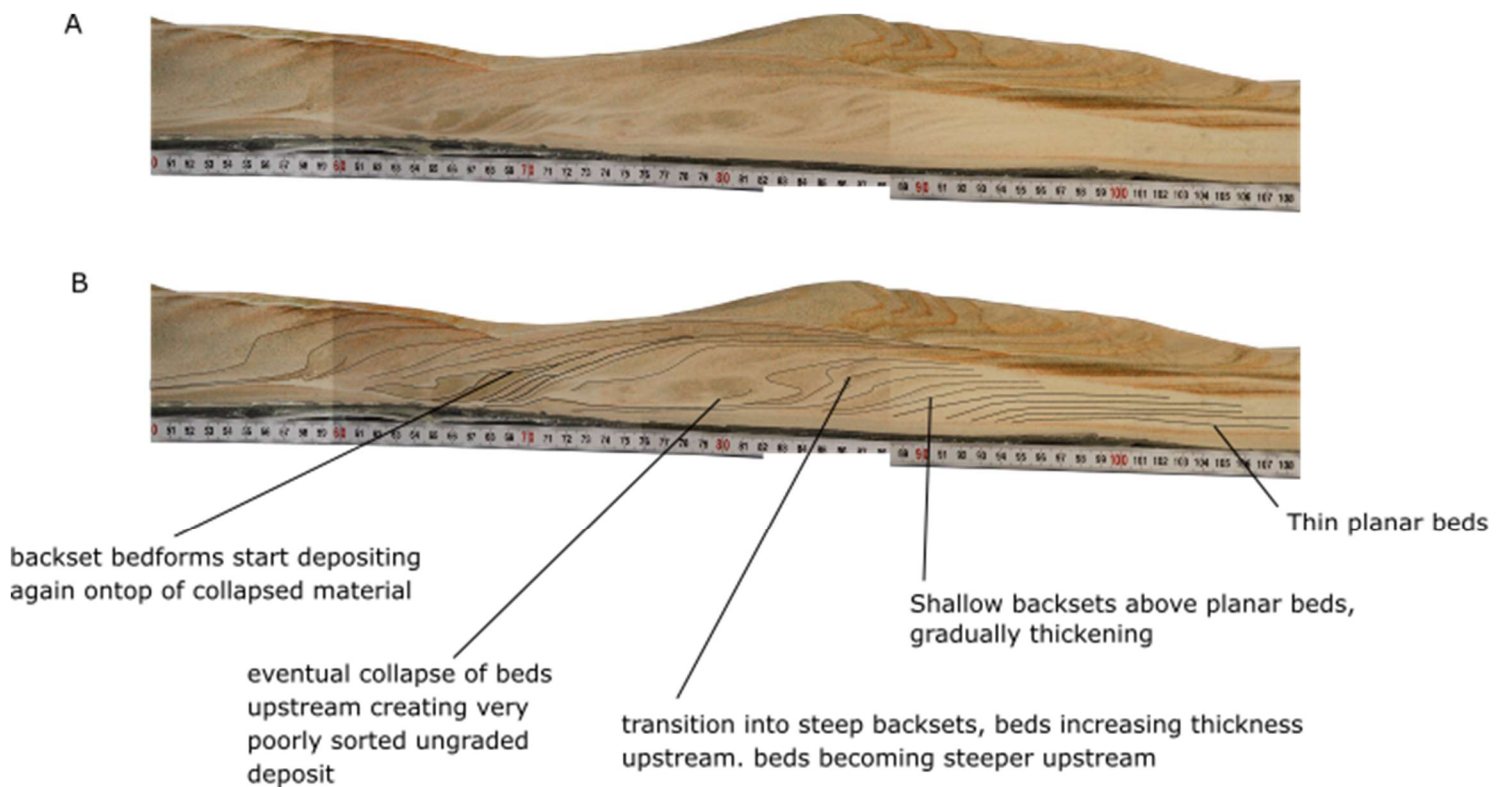


Figure 5.6 (A) Deposit from Experiment 3 using mix 5: 60% fines (White), 20% medium (Orange) and 20% coarse (Green). (B) Deposit from experiment 3 overlain with a sketch detailing the changing bedforms upstream

Bedforms from a typical profile A deposit (Fig. 5.6) show lateral changes in bedding, changing from planar bedding at 100 cm at the base of the deposit to shallow backsets starting at 95 cm, and then to steep backsets at 85 cm. The planar beds downstream (to the right of the figure) are fines rich with the backsets that overlie this gradually getting coarser.

This deposit began depositing around 100 cm, building upwards with planar beds. As the deposit builds the bedforms transitioned from planar bedding to shallow backset bedforms beginning to act as an obstruction to the current and blocking the outgoing current. With continuing sediment supply the deposit continues to propagate upstream and further steepen the beds until they steepen to vertical, at which point they collapse upstream. When the upstream avalanche stops the process begins again. This process is known as a granular bore (Smith et al., 2020). Figure 5.7 shows the formation and evolution of a granular bore.

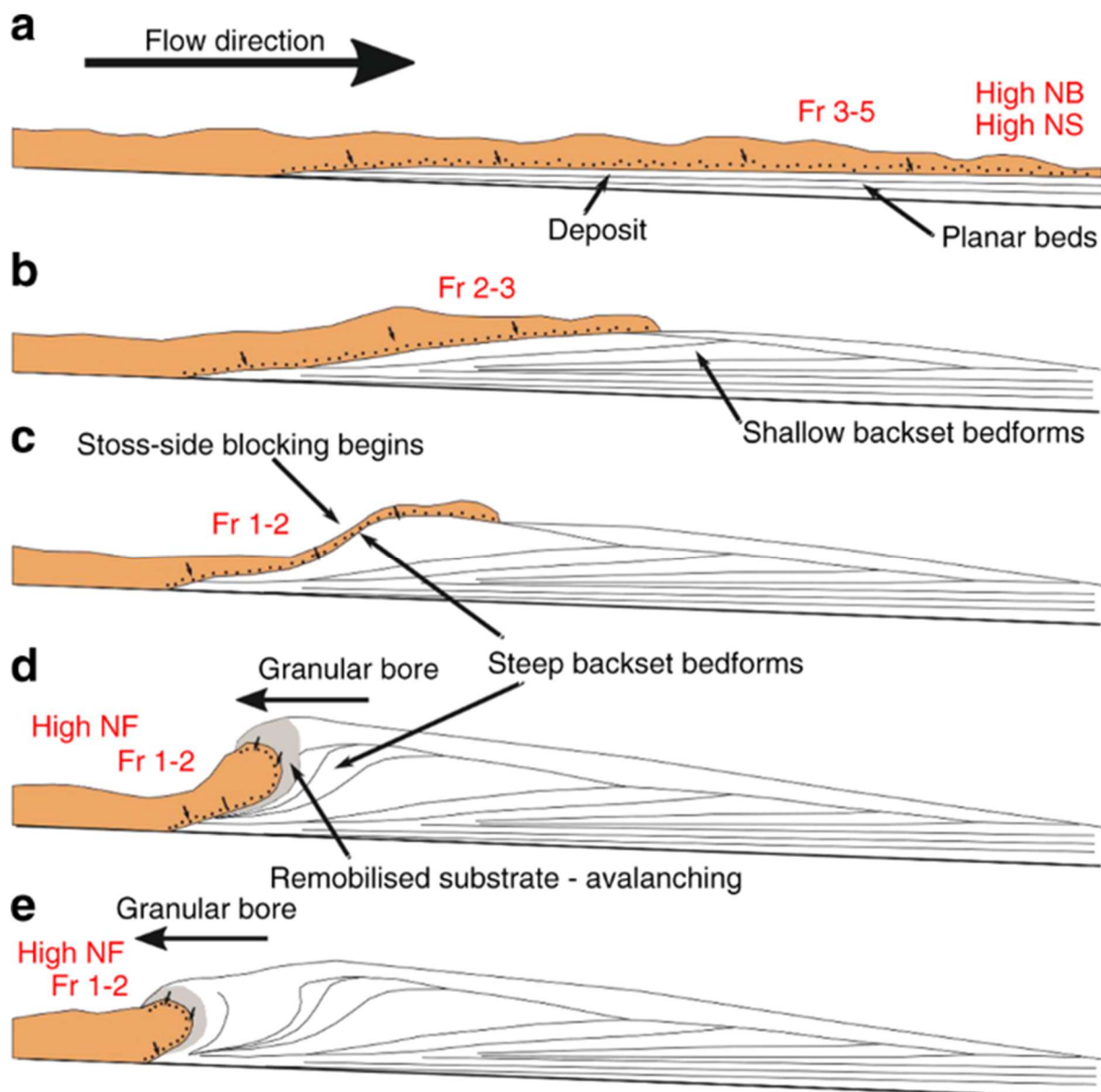


Figure 5.7 the progression from planar beds to steep backset bedforms through a granular bore, numbers in red give representative values for Froude number (Fr), Savage number (NS), Bagnold number (NB) and Friction number (NF) (Smith et al., 2020)

5.4.5 Reverse grading

Image analysis was completed on the reverse graded beds identified. The image analysis uses the same techniques outlined in Chapter 3.3 where each bed is split into 5 equal subsections and then using JMicrovision, 50 random clasts from each section are measured and then Gradistat is used to measure sorting values. Images were selected based on the following criteria: package must be graded, individual package shows all grain sizes, the thickness of deposit must be large enough to split into 5 equal sections for detailed analysis.

5.4.6 Analysis of experiments with varied grain sizes and the same density

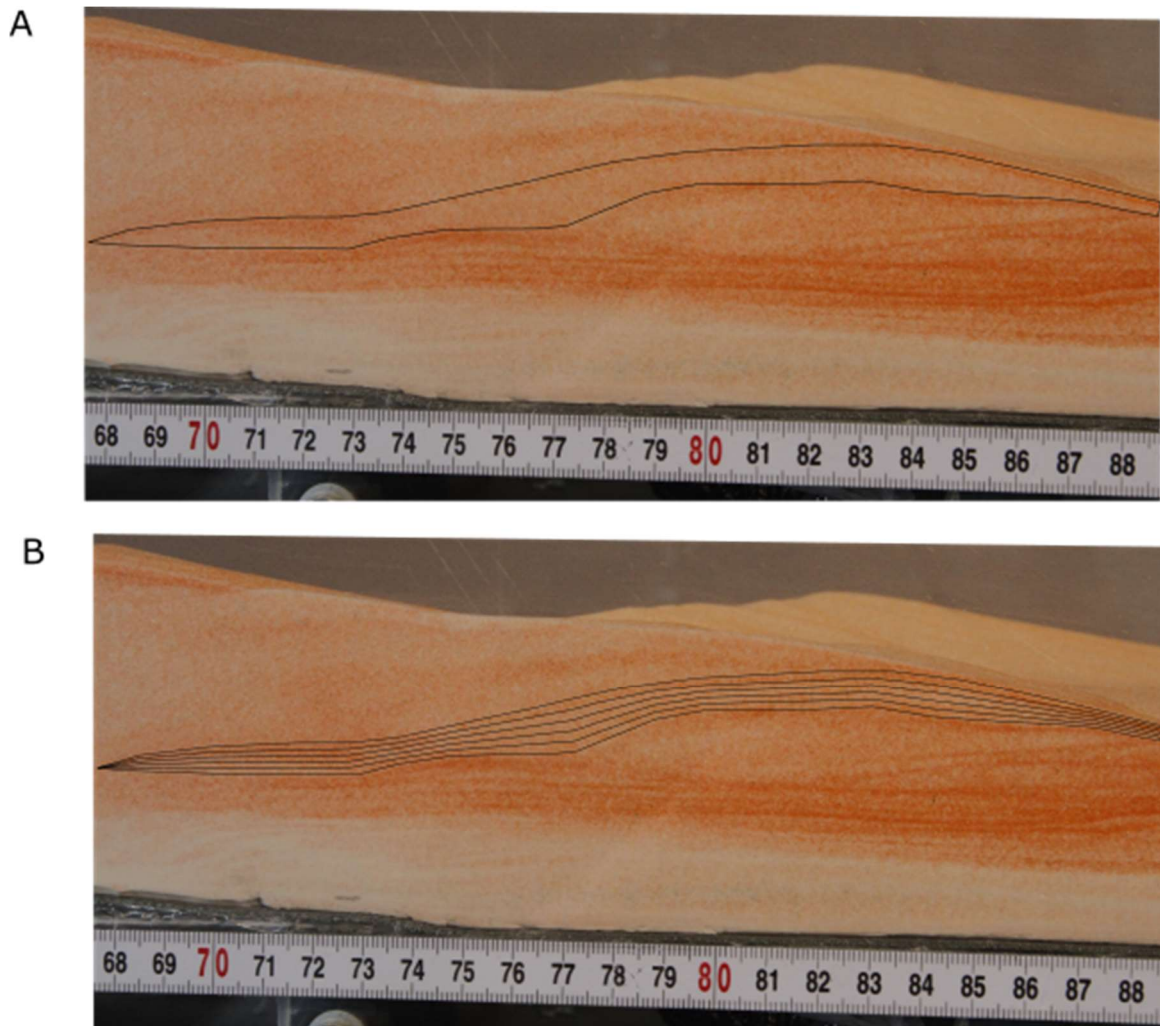


Figure 5.8 A) Reversely graded packages identified in experimental deposit 28 using mix 2 (80% 45-90 μm (White), 20% 125-425 μm (Orange)) . B) Package 1 with 5 equal horizontal subsections outlined for image analysis (Fig 5.9)

Experimental deposit 28 uses the finest combinations of grain sizes available for this investigation, 45-90 microns (white) and 125-425 microns (orange). Fig. 5.8 shows a section of this deposit where thin planar beds transition into thicker shallow backset beds. One of these shallow backset beds is chosen to analyse due to its thickness and length, allowing for a detailed analysis. The planar beds below are too thin to do a full analysis on using this method.

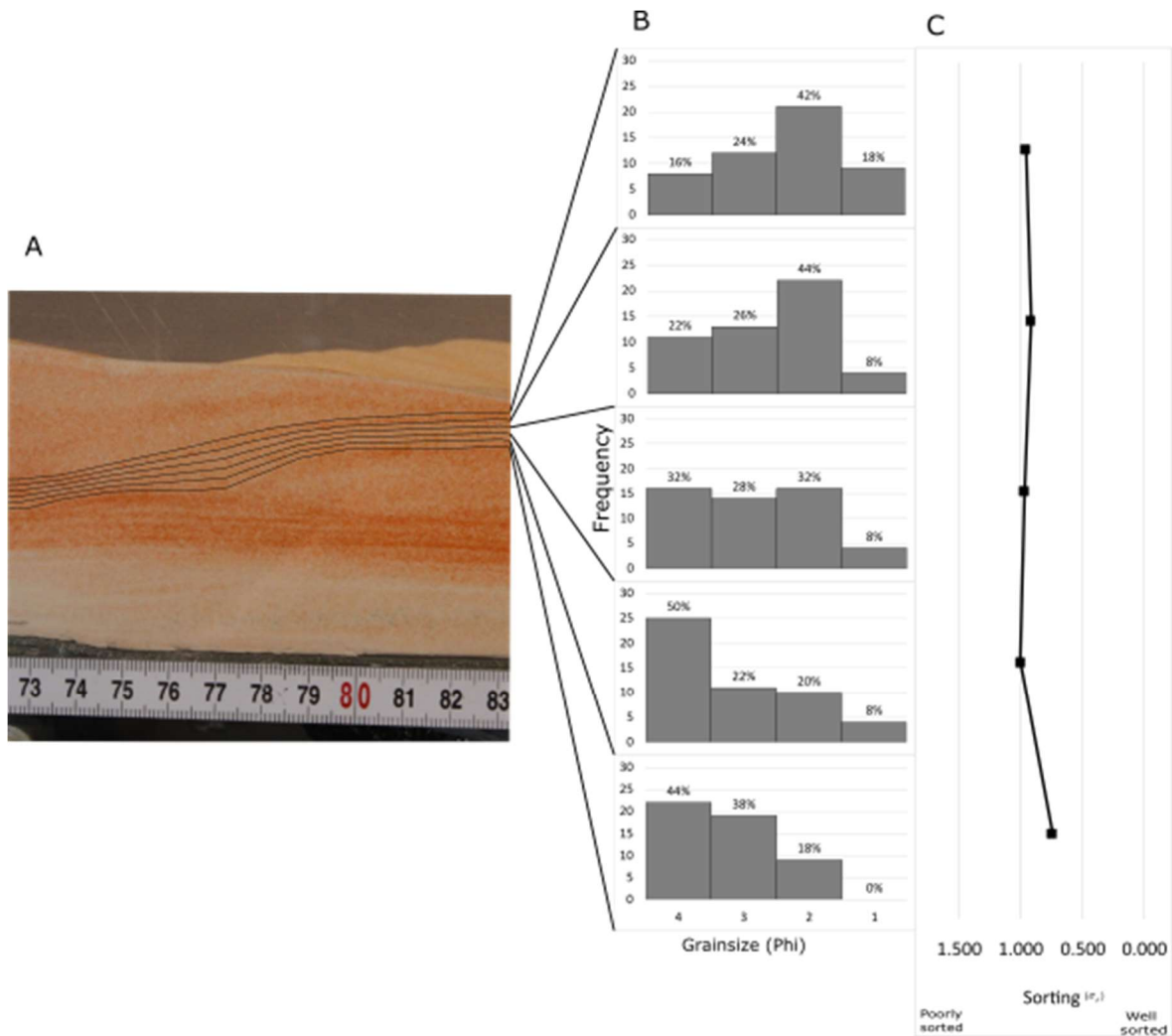


Figure 5.9 A package from experimental deposit 28 split into 5 equal subsections, the image has been cropped for presentation purposes B Grain size data for each subsection collected using JMicrovison C sorting data from each subsection calculated using Gradistat.

The median diameters for these grain sizes are 67.5 and 275 microns giving an average d_s/D_l of 0.25. Quantitative analysis of the deposit (Fig 5.9) shows very gradual changes in grain size, with the smallest grain sizes decreasing from 44% at the base to 16% at the top, meanwhile the largest grain size increases from 0% to 18%. At the base, only 18% of grains are over 125 microns in comparison to 60% at the top section showing a 42% increase in the proportion of large grains.

Sorting in this deposit is best in the basal section at 0.754 (moderately sorted). Upwards the sorting remains similar ranging between 0.918 σ_ϕ and 1.003 σ_ϕ (poorly sorted) as the grain size distributions show similar characteristics while the dominant grain size changes from finer to coarser (Blott & Pye, 2001).

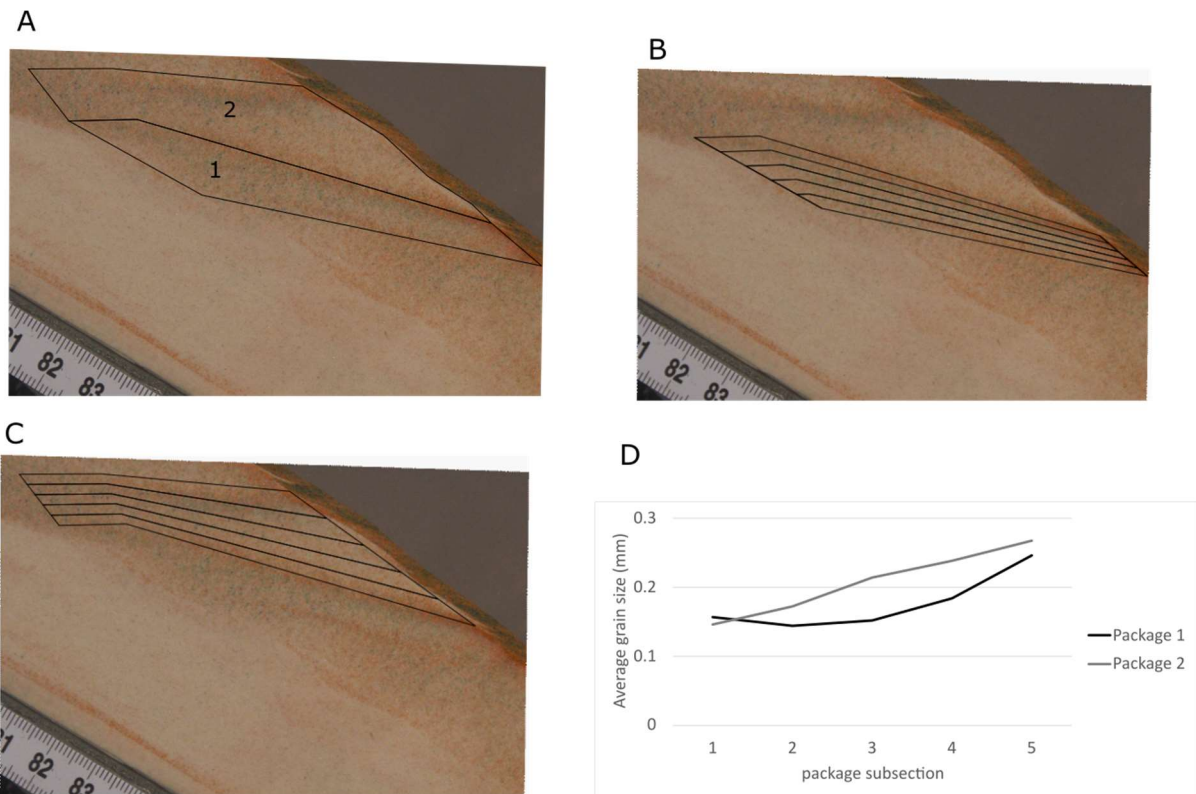


Figure 5.10 A) Reversely graded packages identified in experimental deposit 14 (top) using mix 6 (50% 45-90 μm (White) 30% 125-425 μm (Orange) 15% 425-600 μm (Green) 5% 600-800 μm (Purple)). B) Package 1 with 5 equal horizontal subsections outlined for image analysis (Fig 5.11). C) Package 2 with 5 equal horizontal subsections outlined for image analysis (Fig 5.12). D) average grain size for each subsection for packages 1 and 2

Experimental deposit 14 (Fig. 5.10) uses 4 grain sizes, 45 μm -90 μm , 125 μm -425 μm , 425 μm -600 μm and 600 μm -800 μm . This experiment produced a deposit with a massive, ungraded fines rich deposit overlain by steep backset beds of graded material. Figure 5.10 shows a small section of this deposit with 2 graded beds highlighted. These beds are interpreted to be representative of the current at the time of deposition and are of a suitable thickness and grain size range for a detailed analysis.

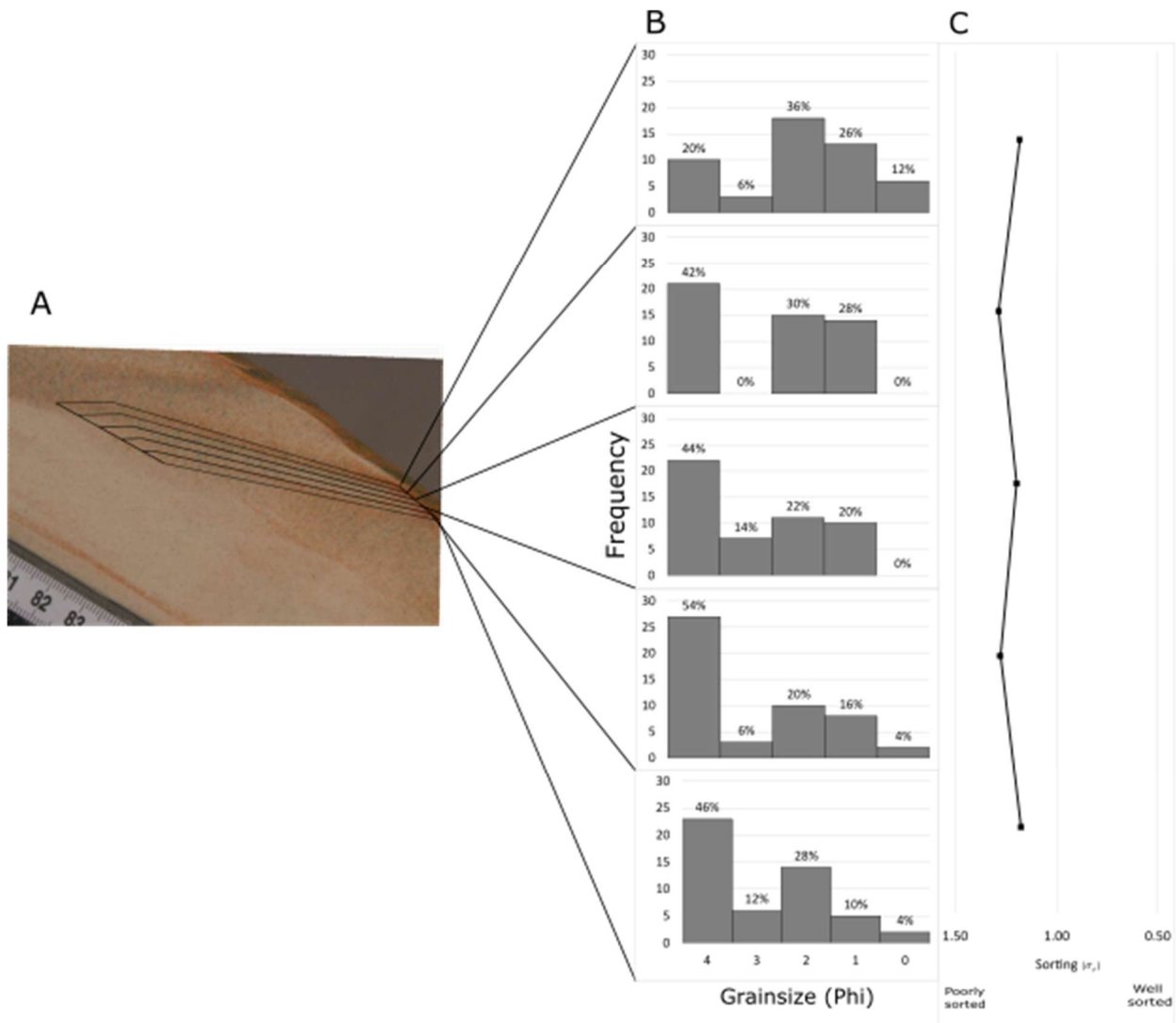


Figure 5.11 A package 1 from experimental deposit 14 split into 5 equal subsections B Grain size data for each subsection collected using JMicrovison C sorting data from each subsection calculated using Gradistat

Data from Figure 5.11 shows a gradual shift from predominately with 46% of particles with a grain size of 4 Phi (62-125micron) at the base to a predominant grain size of 2 Phi (250-300 microns) at the top of the bed. This is a poorly sorted deposit with sorting values remaining between 1.100 and 1.200 throughout (Folk & Ward, 1957; Blott & Pye, 2001).

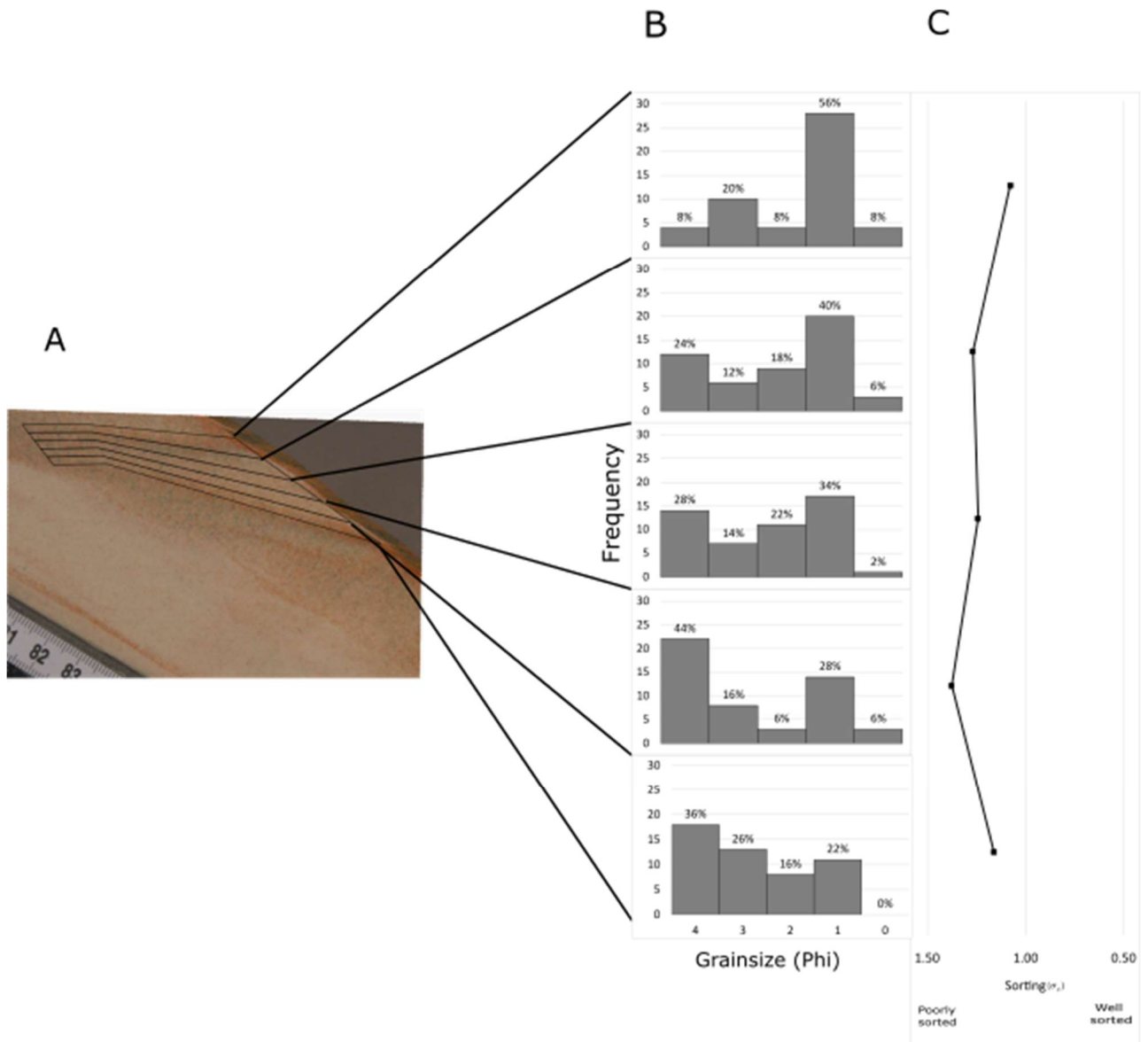


Figure 5.12 A package 2 from experimental deposit 14 split into 5 equal subsections B Grain size data for each subsection collected using JMicrovison C sorting data from each subsection calculated using Gradistat.

Package 2 (figure 5.12) shows a similar transition from fine to coarse to fine particles in package 1 (figure 5.11) in which the base is dominated by grains with a grain size lower than 2 phi (250 microns) totalling 62% of all grain in the subsection, whereas the top section is dominated by grains larger than 1phi (500 microns). The basal and uppermost subsections have the best sorting within this deposit with respective values of 1.161 σ_ϕ and 1.077 σ_ϕ . The deposit remains poorly sorted with values peaking at 1.376 σ_ϕ in the 2nd lowest subsection. Sorting becomes better from the midsections upwards as the subsections become predominantly 1 Phi.

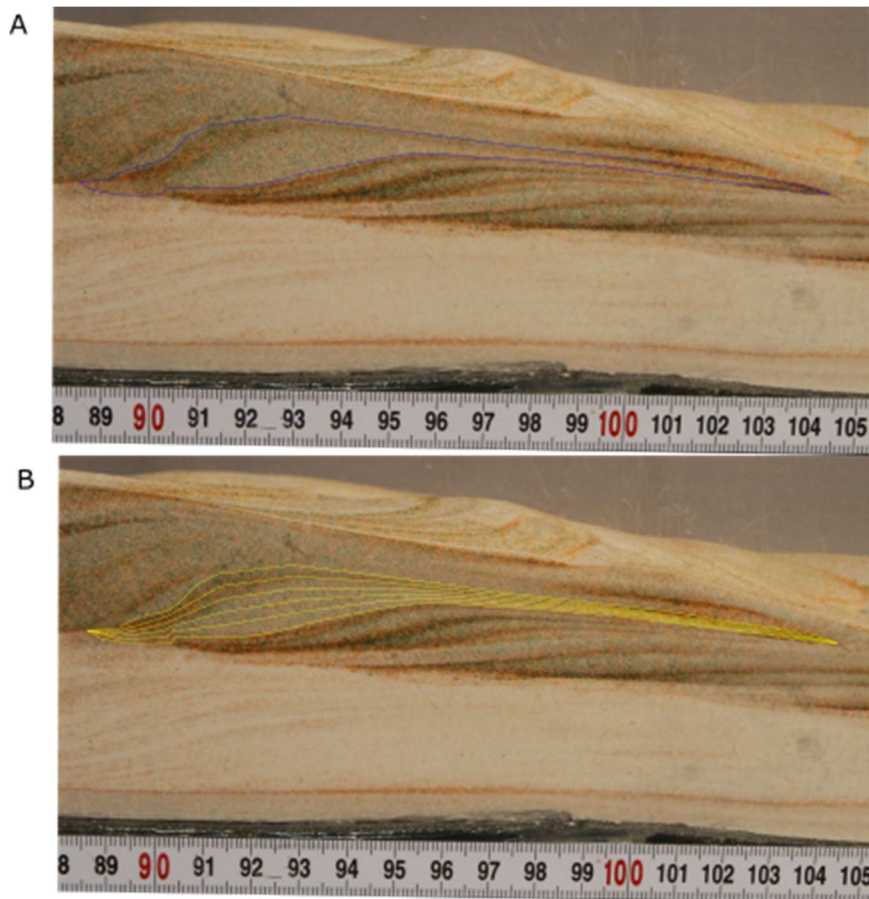


Figure 5.13 A) Reversely graded packages identified in experimental deposit 4 using mix 5 (60% 45-90 μm (White) 20% 125-425 μm (Orange) 20% 425-600 μm (Green)). B) Package with 5 equal horizontal subsections outlined for image analysis (Fig 5.14).

Experimental deposit 4 (Fig 5.13) used 3 grain sizes: 45 μm -90 μm (white), 125 μm -425 μm (orange), and 425 μm -600 μm (green). The deposit shows a ~5 cm build-up of unsorted fine grains overlain by 4 cm of graded beds, with thin planar beds at the base of the graded section changing into backset beds in the upper section. The bed highlighted for analysis is a ~2.5 cm thick backset, which was chosen for analysis due to its thickness and because it shows the full range of grain sizes, interpreted as being representative of the current at the time of deposition.

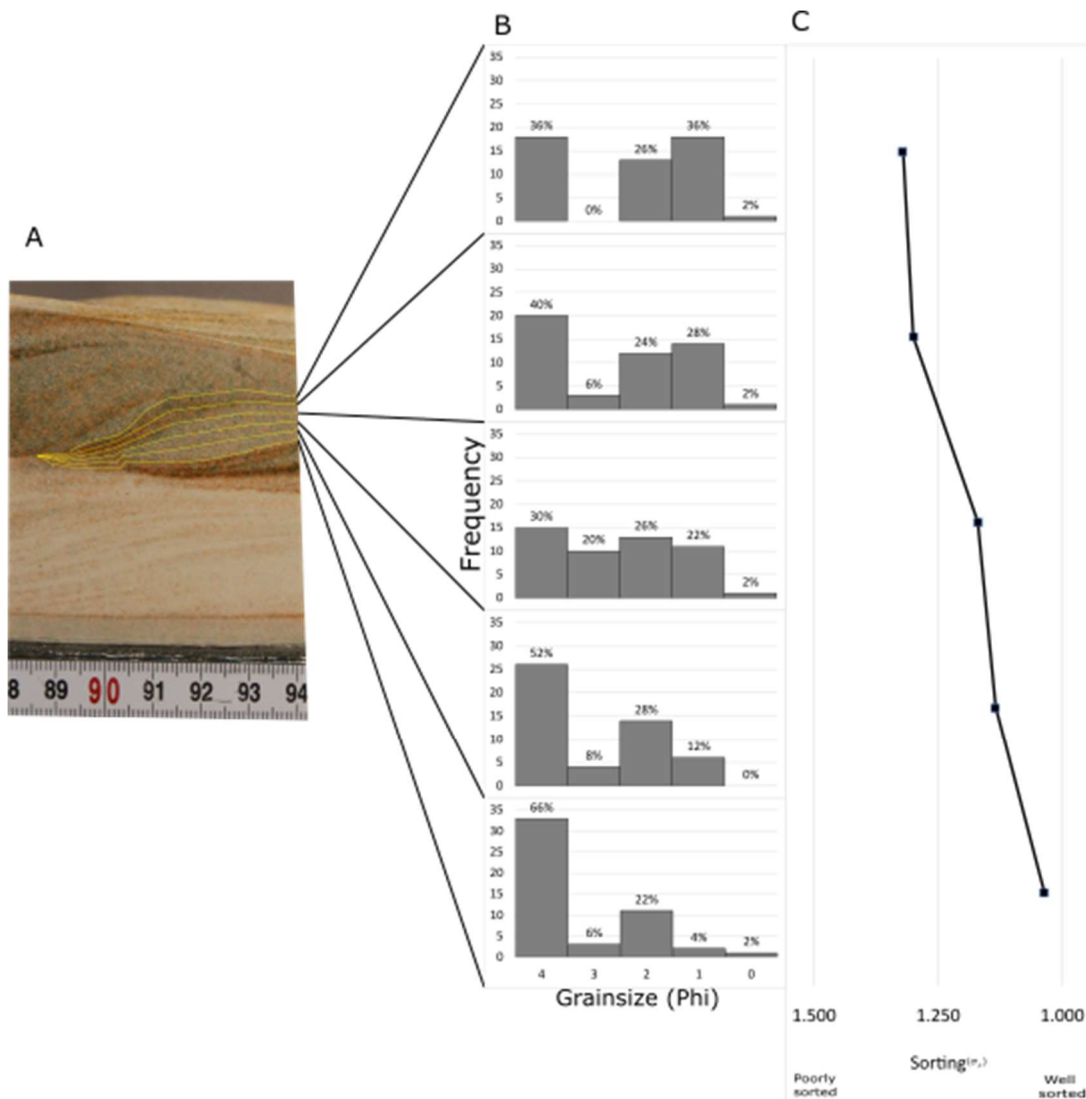


Figure 5.14 A package 2 from experimental deposit 4 split into 5 equal subsections, the image has been cropped for presentation purposes B Grain size data for each subsection collected using JMicrovison C sorting data from each subsection calculated using Gradistat.

Analysis of the graded bed highlighted in Fig. 5.13 displayed in Fig 5.14 shows a very poorly sorted bed with reverse grading. The bed shows an increase in the coarse grains (1 phi and larger) from 6% at the base to 38% in the uppermost section and a 30% depletion in the finest grain size upwards through the bed. Sorting worsens upwards through the deposit from 1.036 σ_ϕ at the base to 1.320 σ_ϕ at the uppermost section remaining in the poorly sorted classification (Folk & Ward, 1957; Blott & Pye, 2001). The basal section is predominantly 4 Phi (66%), with the rest of the subsection consisting of all grain sizes used, as a result, the subsection shows to be the best sorted. Upwards through the bed to the mid subsection, the grain size concentrations become more equal before a reduction in 3 Phi grains occurs increasing the concentration of other grain sizes and producing a more poorly sorted bed.

5.4.7 Analysis of experiments with varied grain sizes and different density

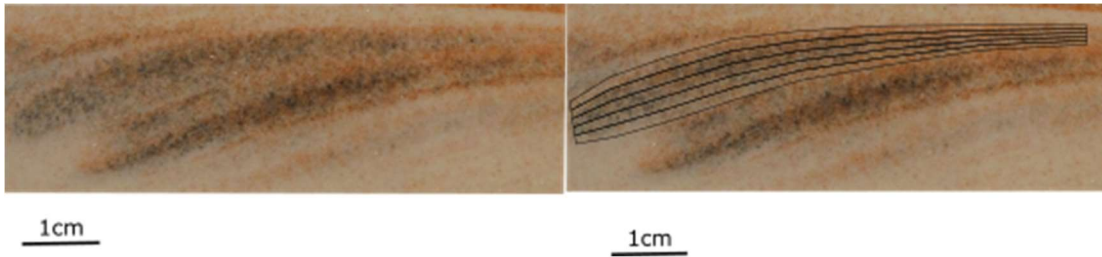


Figure 5.15 reverse graded bed from experiment 31 using mix 3 (80% 45-90 μm (White) 20% 125-425 μm (orange) 20% 125-425 μm dense (Black)) (left) same bed with linework splitting into 5 equal subsections (right)

Experimental deposit 31 (Fig 5.15) produced a profile type B deposit with mostly shallow backset and planar bedding. The planar beds which were concentrated at the base of the deposit consists of mostly fine grains, whilst the backsets above presented all grain sizes graded. Figure 5.15 shows a backset bed from deposit 31 that was used for analysis due to its thickness and presence of all grain sizes which allow for a detailed analysis in Figure 5.16.

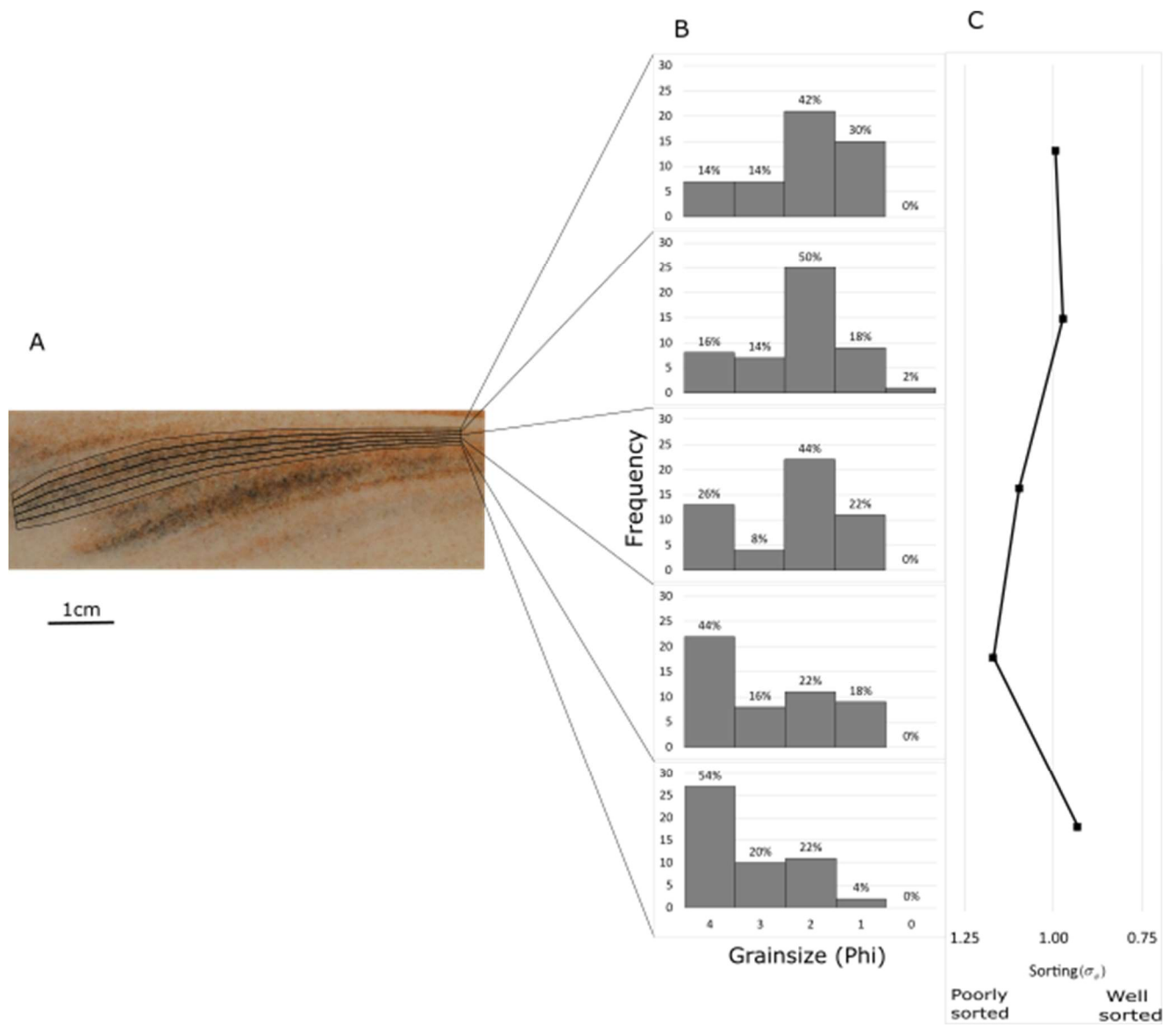


Figure 5.16 A reverse graded bed from experimental deposit 31 split into 5 equal subsections B Grain size data for each subsection collected using JMicrovison C sorting data from each subsection calculated using Gradistat.

Grain size analysis for the reverse graded bed in experiment 31 (Fig 5.16) shows an overall increase in grain size from a majority of grains (54%) at 4 phi at the base rising to 72% of grains at 2 phi in the top section. The second to top subsection also shows a predominately larger grain size with 70% of grains larger than 2 phi. This subsection contains a large portion of dense larger grains while the top contains a larger proportion of both coarse light and dense grains. Sorting values calculated from grain size analysis of the experimental deposit indicate a poorly sorted deposit with values ranging from 0.931 to 1.169 σ_ϕ (Folk & Ward, 1957). The basal subsection is the best sorted subsection with a concentration of the finest grains and few larger grains, becoming more poorly sorted to the 2nd lowest subsection where a wider range of grain sizes is introduced. Rising upwards through the bed sorting becomes better as the grain size range begins to reduce again as the bed becomes coarser.

5.4.8 Current velocity

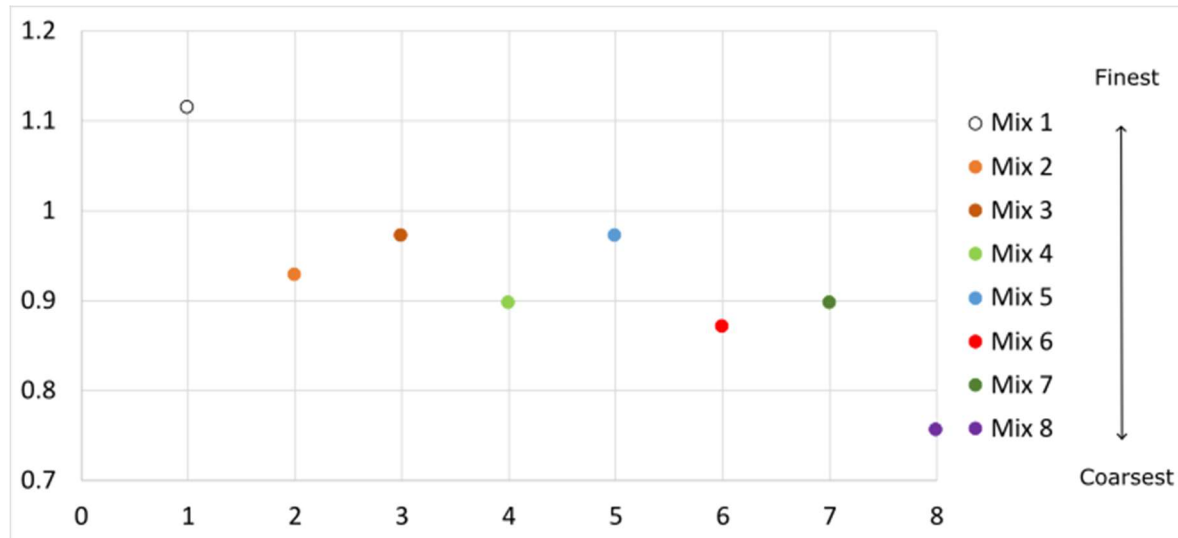


Figure 5.17 average flow front velocity vs current mixture from finest (mix 1) to coarsest (mix 8).

Velocity measurements displayed in Figure 5.17 indicate that there is a relationship between grain size and velocity, with the coarser currents generally having a slower velocity, with the exception of the mix using 60% 45 μm -90 μm 20% 125 μm -425 μm 20% 425 μm -600 μm . Interestingly both dense mix currents (Mix 3 and Mix 7) had a marginally higher velocity than the low density currents using the same size grains despite having a higher proportion of coarse grains and a higher bulk density.

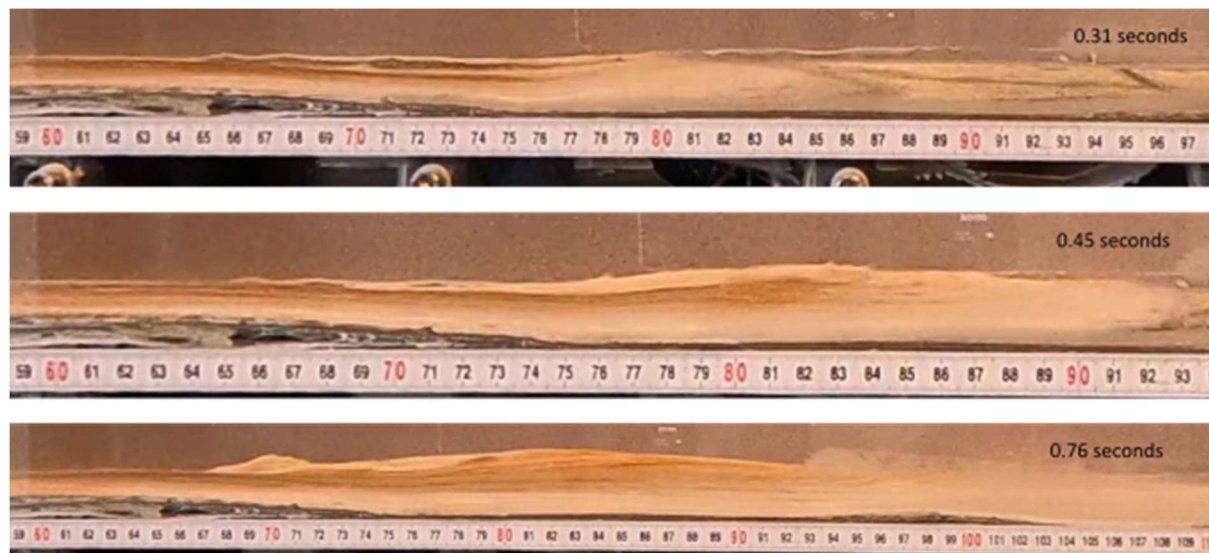
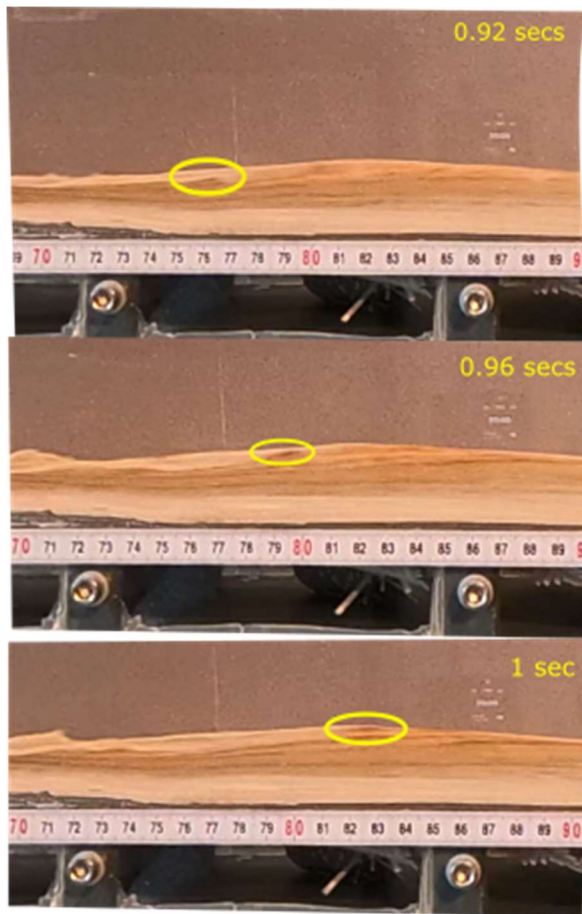


Figure 5.18 Timelapse of current showing segregation of larger beads from the bulk of the current in experiment 14 (timestamps mark time passed since current enters video frame). (see supplementary [video 5.2](#))

Videos of the currents show that segregation occurs before the current enters the frame. Fig.5.18 shows the coarser grain sizes of 425 μm -600 μm , and 600 μm -800 μm (coloured purple and green) have already segregated from the finest grains (white), whilst the 125 μm -425 micron beads have

not fully segregated. However, it appears that the orange colour of the 125 μm -425 μm beads is moving upwards with a large degree of mixing still present in the lower section of the current.



In figure 5.19 a small package of coarser material is seen moving within the current in experiment 14

Video frames allow us to observe the movement of coarser grains within the current. Figure 5.19 shows an example of a small package of coarse grains moving towards the surface over a period of 0.08 seconds after the current first entered the frame. Velocity analysis measured this package moving at 0.8 m/s and the same was recorded for the rest of the current during this time, showing no lag of coarse sediment within the current. The video footage only had a resolution capable of accurately viewing down to ~ 1 mm while the coarsest grains here are at 600 μm thus no observation of how these grains were able to segregate can be accurately recorded.

5.4.9 Current stratification

Current stratification is seen across multiple currents with different grain sizes and densities (Fig 5.20). In experiment 22, which uses the finest of the mixtures, a small change in composition upwards through the current is seen, where the base is almost exclusively fine grains (white), with an increase in larger grains (orange) towards the top. The deposit forming under the current at this point appears to be recording the base of the current, appearing to be mostly fines with occasional layers of coarser material. Experiment 5 (Fig 5.20) shows a coarser current with 3 different grain sizes: 45-90 (white), 125-425 (orange) and 425-600 (green) microns. The frame shows a very thin line of the fine white grains at the base in contact with the deposit surface, overlain by the medium sized grains which are then overlain by the coarse grains at the top. As with experiment 22, the

deposit reflects the base of the current at the time of deposition, with the base of the deposit downstream (Right-hand side of frame) showing a large concentration of the finer grains and a mixture of the finer and medium grains. There appears to be little of the coarsest grains deposited at this point, which are found at the top of the stratified current overpassing the finer grains as they are not able to reach the flow boundary to be deposited. Experiment 30 (Fig 5.20) shows how a stratified current not only allows for segregation of grains by size but also by density. The base of this current in contact with the deposit is a high concentration of fine grains, above this, there are grains of the same size range (125 μm -425 μm) but two different densities (orange coloured beads have a density of 2.5 g/cm^3 where the black beads have a density of 3.0 g/cm^3). In the frame, the black denser beads are below the lighter orange beads showing some density segregation.

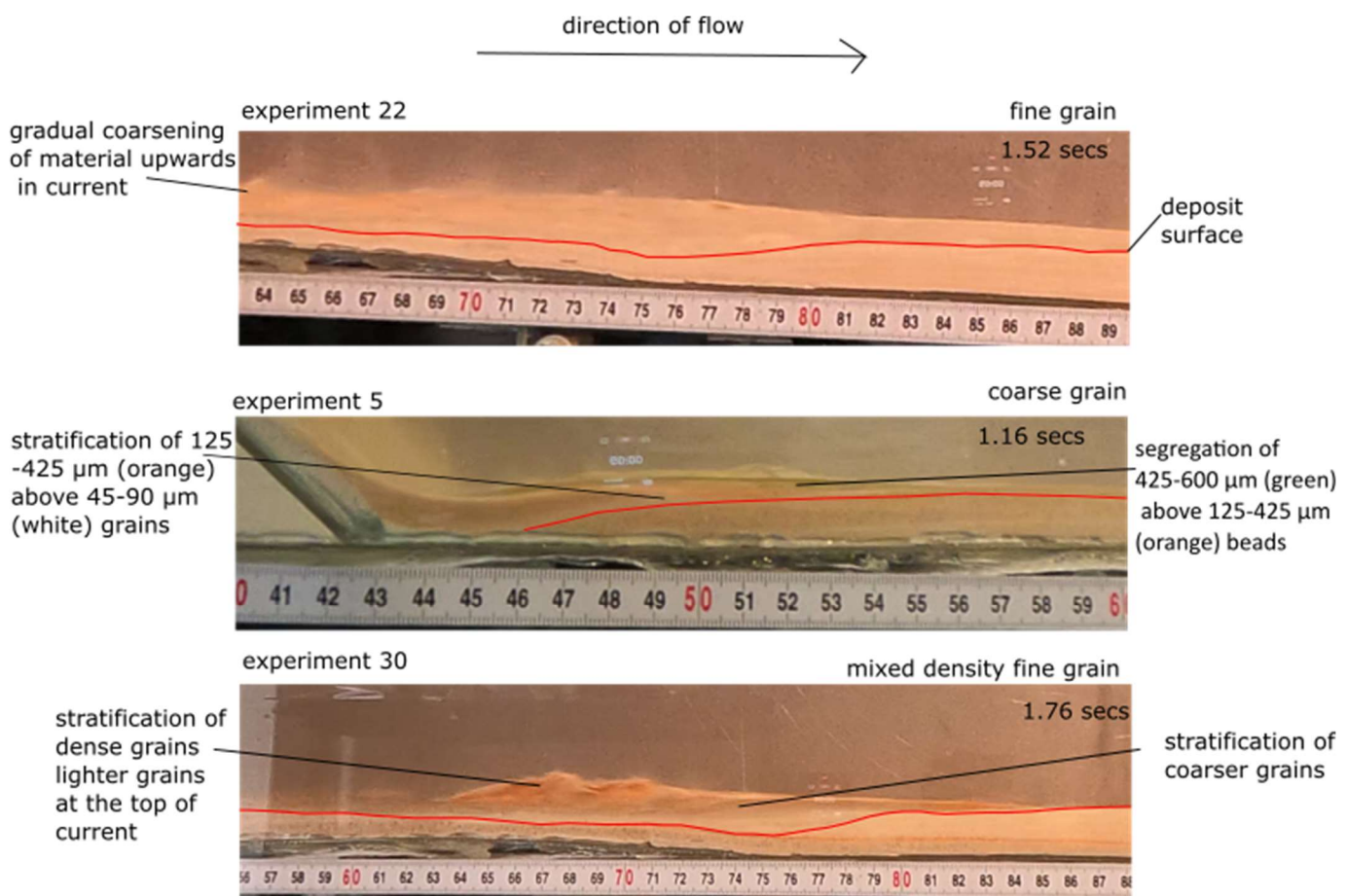


Figure 5.20 Stratification of currents shown across different grain sizes and densities. Red lines show the deposit surface, frames timestamped in the top right corner, and time in seconds since the current entered frame. Experiment 22 (see supplementary [video 5.5](#)) shows a fine-grained current with small levels of stratification particularly evident on the left of the frame. Experiment 5 (see supplementary [video 5.6](#)) shows a coarse-grained current with a much greater level of stratification than shown in a fine-grained current across two waves, grain size change is abrupt in the lower section and gradual in the upper section. Experiment 30 (see supplementary [video 5.7](#)) shows a fine-grained current with mixed density grains. The stratification shows a grain size segregation and a density segregation, with fines at the base of current, underneath coarse dense grains which are underneath coarse light grains.

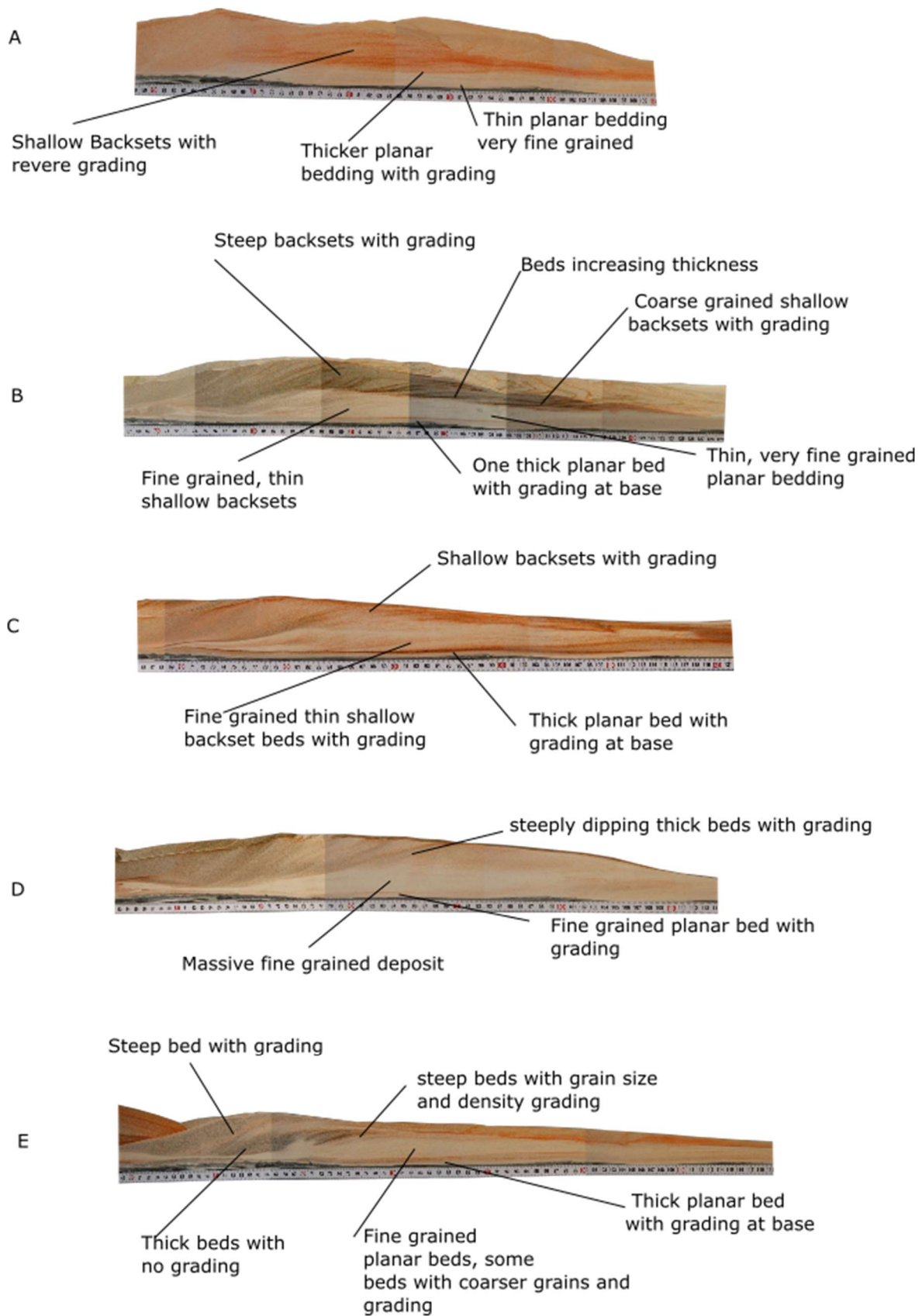


Figure 5.21 (A) fine-grained experimental deposit (experiment 28) using Mix 2, (B) Medium grain size experimental deposit (experiment 4) using mix 5, (C) coarser grained experimental deposit (Experiment 17) using mix 6, (D) coarse grained experimental deposit (experiment 14) using mix 8, (E) dense experimental deposit (experiment 31) using mix 3

Figure 5.21 shows deposits for each of the grain size mixtures analysed as part of this study. Each of the deposits shows different characteristics including types of prevalent bedding and each shows different degrees of sorting and grading. However, all of the above examples share a similar trait; each has a relatively fine-grained lower section and a coarser-grained upper section. All except A (experiment 28) show a thick graded planar bed at the base of the deposit. A and C also do not show steep backset beds.

The evidence shown in figures 5.20 and 5.21 suggest that the deposits are created by a stratified current which is depositing fines first and shows depletion of fines over time. In the first phase of deposition which is inferred as the fine-grained deposit, the deposit aggrades progressively from the flow boundary.

5.5 Discussion

5.5.1 Deposit Characteristics

5.5.1.1 *General characteristics*

Deposit analysis detailing deposit profile, internal architecture and grading patterns revealed that reverse grading can occur within both planar beds and steeper bedding. However as shown in figures 5.3, 5.5, and 5.7 many steeper beds and near vertical beds show no grading at all. This could suggest that there is a maximum angle at which reverse grading can evolve likely due to avalanching of material destroying any evidence of grading. In some cases, this is also likely due to gravitational collapse upstream caused by a granular bore. Deposit sketches also reveal that normal grading is very common within these currents, deposits often forming between reversely graded beds, or chronologically after reversely graded beds perhaps suggesting that changing conditions within the current once a deposit is formed may affect the way particles interact. This may also be linked to the gas injection through the base of the flume getting blocked off by an aggrading deposit which then reduces fluidisation of the over passing current possibly reducing the spaces available between particles for coarser grain to percolate resulting in normal or lack of grading in these zones. However, it is not possible to determine this without further testing.

5.5.1.2 *Grain size distribution*

Image analysis collected on the reversely graded packages identified within the deposit shows that in both dense and non-dense currents the base of the deposit is predominantly under 125 μm whereas grains over 250 μm often make up over 70% of the top layer.

The larger the grain size difference the better a current would segregate, much like the static experiments e.g. currents using Mix 2 (80% 45 μm -90 μm , 20% 125 μm -425 μm) would have graded beds where the base would be predominantly fine grains, whereas the top would be the coarser grains. Additionally, the middle sections would show a large extent of mixing with very little grain size change. However, the currents using mix 5 (50% 45 μm -90 μm , 25% 125 μm -425 μm , 20% 425 μm -600 μm , 5% 600-800 μm) would show larger grain size variations, with the base predominantly the finest grain, the second subsection, a mix between the 45 μm -90 μm and 125 μm -425 μm grains, with the next two higher subsections showing a mix between a majority of the 125 μm -425 μm and 425 μm -600 μm grains with very few 45 μm -90 μm and 600 μm -800 μm grains. The top subsection would show a majority of 425 μm -600 μm grains with 600-800 μm and some of the finer grains included.

5.5.1.3 Density

Currents with dense grains show another form of reversely graded beds where the fine 45-90 μm beads formed the base and were then covered by the coarse dense beads with the coarse light beads of the same grain size (125-425 μm) above. The presence of these beds suggests that when there is a size difference between grains, sorting of size is the strongest sorting mechanism, whereas between grains of the same size but different density, gravitational settling is the dominant mechanism whereby the denser grains are deposited first.

Deposits from currents using different densities showed the same grain size grading presented in the non-dense currents, and in addition, they also presented with density grading. When two grains were the same size they would separate according to the density of the grain, with the lighter grains rising above the denser grains. This is demonstrated in experiment 31 where a deposit was created with 125 μm -425 μm beads overlying the 45 μm -90 μm beads, and within the 125 μm -425 μm beads there was a separation of the denser beads below the lighter beads (Fig. 5.16). This can also be seen within the static experiments and could suggest the same processes taking place where the denser particles will percolate faster than the light particles of the same size whilst the light particle will uplift faster than the dense particles of the same size, producing a deposit where dense particles lie below similarly sized light particles.

5.5.1.4 Sorting

All deposits show poor sorting based on sorting values collected using Gradistat (Folk & Ward, 1957; Blott & Pye, 2001); the finest deposit (deposit 28) showed the best sorting. The coarsest deposits (deposit 14) showed similar sorting to the medium grained deposits (deposit 4) both with sorting values between 1.00 and 1.40 σ_ϕ . The dense experimental deposit used the same grain sizes as the fine-grained currents, the sorting values indicated that the deposit was more poorly sorted than the fine-grained experimental deposits but not as poorly sorted as the coarser-grained non-dense experiment deposits. When we compare the sorting values between the flume experiments and the sorting values collected in the muesli experiments, we find that the values sit in a similar range with the shaking experiments where the non-dense currents are slighter and better sorted than the dense currents as in the shaking experiments. Based on deposit analysis data, we suggest a possible link between the muesli effect and reverse grading within the experimental currents.

Sorting in the deposits was also better in the finer deposits than the coarser deposits in both field and experiments. In the experiments, fine experiments averaged a sorting value of 0.9 σ_ϕ (moderate – poor sorting), medium grained experiments (Mix 5) had an average sorting value of 1.1 σ_ϕ (poorly sorted) and the coarser experiments had sorting values around 1.2 σ_ϕ (poorly sorted). This is a similar trend to what is experienced in the field deposits where the fine deposits, 1 and 2, showed average overall sorting values of 0.715 σ_ϕ (range 0.63 to 0.83 σ_ϕ) (moderate sorting) compared to the coarser deposits which often hovered around 1.08 σ_ϕ (range 0.8-1.36 σ_ϕ) (poor sorting).

Analysis of the muesli effect found that in the Type 1 experiments (similar density material) which used finer materials than Type 2 (high density material) showed sorting values of 0.86 σ_ϕ (Range 0.59-1.28 σ_ϕ) in comparison with a value range of 0.93 σ_ϕ (0.74-1.05 σ_ϕ) respectively. This suggests that the muesli effect allows for a similar level of segregation as witnessed in field deposits supporting the hypothesis that the muesli effect is linked to grading in field deposits.

5.5.2 Flow behaviour

The timelapse in Fig. 5.19 shows larger and finer beads moving at the same speed with the largest grains having already segregated before entering the frame and small levels of segregation between the two finer grain sizes can be seen taking place in the current. This shows that reverse grading is not a product of coarse material transport lag as sometimes suggested in turbidity currents (Hand, 1997) but may be a product of particle interaction most likely taking place within the hopper when particles are first released causing agitation or when the grains first enter the flume. The camera resolution and frame rate are not high enough to observe kinetic sieving (The Muesli Effect), but we can compare the results of the qualitative and quantitative analysis conducted on the Muesli effect discussed in chapter 4 to assess whether the muesli effect is the most likely cause of the reverse grading in these flume deposits.

The lack of significant segregation in the 45-90 μm (white) and 125-425 μm (orange) beads may support the findings of Sohn and Chough (1993) that particles with greater differences in size will segregate faster than those with small differences.

For instant segregation of different sized particles, the diameter of the smaller particles (d_s)/diameter of the larger particles (D_l) must be ≤ 0.25 (Sohn & Chough, 1993). The average d_s/D_l for white beads vs orange, white vs green and white vs purple beads are 0.25, 0.13 and 0.01 respectively, all of which are equal to or less than 0.25 qualifying them for instant segregation. However, the diameter difference of the coarsest 45-90 μm white beads and the smallest 125-425 μm orange beads are not significantly different enough for instant segregation with a d_s/D_l of 0.72 resulting in the bulk of the lower deposits being a poorly sorted mix of these two grain sizes. The d_s/D_l for 125-425 μm (orange) vs 425-600 μm (green) and orange vs 600-800 μm (purple) grains are 0.54 and 0.39 respectively whilst the green vs purple is 0.73. In the deposits, there is often a partial segregation between the orange and green beads with a significant amount of mixing, whilst the purple beads and orange beads are normally slightly more segregated, with the orange beads tending to be concentrated between the 2nd and 3rd lowest subsections while the purple is within the upper two. The green beads are found mostly between the top 3 subsections. A partial but not full segregation of the orange beads from the green and purple and heavy mixing between green and purple fits in with the values calculated by Sohn and Chough (1993) and in chapter 4 where they do not segregate instantly but will segregate over time if there is a size difference.

5.5.3 Stratified currents

Fig. 5.20 shows how currents are entering the flume showing stratification within the current. The flow boundary at this point is interpreted as being at the base of the current in steady conditions (Branney & Kokelaar, 2002) with continued sediment supply and fluidisation. During deposition the large clasts at the top of the current are not being deposited as they are not in contact with the flow boundary, only the smaller clasts which are in the flow boundary zone can be deposited. In steady conditions, the deposition of finer material is maintained by continued supply of fine material by the stratified current, producing a thick non-graded fine-grained deposit not representative of the whole current. The segregation of clasts may cause changes in the rheology of the lowermost part of the current, causing the flow boundary to jump upward in a process known as stepwise aggradation preserving the current's inverse grading. In a steady current, the deposit will aggrade as a fine-grained deposit until a critical point is reached where the fines have been depleted enough to cause a rheological change leading to an unsteady current (Branney & Kokelaar, 2002). In unsteady conditions the rate of deposition is not uniform. In this case unsteady conditions are causing the flow boundary to jump (Branney & Kokelaar, 2002; Sulpizio et al., 2007; Douillet et al., 2019). Branney and Kokelaar (1992) propose that in a deposit formed by progressive aggradation the basal

section would be dominated by a massive fines rich deposit. The transition to stepwise aggradation will be evident by graded beds where the internal structure of the current has been preserved (Branney & Kokelaar, 2002).

Fig. 5.21 shows final deposits with a fine basal section of planar beds with little or no grading, which are overlain by thicker coarse grained backset bedforms that are graded. The basal section is interpreted as showing a stratified current with the flow boundary at the base of the layer causing a fine-grained deposit to aggrade. The layer of graded beds above shows where a change in flow behaviour induced by lack of gas supply and depletion of fine grains causes deposition with stepwise aggradation or *en masse* deposition where the deposit reflects the current at that time of deposition, agreeing with the proposed stratigraphy in Branney and Kokelaar (2002). The deposit rapidly builds regressive graded beds as the outgoing current is blocked off by the aggrading deposit (Granular jamming/ stoss side blocking) (Douillet et al., 2019; Smith et al., 2020).

As the deposit surface aggrades the larger clasts that have segregated to the top of the current may overpass depositing further downstream. Current unsteadiness caused by changes to rheology or waning of the current affect the segregation of the depositing current so that larger clasts are more able to reach the flow boundary zone (Branney & Kokelaar, 2002). The overpassing coarse material that was deposited downstream can be seen in some pictures looking down on the final deposit, suddenly becoming what appears to be a normally graded deposit. In this section it is believed that gas rising through the deposit has elutriated fine grains to the top of the deposit obscuring the original grading. This was not investigated as it was out of the scope of this study.

5.5.4 Applications to field volcanology

Similar properties were found between the flume deposits and field deposits examined. In coarser deposits such as those using mix 6 and 8 in the flume experiments, grading appears more extreme in that it was more visible. Quantitative analysis showed that the average grain size increased from the base to the top by 1.03 for the fine-grained experiment and 1.07 for the coarse grained experiment. Though the relative size changes were similar the actual average grain size change from the base to the top was 70 microns for the fine-grained experiments and 120 microns for coarse grained.

In the field deposits 1, 2 and 3 were fine and 4, 5 and 6 were coarse, as, in the flume, deposits 4, 5 and 6 grading was much more visible than in the finer deposits.

5.6 Conclusions

Examination of the deposits formed through experimentation has allowed for the identification and characterisation of different types of grading. Analysis indicated that reversely graded deposits can be formed at any height in a deposit and anywhere from proximal to medial distance in the deposit with few examples in the distal end.

Current stratification is a significant factor in producing reverse graded deposits in fluidised granular currents. Stratification controls the supply of grains to the flow boundary zone with finer grains deposited first producing a fines rich base in deposits while larger clasts bypass to the distal end on the deposit. Grading records stepwise aggradation in currents where the flow boundary zone jumps upwards preserving the internal grading of the current. Aggradation of steepening backset bedforms leads to granular jamming or stoss side blocking of the current, jamming leads to rapid deposition via stepwise aggradation of pulses stopping *en masse* or the propagation of a granular bore.

Overall, a mix of qualitative and quantitative data collected on experimental flume deposits and currents shows that size segregation is the dominant sorting mechanism even among grains of similar sizes, although currents with bigger grain size differences will exhibit this to a greater extent. Comparison with data collected on static grains shows that deposits exhibit similar characteristics to those formed by the muesli effect suggesting that the muesli effect has at least a partial involvement in the size sorting of grains in a granular current.

6. Discussion

This study has used digital analysis and analogue modelling to investigate graded ignimbrites and their implications for flow dynamics. This study set out to quantify the characteristics of reversely graded ignimbrites, investigate sorting behaviours that occur in a static system, and investigate behaviours responsible for reverse grading in a polydisperse fluidised granular current. In this chapter, key findings are discussed and potential areas for further study of particle sorting are outlined.

Grading in ignimbrites has sometimes been used to infer changing conditions within a PDC such as waxing and waning (Branney & Kokelaar, 2002; Brown et al., 2007; Brown & Branney, 2013; Smith & Kokelaar, 2013), whereby as the current wanes and loses energy it deposits larger clasts onto an aggrading deposit of fines, although the relationship between grading and PDC behaviour has remained unclear.

For this investigation fieldwork visiting reverse graded sites was not required, and digital analysis of deposits using images collected by volcanologists was undertaken (courtesy of Drs Natasha Dowey, Rebeca Williams, and Richard Brown), by using qualitative data collected by volcanologists along with digital analysis, a detailed account of characteristics was recorded on 6 reverse graded deposits.

The results from the digital analysis were compared to the results of a series of analogue tests. The analogue tests used static and dynamic fluidised systems to collect data on grain size segregation mechanisms and granular current behaviours that influenced the reverse grading of grains by size and density. By using the same digital analysis across real ignimbrite deposits and experimental deposits, an in-depth qualitative and quantitative comparison was completed, discussing the possibility of segregation mechanisms in PDCs.

6.1. Key factors involved in segregation processes

Experimentation reveals that kinematic sieving is the dominant process in grain size segregation within granular material. Investigation into the sorting mechanism within static and fluidised currents reveals that the effectiveness of the process is controlled by variables including, grain size difference, grain shape and density.

6.1.1. Grain size range

Sparks (1976) suggests that only coarse clasts are graded and assumes the matrix or clasts under 0.5 mm remains constant throughout. In this study, the grain size distribution data suggests that this is accurate as clasts under 2 mm can be found through all subsections in real ignimbrite deposits. Shake table experiments also revealed that the smallest grain sizes could be found across all subsections, with decreasing levels upwards through deposits. Deposits from flume experiments showed that the majority of fines would flow at the base of the current while a small percentage would be distributed across the upper sections. These results suggest that the statement of Sparks (1976) is partially correct in that fine particles will remain present throughout the deposit although their proportion will not remain constant, they will show decreasing levels upwards.

The data does however suggest that there is a relationship between particle size and grading with coarser deposits displaying more intense grading. Those deposits with larger grain sizes show greater increases in the percentage of larger grain sizes upwards through the deposit, with a larger overall grain size increase from base to top.

Sohn and Chough (1993) propose that when two grains have a diameter difference of $D d_s/D_l = \leq 0.25$ the grains will segregate instantly. This study has shown that grains with a diameter difference of ≤ 0.16 will begin to segregate instantly while grains with diameter differences of ≥ 0.42 will not begin to segregate instantly, the results found to broadly agree with the findings of Sohn and Chough (1993).

6.1.2. Grain density

Aside from grain size, this study has shown that density is the biggest factor in grain segregation. Shake table analysis showed that the Sohn and Chough (1993) value of 0.16 for instant segregation is accurate for grains of the same density, however for grains with different densities, the value for denser grains is closer to 0.25, and an exact value couldn't be determined. This shows that density variations increase a grain's ability to segregate.

In field deposits, lithics have sometimes been described as normally graded whereas pumices are described as reversely graded. This study has found that both pumice and lithics are often reversely graded. In analysed deposits there is generally a wider grain size range for pumices and ash in comparison to lithics, the relative size increase is often larger for pumices than lithics as shown in two-thirds of analysed deposits. This relatively larger change in grain size makes the grading in pumices much more obvious than lithics, with the pumice size increasing at a much greater rate in some cases. Therefore without measuring the clasts, the lithics would appear to remain a similar size or even decrease in size. Visual descriptions of normal grading of lithics in the field may therefore be incorrect and these descriptions improved by quantification.

Quantitative analysis of the muesli effect (chapter 4) revealed that in a static system the dominating factor of segregation in any polydisperse mixture is the grain size, with all non-dense and dense experiments showing reverse grain size grading after 2 minutes of shaking. However, in type 2 (different density) experiments, density displayed a significant role in the segregation of grains. Observations showed that when a mixture of grains with different densities is shaken that a dense grain would percolate up to 1.55 times faster than a light grain of the same size. However, a large light grain would uplift up to 1.37 times faster than a large dense grain.

This study shows that in field deposits, the base of the deposit is often ash-sized particles, while the uppermost section is often dominated by large pumices. This may suggest that pumices are rising through currents better than large lithics can, however with the base dominated by ash-sized grains, a composition analysis cannot be completed using image analysis to determine how much of the base may be dense lithics as opposed to light pumices. To understand this relationship further, field deposits could undergo greater quantitative analysis such as more regular image analysis on deposits to increase data on the distribution of lithics and pumices across deposits.

Experimental results in chapters 4 and 5 revealed a pattern not found in the ignimbrites of chapter 3, where grains would be sorted according to density. During agitation when two grains of the same size but different densities interacted, the denser grain would fall below the lighter grain. This pattern was found in all varied density experiments in chapter 5 and across small grains in chapter 4 but only occasionally in larger grains. The density grading however was not as powerful as the grain size grading as observed in Fig. 5.16 where dense grains are deposited below similar-sized light grains but above smaller light grains.

Composition analysis of ignimbrite in chapter 3 shows that lithic fragments made up between 20 and 36% of all visible grains across the deposits. Those with higher lithic counts displayed poorer sorting than deposits with fewer lithics, which could be a result of differing segregation rates of lithic

fragments or possibly due to different flow conditions, as deposits with larger lithic counts were also larger than the other deposits, suggesting larger events created these deposits. Further study to investigate the sorting of deposits with a wider range of lithic composition, and experiments using a range of densities to determine how increasing the lithic volume may impact the flow conditions of a PDC are recommended.

6.1.3. Grain shape

This study has found that shape has a significant impact on segregation. Fernlund (1998) notes that the least cross-sectional area is most important, and usually, the longest dimension of a particle has little effect on sieve results. If the longest axis is curved particles may rotate through a sieve. This has proved to also be true for the muesli effect as witnessed in experiments in chapter 4 whereby large >4 mm oats would fall through gaps of only 0.5 mm as the shortest axis of the oats measure less than 0.5 mm.

Grains with a spherical shape have higher mobility than angular clasts, along with local bridging of particles, which allows for a high initial rate of segregation of fine spherical particles. As the bridges collapse and the fine particles form a more stable structure with low void spaces the rate of segregation for spherical particles will reduce, whereas for angular clasts the lower mobility slows down the segregation in the initial phase. Due to their shape, angular particles will have higher void spaces as the settling structure changes allowing for continued relatively high segregation rate in comparison to the later phase of spherical particle movement (Jha et al., 2008; Shimosaka et al., 2013).

6.1.4. Grain size distribution

Ignimbrites are often described as poorly or very poorly sorted (Smith & Kokelaar, 2013; Brown & Andrews, 2015). The results of this study show that reversely graded ignimbrites are often poorly sorted, however they range from moderately well sorted to poorly sorted. Results show that sorting is influenced by multiple factors including grain size ranges, density, and shape.

Results show that deposits with small grain size ranges have moderate to moderately well sorting (<1.00) (Blott & Pye, 2001). As grain size ranges increase the likelihood of subsections to be predominantly one-grain size decreases, and as a result, the deposits become increasingly poorly sorted.

Analysis of real ignimbrites revealed that in addition to grain size impacting the sorting values of deposits, the deposits with a higher lithic count have poorer sorting than deposits with fewer lithics (See chapter 3). Following this experimental data collected in chapters 4 and 5 investigated the impact of increasing the percentage of dense material in a package and recording the sorting data. Results showed that small dense grains could percolate up to 1.55 times faster than a lighter grain of the same size, however, the rate at which large dense grains rose was reduced in comparison to large light grains. This led to basal sections which leads to poor sorting in denser deposits where finer light material is often littered with coarser dense material that was able to percolate further than light grains of similar sizes and large grains that were restricted from rising.

6.1.5. Impact of fluidised flow

Fluidised granular currents produce a range of features that cannot be seen in a static system. When a granular current is fluidised and passed down a flume, flow conditions change over time as the

current deposits material, causing a rheological change. These conditions are recorded in the deposit through bedding, structures, and grading. This study used a flume set-up inspired by Smith et al. (2018), with a ramp included increasing the mobility of the coarser and denser currents used in this study. Bedforms identified in these experiments used the same naming system as used in Smith et al. (2020).

Experimental aerated dense granular currents show an initial steady state during supply followed by rapid waning leading to unsteady conditions. Polydisperse currents record changing conditions at the base of the current in a region termed the 'flow boundary zone' (Branney & Kokelaar, 1992) through bedding and structures within the deposit. The initial massive fine-grained deposit is a characteristic of a progressively aggrading stratified current where small grains are continuously percolated downwards throughout the current, replacing those that are deposited and maintaining the grading of the current (Branney & Kokelaar, 1992; Branney & Kokelaar, 1997; 2002). The steady deposition produced a thick fine-grained deposit not representative of the whole current showing steady conditions in the current (Branney & Kokelaar, 1992; Branney & Kokelaar, 2002). Aggrading deposits will build planar beds during steady conditions. Planar bed sets in granular current represent a fast current with high viscous stresses and low frictional stresses, dominated by particle collision (Smith et al., 2020). High particle collision regimes are known to increase the effectiveness of kinematic sorting (Sulpizio et al., 2007). The planar beds are often fine-grained with weak inverse grading. Upper beds are found to be coarser in experimental conditions. Continued aggradation of the deposit presents increased frictional stresses. When frictional stresses in the current are greater than the viscous stresses backset beds will begin to form in the deposit (Douillet et al., 2019; Smith et al., 2020). Backset beds promote increased deposition on the stoss side, causing each bed to be steeper than the last. As the beds steepen, the frictional forces acting upon the base of the current increase to a critical point where the current no longer has the momentum to pass over the beds in an event known as granular jamming (Douillet et al., 2019) and the deposit will rapidly aggrade backwards.

As the deposit transitions from massive and planar beds to backset beds the rheological conditions in the current change sufficiently to transition from a progressively aggrading flow boundary to a stepwise flow boundary. Stepwise aggradation occurs when the flow boundary suddenly 'jumps upwards' freezing sections of the current (Branney & Kokelaar, 2002), referred to as stoss side aggradation (Sulpizio et al., 2007; Douillet et al., 2013; Sulpizio et al., 2014; Douillet et al., 2019; Smith et al., 2020). This process allows for a single pulse to be considered a flow boundary zone for its entire thickness, as each pulse deposits *en masse*. As the deposition rate remains constant this can be considered progressive aggradation (Fig 6.1) (Sulpizio et al., 2007).

Stepwise aggradation of stratified granular pulses

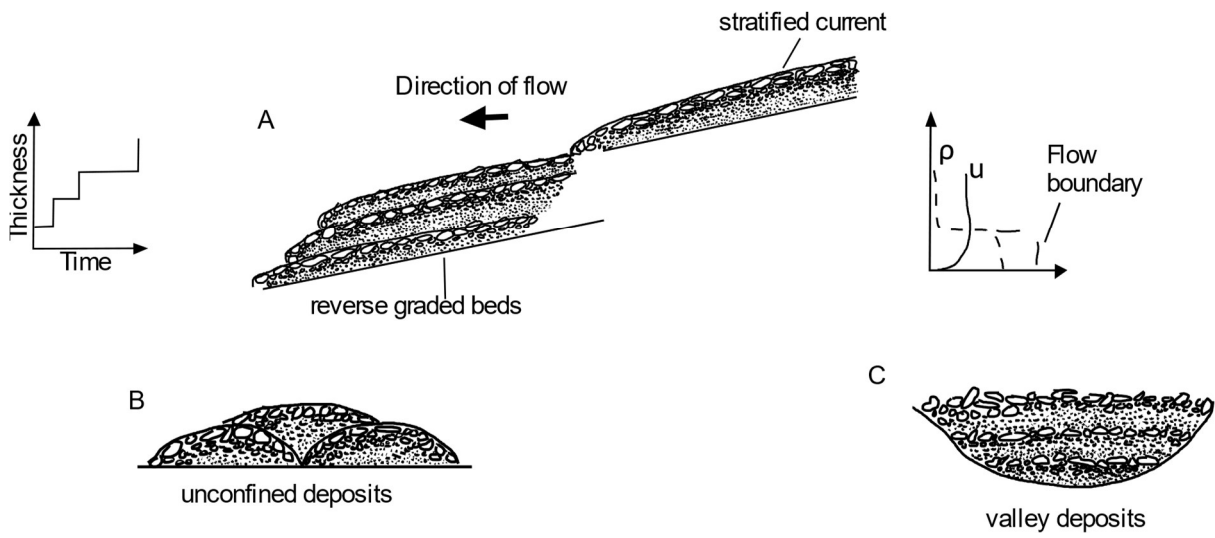


Figure 6.1 (A) Stepwise aggradation of granular surges. A schematic diagram of density (ρ) and velocity (u) profiles is also presented; (B) sketch of a transverse section through unconfined deposits; (C) sketch of a transverse section through valley pond deposit (Sulpizio et al., 2007)

Experimental data supports Sulpizio et al. (2007) that a pulse in its entirety can be considered a flow boundary zone that will be deposited *En masse* where the whole section of the current freezes and preserves any internal grading (Shultz, 1984; Allen & Cas, 1998; Branney & Kokelaar, 2002) followed by the next pulse depositing above *En masse*. However experiments create one large pulse at a constant rate. During deposition, the flow head deposits *En masse*, the current behind carries momentum and overpasses the deposit to deposit *En masse*, creating a deposit showing the same characteristics as proposed by Sulpizio et al. (2007) (Fig 6.2).

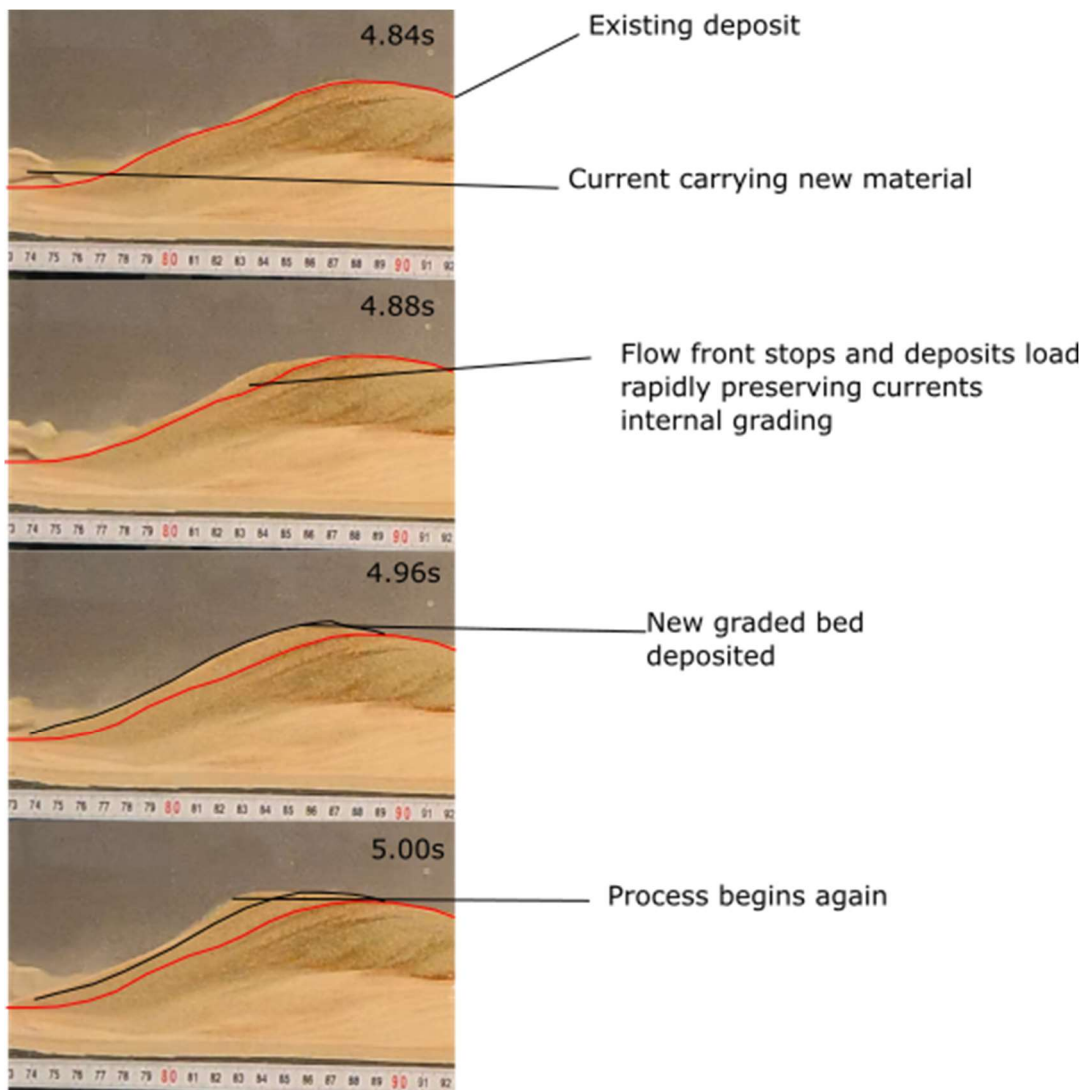


Figure 6.2 Video frames from experimental current showing an aggrading deposit from a stratified current, flow head enters the frame at 4.84 seconds. At 4.96 seconds a new graded bed is formed and the current behind continues to flow and overpass the deposited bed for the process to begin again and force the deposit to aggrade regressively.

During progressive aggradation, only the base of the current is deposited while the rest will overpass and deposit further downstream. In experimental conditions a lack of gas flux forces the current to deposit rapidly at the distal end creating a reverse graded deposit. Continued gas flux will elutriate fines upwards, releasing fine grains back to the surface of the deposit (Fig 6.3). Mass elutriation during degassing may lead reverse graded deposits to lose evidence of grading or produce more normally graded deposits as a result of fines being lifted above coarser grains.

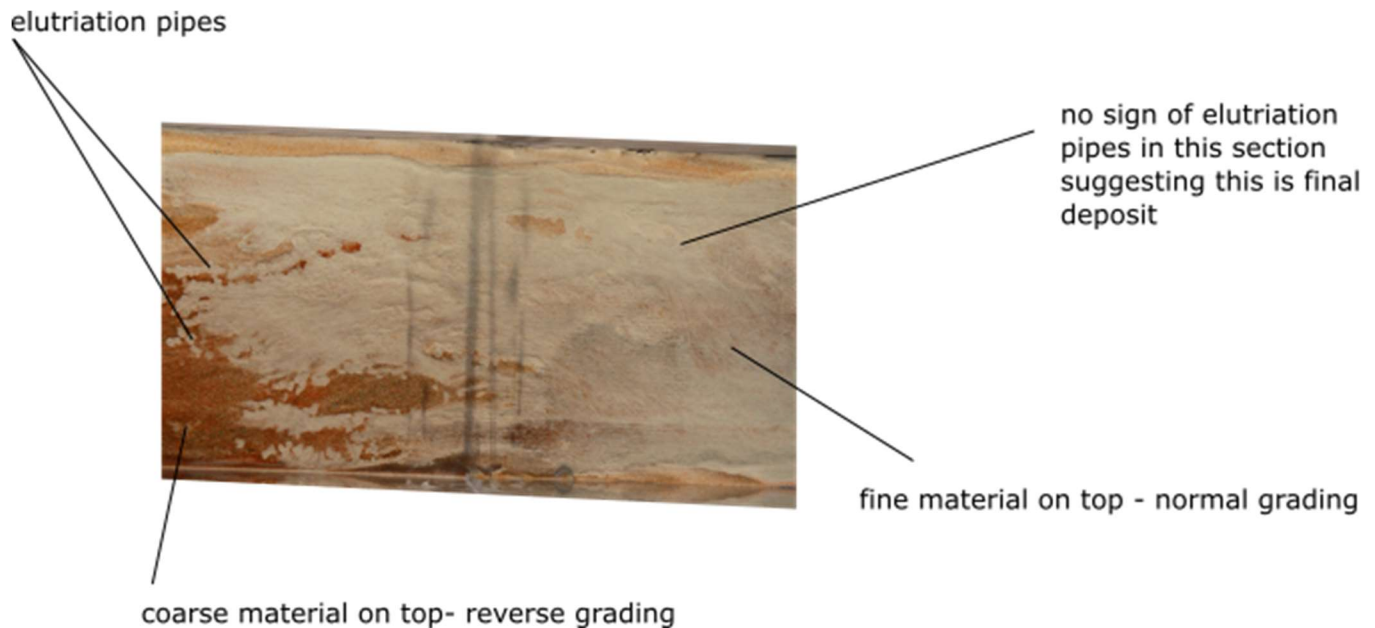


Figure 6.3 elutriation pipes at the surface of the distal end of the deposit, displaying evidence of fine grains elutriating and transporting down current after deposition

Experimental granular currents show that greater grading in regressive bedforms is due to stepwise aggradation of stratified currents where the flow boundary of the current suddenly jumps upwards freezing the full flow head or pulse, as proposed by Sulpizio et al. (2007). This study has shown that reverse grading is likely in all planar and backset beds. However, it shows that backset beds will show larger ranges in available grain sizes.

Fluidised currents in a flume present a sidewall effect where the deposit at the sidewall of the flume was markedly different from the deposit on the interior. The unconsolidated nature of the granular material used made it impossible to gain any meaningful data on this effect. Further study is required to understand the effect better. Monitoring the movement of grains on the sidewall versus the centre of the current, and/or overhead cameras recording the surface of the current, and/or setting the deposits with a cohesive glue or gel could provide an insight into how the deposits show different conditions on the edge and in the centre of a current.

6.2. Implications for PDC behaviour

Shake table experiments used a mixture of muesli; a well-known analogue for recording the muesli effect. This ensured that what we would observe was kinematic sieving. Muesli also presents a range of grain sizes, densities and shapes making it comparable to an ignimbrite.

Stratified currents (Branney & Kokelaar, 2002) show a model where *En masse* deposition creates overlapping bedforms (Sulpizio et al., 2007) as the continued supply of material builds the deposit. Is this more common than believed, or does this occur only under the specific conditions we have demonstrated i.e., rapid deaeration? This could be the focus of future study.

This study has indicated that in steady supply conditions, where the current has a constant gas supply, a current will always be stratified, separating grain sizes from fines at the base to coarsest grains at the free surface. This has been shown to occur in any current using single density material and in granular currents with different densities. When these currents are waning the current will stop *En masse*, and the current will overlap. To investigate this further, field studies examining deposits of dense granular currents should look at bedforms comparing them to the bedforms identified in this study and by Sulpizio et al. (2014).

Stratification within the current dominates the supply to the deposit interface in the flow boundary zone. The deposit aggrades from the base of the current, with the base dominated by fines; coarse particles are carried above the flow boundary and cannot be deposited until the flow boundary rises to them. Continued supply in a steady current leads to the build-up of fines at the base. As the current wanes and the supply reduces aggradation rates increase rapidly effectively depositing the current *en masse* at the flow front. Continued flow behind causes overlapping of beds (Sulpizio et al., 2014). This occurs in the steep backset beds and is not observed in planar beds.

6.3. Applications to field volcanology

The use of JMicrovison (Roudit, 2008) and Gradistat (Blott & Pye, 2001) have enabled quantitative data to be used to back up or oppose the qualitative findings in the field. For example, Smith and Kokelaar (2013) identify a deposit as having reversely graded pumices and normally graded lithics, this study however has found that both pumice and lithics are reversely graded. This could suggest that image analysis could be used more often to back up qualitative findings. Furthermore, using quantitative data will allow for better comparisons of deposits from different regions which could be useful in spotting patterns in PDC behaviour.

Experiments have revealed that steep regressive bedforms in granular currents show stronger grading in comparison to shallow backsets and planar beds. This is inferred to be a result of current stratification and stepwise aggradation in steep bedforms. Comparisons to field deposits could provide an insight into whether this process is occurring in real ignimbrites. If current stratification is occurring in PDCs then using flume experiments such as this could provide crucial insights into the rheological behaviour of PDCs

We need more details on bedforms in deposits analysed in the field. Comparing the results of this study to real ignimbrites is hampered by the lack of published quantified deposit and bedform descriptions. Future study could assess whether reverse grading in the field is more prevalent on regressive bedforms as is suggested by the flume experiments in this study.

Elutriation pipes in the flume experiments destroyed any potential evidence of grading in the thinner sections of the deposit. The effect of gas elutriation on sedimentary structures and deposit architecture more broadly could be investigated using flume experiments pumping gas into a graded deposit and observing how it changes. The resultant deposits could be compared to field deposits to determine whether elutriation affects the grading of deposits.

The sidewall effect occurs in flume experimentation whereby the sidewalls of the flume produce different flow conditions to the centre of the flume. As a result, the deposit in the centre of the flume and at the sidewalls produce different characteristics. This could be connected to PDCs that flow through valleys where the valley walls constrain the currents similarly to how the sidewalls constrain the current into the flume. By investigating a deposit across a valley insight into how the flow conditions change from the valley walls in the centre could be provided.

6.4. Conclusions

Sedimentological characterisation of ignimbrites from Tenerife has shown that these reversely graded deposits are generally moderate to poorly sorted ($0.5-1.5 \sigma_{\phi}$) and that this may be dependent on the grain size and density of clasts in the current that forms the deposit. Image analysis of the ignimbrites shows that both pumices and lithic clasts may be reversely graded, and pumices are often more strongly graded than lithics. This is contrary to how these deposits are often recorded in the field by qualitative visual inspection; the deposits analysed were all recorded as normally graded in lithics in the field. Grading is more visible in coarser deposits. Results from this study show that the average grain size difference from the base to the top may be up to 5x larger in coarse deposits whilst in finer deposits it may be as little as 1.9x larger. This means that this grading is harder to visually observe, which may lead to misinterpretation in the field. This study demonstrates that quantitative analysis of sedimentological characteristics, such as sorting and grain size, may provide more accurate descriptions of the deposits and this can be done by image analysis rather than collecting samples.

Mechanisms of sorting and grading in polydisperse sediments were assessed in static (shake table) and dynamic (flume) settings. In static systems with grains of the same density but different grain sizes, grains with a diameter difference of $d_s/D_l \leq 0.16$ will begin to segregate instantly. Over this threshold, grains will segregate but will take longer, and may not fully segregate when time is constrained. This value is less than the threshold proposed by Sohn and Chough (1993). In static systems with grains with varying density and grain size, the grain size is the dominant factor in a grain's ability to percolate. Experiments showed that density has a significant impact on a grain's ability to segregate; denser particles are able to percolate downwards more than lighter particles of the same grain size and lighter coarse particles rose to the top above coarse dense particles. Grains of similar size, but different densities were able to percolate with the diameter difference for instant percolation at ≤ 0.25 , which is consistent with the threshold value proposed by Sohn and Chough (1993).

In fluidised systems grains are sorted in a stratified current. Stratification arises from kinematic sorting within the current, this is evident from the deposits which show similar characteristics to deposits formed by kinematic sieving, such as the complete segregation of the largest grain from the smallest grains and the mixture of grain sizes that are similar, conforming to the threshold value of 0.25, furthermore the conditions were kept constant through all currents, ruling out any impact from waxing and waning. Video recording and deposits show that deposits of stratified currents begin aggrading progressively producing massive and fine grained deposits, followed by weakly graded planar beds. Increased frictional stress leads to currents depositing backset beds, as the fines are depleted. As friction stresses continue to increase stepwise aggradation occurs freezing pulses and preserving the internal grading of the current.

In currents where the grains all have the same density but varying grain size the currents will sort the grains by size to deposit reversely graded beds. Gravitational settling does appear to have a minor

role in currents with varying grain density and grain size, as when two grains of the same size but varying density are together they will sort according to density as is expected in gravitational settling. Gravitational settling is not thought to be a major impacting factor in these currents, as evident in experiment 31 the dense beads did not sink below the less dense beads and in fact ended up sorted according to size as is to be expected from kinematic sorting. The currents will sort predominantly according to grain size, with dense grains percolating below lighter grains of similar grain size but not through smaller grains. Analysis of the deposits shows similar characteristics to the real ignimbrites, with sorting values for current deposits ranging between 0.63 and 1.36. When compared to kinematic sorting experiments with values ranging from 0.5-1.1, the values sit within similar ranges suggesting a link between the two, the slight differences could be attributed to fluidisation of the currents or the minor role of other segregation mechanisms such as gravitational settling. This study concludes that there is a direct link between kinematic sieving and reverse grading in ignimbrites. Stratification of the current controls the composition of the flow boundary zone and the clasts which are able to deposit. Reverse graded ignimbrites are likely a result of kinematic sieving occurring during flow, creating stratified currents that aggrade in a stepwise fashion preserving the internal structure. The impact of waxing currents introducing increasingly larger clasts which are later deposited by waning of the currents could not be investigated in this study. Further work should be completed to investigate this alternative interpretation of reverse grading in granular currents.

References

- Allen, S. & Cas, R. A. (1998) Rhyolitic fallout and pyroclastic density current deposits from a phreatoplinian eruption in the eastern Aegean Sea, Greece. *Journal of Volcanology and Geothermal Research*, 86(1-4), 219-251.
- Arasan, S., Akbulut, S. & Hasiloglu, A. S. (2011) Effect of particle size and shape on the grain-size distribution using Image analysis. *International journal of civil and structural engineering*, 1(4), 968-985.
- Auker, M. R., Sparks, R. S. J., Siebert, L., Crosweller, H. S. & Ewert, J. (2013) A statistical analysis of the global historical volcanic fatalities record. *Journal of Applied Volcanology*, 2(1), 2.
- Bagnold, R. A. (1954) Experiments on a gravity-free dispersion of large solid spheres in a Newtonian fluid under shear. *Proceedings of the Royal Society of London. Series A. Mathematical and Physical Sciences*, 225(1160), 49-63.
- Bartali, R., Rodríguez Liñán, G. M., Torres-Cisneros, L. A., Pérez-Ángel, G. & Nahmad-Molinari, Y. (2020) Runout transition and clustering instability observed in binary-mixture avalanche deposits. *Granular Matter*, 22(2).
- Blott, S. J. & Pye, K. (2001) GRADISTAT: a grain size distribution and statistics package for the analysis of unconsolidated sediments. *Earth Surface Processes and Landforms*, 26(11), 1237-1248.
- Bonadonna, C., Cioni, R., Pistolesi, M., Connor, C., Scollo, S., Pioli, L. & Rosi, M. (2013) Determination of the largest clast sizes of tephra deposits for the characterization of explosive eruptions: a study of the IAVCEI commission on tephra hazard modelling. *Bulletin of Volcanology*, 75(1).
- Branney, M. J. & Kokelaar, P. (1992) A reappraisal of ignimbrite emplacement: progressive aggradation and changes from particulate to non-particulate flow during emplacement of high-grade ignimbrite. *Bulletin of Volcanology*, 54(6), 504-520.
- Branney, M. J. & Kokelaar, P. (1997) Giant bed from a sustained catastrophic density current flowing over topography: Acatlan ignimbrite, Mexico. *Geology*, 25(2), 115-118.
- Branney, M. J. & Kokelaar, P. (2002) Pyroclastic density currents and the sedimentation of ignimbrites: Geological Society of London.
- Brown, R. J. & Andrews, G. D. (2015) Deposits of pyroclastic density currents, *The Encyclopedia of Volcanoes* Elsevier, 631-648.

Brown, R. J. & Branney, M. J. (2004a) Bypassing and diachronous deposition from density currents: Evidence from a giant regressive bed form in the Poris ignimbrite, Tenerife, Canary Islands. *Geology*, 32(5), 445.

Brown, R. J. & Branney, M. J. (2004b) Event-stratigraphy of a caldera-forming ignimbrite eruption on Tenerife: the 273 ka Poris Formation. *Bulletin of Volcanology*, 66(5), 392-416.

Brown, R. J. & Branney, M. J. (2013) Internal flow variations and diachronous sedimentation within extensive, sustained, density-stratified pyroclastic density currents flowing down gentle slopes, as revealed by the internal architectures of ignimbrites on Tenerife. *Bulletin of Volcanology*, 75(7).

Brown, R. J., Kokelaar, B. P. & Branney, M. J. (2007) Widespread transport of pyroclastic density currents from a large silicic tuff ring: the Glaramara tuff, Scafell caldera, English Lake District, UK. *Sedimentology*, 54(5), 1163-1190.

Brown, S. K., Jenkins, S. F., Sparks, R. S. J., Odbert, H. & Auken, M. R. (2017) Volcanic fatalities database: analysis of volcanic threat with distance and victim classification. *Journal of Applied Volcanology*, 6(1).

Buckland, H. M., Saxby, J., Roche, M., Meredith, P., Rust, A. C., Cashman, K. V. & Engwell, S. L. (2021) Measuring the size of non-spherical particles and the implications for grain size analysis in volcanology. *Journal of Volcanology and Geothermal Research*, 107257.

Burden, R. E., Phillips, J. C. & Hincks, T. K. (2011) Estimating volcanic plume heights from depositional clast size. *Journal of Geophysical Research: Solid Earth*, 116(B11), n/a-n/a.

Buser, O. & Bartelt, P. (2011) Dispersive pressure and density variations in snow avalanches. *Journal of Glaciology*, 57(205), 857-860.

Cagnoli, B. (2005) Vertical segregation in granular mass flows: A shear cell study. *Geophysical Research Letters*, 32(10).

Campbell, C. S. (1990) Rapid Granular Flows. *Annual Review of Fluid Mechanics*, 22(1), 57-90.

Capaccioni, B., Valentini, L., Rocchi, M. B. L., Nappi, G. & Sarocchi, D. (1997) Image analysis and circular statistics for shape-fabric analysis: applications to lithified ignimbrites. *Bulletin of Volcanology*, 58(7), 501-514.

Cas, R. & Wright, J. (1987) Volcanic successions, modern and ancient: London–New York–Tokyo–Melbourne–Madras. Chapman & Hall.

Choux, C. & Druitt, T. (2002) Analogue study of particle segregation in pyroclastic density currents, with implications for the emplacement mechanisms of large ignimbrites. *Sedimentology*, 49(5), 907-928.

Choux, C., Druitt, T. & Thomas, N. (2004) Stratification and particle segregation in flowing polydisperse suspensions, with applications to the transport and sedimentation of pyroclastic density currents. *Journal of Volcanology and Geothermal Research*, 138(3-4), 223-241.

Douillet, G. A., Bernard, B., Bouysson, M., Chaffaut, Q., Dingwell, D. B., Gegg, L., Hoelscher, I., Kueppers, U., Mato, C., Ritz, V. A., Schlunegger, F. & Witting, P. (2019) Pyroclastic dune bedforms: macroscale structures and lateral variations. Examples from the 2006 pyroclastic currents at Tungurahua (Ecuador). *Sedimentology*, 66(5), 1531-1559.

Douillet, G. A., Pacheco, D. A., Kueppers, U., Letort, J., Tsang-Hin-Sun, È., Bustillos, J., Hall, M., Ramón, P. & Dingwell, D. B. (2013) Dune bedforms produced by dilute pyroclastic density currents from the August 2006 eruption of Tungurahua volcano, Ecuador. *Bulletin of Volcanology*, 75(11).

Druitt, T. (1998) Pyroclastic density currents. *Geological Society, London, Special Publications*, 145(1), 145-182.

Fernlund, J. M. R. (1998) The effect of particle form on sieve analysis: a test by image analysis. *Engineering Geology*, 50(1-2), 111-124.

Folk, R. L. & Ward, W. C. (1957) Brazos River bar [Texas]; a study in the significance of grain size parameters. *Journal of Sedimentary Research*, 27(1), 3-26.

Francus, P. (1998) An image-analysis technique to measure grain-size variation in thin sections of soft clastic sediments. *Sedimentary Geology*, 121(3-4), 289-298.

Geldart, D. (1973) Types of gas fluidization. *Powder technology*, 7(5), 285-292.

Giachetti, T., Burgisser, A., Arbaret, L., Druitt, T. H. & Kelfoun, K. (2011) Quantitative textural analysis of Vulcanian pyroclasts (Montserrat) using multi-scale X-ray computed microtomography: comparison with results from 2D image analysis. *Bulletin of Volcanology*, 73(9), 1295-1309.

Giannetti, B. & De Casa, G. (2000) Stratigraphy, chronology, and sedimentology of ignimbrites from the white trachytic tuff, Roccamonfina Volcano, Italy. *Journal of Volcanology and Geothermal Research*, 96(3-4), 243-295.

Gilbertson, M. A., Jessop, D. E. & Hogg, A. J. (2008) The effects of gas flow on granular currents. *Philosophical Transactions of the Royal Society A: Mathematical, Physical and Engineering Sciences*, 366(1873), 2191-2203.

Gravina, T., Lirer, L., Marzocchella, A., Petrosino, P. & Salatino, P. (2004) Fluidization and attrition of pyroclastic granular solids. *Journal of Volcanology and Geothermal Research*, 138(1-2), 27-42.

- Hand, M., Bryce. (1997) Inverse Grading Resulting from Coarse-sediment Transport Lag. *SEPM Journal of Sedimentary Research*, Vol. 67.
- Hill, K. M., Khakhar, D. V., Gilchrist, J. F., McCarthy, J. J. & Ottino, J. M. (1999) Segregation-driven organization in chaotic granular flows. *Proceedings of the National Academy of Sciences*, 96(21), 11701-11706.
- Jha, A. K., Gill, J. S. & Puri, V. M. (2008) Percolation Segregation in Binary Size Mixtures of Spherical and Angular-Shaped Particles of Different Densities. *Particulate Science and Technology*, 26(5), 482-493.
- Kwan, A. K. H., Mora, C. F. & Chan, H. C. (1999) Particle shape analysis of coarse aggregate using digital image processing. *Cement and Concrete Research*, 29(9), 1403-1410.
- Le Roux, J. (2003) Can Dispersive Pressure Cause Inverse Grading in Grain Flows?: Discussion. *Journal of Sedimentary Research*, 73(2), 333-334.
- Legros, F. o. (2002) Can dispersive pressure cause inverse grading in grain flows? *Journal of Sedimentary Research*, 72(1), 166-170.
- Lindqvist, J. & Åkesson, U. (2001) Image analysis applied to engineering geology, a literature review. *Bulletin of Engineering Geology and the Environment*, 60(2), 117-122.
- Lube, G., Breard, E. C. P., Esposti-Ongaro, T., Dufek, J. & Brand, B. (2020) Multiphase flow behaviour and hazard prediction of pyroclastic density currents. *Nature Reviews Earth & Environment*, 1(7), 348-365.
- Marks, B., Rognon, P. & Einav, I. (2012) Grainsize dynamics of polydisperse granular segregation down inclined planes. *Journal of Fluid Mechanics*, 690, 499-511.
- Mertens, G. & Elsen, J. (2006) Use of computer assisted image analysis for the determination of the grain-size distribution of sands used in mortars. *Cement and Concrete Research*, 36(8), 1453-1459.
- Middleton, G. V. (1970) Experimental studies related to flysch sedimentation. *Flysch sedimentology in North America*, 7, 253-272.
- Möbius, M. E., Lauderdale, B. E., Nagel, S. R. & Jaeger, H. M. (2001) Size separation of granular particles. *Nature*, 414(6861), 270-270.
- Ottino, J. M. & Khakhar, D. V. (2000) Mixing and Segregation of Granular Materials. *Annual Review of Fluid Mechanics*, 32(1), 55-91.

Palladino, D. M. & Valentine, G. A. (1995) Coarse-tail vertical and lateral grading in pyroclastic flow deposits of the Latera Volcanic Complex (Vulsini, central Italy): origin and implications for flow dynamics, 69(3-4), 343-364.

Pudasaini, S. P. & Hutter, K. (2007) *Avalanche dynamics: dynamics of rapid flows of dense granular avalanches*. Springer Science & Business Media.

Riley, C. M., Rose, W. I. & Bluth, G. J. S. (2003) Quantitative shape measurements of distal volcanic ash. *Journal of Geophysical Research: Solid Earth*, 108(B10).

Roduit, N. (2008) JMicroVision: Image analysis toolbox for measuring and quantifying components of high-definition images. *Ver*, 1(7), 2002-2007.

Roduit, N. (2020) *JMicroVision: Image analysis toolbox for measuring and quantifying components of high-definition images*. version 1.3.4. Available online: <https://jmicrovision.github.io/> [Accessed 10/02/2021].

Rosato, A., Strandburg, K. J., Prinz, F. & Swendsen, R. H. (1987) Why the Brazil nuts are on top: Size segregation of particulate matter by shaking. *Physical review letters*, 58(10), 1038.

Rowley, P. J., Roche, O., Druitt, T. H. & Cas, R. (2014) Experimental study of dense pyroclastic density currents using sustained, gas-fluidized granular flows, 76(9).

Sanders, J. (2008) *Veusz-a scientific plotting package* 26/05/21].

Savage, S. & Lun, C. (1988) Particle size segregation in inclined chute flow of dry cohesionless granular solids. *Journal of fluid mechanics*, 189, 311-335.

Schnautz, T., Brito, R., Kruelle, C. A. & Rehberg, I. (2005) A Horizontal Brazil-Nut Effect and Its Reverse. *Physical Review Letters*, 95(2).

Scott, A. M. & Bridgwater, J. (1975) Interparticle percolation: a fundamental solids mixing mechanism. *Industrial & Engineering Chemistry Fundamentals*, 14(1), 22-27.

Shimosaka, A., Shirakawa, Y. & Hidaka, J. (2013) Effects of Particle Shape and Size Distribution on Size Segregation of Particles. *Journal of Chemical Engineering of Japan*, 46(3), 187-195.

Shinbrot, T. & Muzzio, F. J. (1998) Reverse buoyancy in shaken granular beds. *Physical Review Letters*, 81(20), 4365.

Shultz, A. W. (1984) Subaerial Debris-Flow Deposition in the Upper Paleozoic Cutler Formation, Western Colorado. *SEPM Journal of Sedimentary Research*, Vol. 54.

- Smith, G., Rowley, P., Williams, R., Giordano, G., Trolese, M., Silleni, A., Parsons, D. R. & Capon, S. (2020) A bedform phase diagram for dense granular currents. *Nature Communications*, 11(1).
- Smith, G. M., Williams, R., Rowley, P. J. & Parsons, D. R. (2018) Investigation of variable aeration of monodisperse mixtures: implications for pyroclastic density currents. *Bulletin of Volcanology*, 80(8).
- Smith, N. J. & Kokelaar, B. P. (2013) Proximal record of the 273 ka Poris caldera-forming eruption, Las Cañadas, Tenerife. *Bulletin of Volcanology*, 75(11).
- Sohn, Y. (1997) On traction-carpet sedimentation. *Journal of Sedimentary Research*, 67(3), 502-509.
- Sohn, Y. K. & Chough, S. K. (1993) The Udo tuff cone, Cheju Island, South Korea: transformation of pyroclastic fall into debris fall and grain flow on a steep volcanic cone slope, 40(4), 769-786.
- Sparks, R. S., S. and Walker, G.P.L (1973) Products of an ignimbrite. *Geology*, 1(3), 115-118.
- Sparks, R. S. J. (1976) Grain size variations in ignimbrites and implications for the transport of pyroclastic flows. *Sedimentology*, 23(2), 147-188.
- Sparks, R. S. J. (1978) Gas release rates from pyroclastic flows: a assessment of the role of fluidisation in their emplacement. *Bulletin Volcanologique*, 41(1), 1-9.
- Staron, L. & Phillips, J. C. (2015) Stress partition and microstructure in size-segregating granular flows. *Physical Review E*, 92(2).
- Sulpizio, R., Dellino, P., Doronzo, D. M. & Sarocchi, D. (2014) Pyroclastic density currents: state of the art and perspectives. *Journal of Volcanology and Geothermal Research*, 283, 36-65.
- Sulpizio, R., Mele, D., Dellino, P. & La Volpe, L. (2007) Deposits and physical properties of pyroclastic density currents during complex Subplinian eruptions: the AD 472 (Pollena) eruption of Somma-Vesuvius, Italy. *Sedimentology*, 54(3), 607-635.
- Trofimovs, J., Sparks, R. S. J. & Talling, P. J. (2008) Anatomy of a submarine pyroclastic flow and associated turbidity current: July 2003 dome collapse, Soufrière Hills volcano, Montserrat, West Indies. *Sedimentology*, 55(3), 617-634.
- Walker, G. P. L. W., C.J.N.; Froggatt, P. C. (1980) Fines-depleted ignimbrite in New Zealand — The product of a turbulent pyroclastic flowUnknown article. *Geology (1980) 8 (5): 245–249*.
- Walton, O. R. & Braun, R. L. (1986) Viscosity, granular-temperature, and stress calculations for shearing assemblies of inelastic, frictional disks. *Journal of Rheology*, 30(5), 949-980.

Wilson, C. J. N. (1980) The role of fluidization in the emplacement of pyroclastic flows: An experimental approach. *Journal of Volcanology and Geothermal Research*, 8(2-4), 231-249.

Wilson, C. J. N. & Walker, G. P. L. (1982) Ignimbrite depositional facies: the anatomy of a pyroclastic flow. *Journal of the Geological Society*, 139(5), 581-592.

7. Appendix I

- 7.1. Digital version of all JMicrovison and Gradistat data used in Chapter 3

<https://universityofhull.app.box.com/folder/172766463099?s=xx7io264d3aqlrxygnveqseunn09hu1x>

8. Appendix II

- 8.1. Digital version of all JMicrovison and Gradistat data used in Chapter 4 with videos of all experiments

<https://universityofhull.app.box.com/folder/172786366595?s=nwc0me6dxj2w51y3p8goz74mv17khr1z>

9. Appendix III

- 9.1. Digital version of all JMicrovison and Gradistat data used in Chapter 5 with videos of all representative experiments

<https://universityofhull.app.box.com/folder/172713675518?s=lræydojlha4vxxnpoggothvb2s2dkd8>

10. Appendix IV

- 10.1. Link to online versions of highspeed videos

<https://www.youtube.com/channel/UC7GqAGTwOi5aJgkTjT1gXfQ>

- 10.2. Link to online version of High resolution photos

<https://www.flickr.com/photos/198477086@N07/>